Electric Power System Operations with a Variable Series Reactor

A Dissertation Presented for the

Doctor of Philosophy

Degree

The University of Tennessee, Knoxville

Xiaohu Zhang

May 2017

© by Xiaohu Zhang, 2017
All Rights Reserved.

Dedicated to My Parents

Acknowledgements

I would like to express my highest gratitude to my supervisor, Professor Kevin Tomsovic, for his time and dedication, great guide and support throughout the whole work. Moreover, with his wonderful personality, he has been an outstanding mentor and very influential in regards to not only my professional development, but also my personal life.

I would also like to thank Dr. Aleksandar Dimitrovski, Dr. Fran Li and Dr. Xueping Li for their time and effort in serving as my committee member. Without their invaluable suggestions and comments, the dissertation would not reach the same level as it is today.

My gratitude also goes to all the professors, staff and students in the CURENT research center. Their encouragement and help are very beneficial to my research work.

And last but not least, I would like to express my heartfelt appreciation to my family, especially my wife, Xizi Cai, for their endless love and support during my education abroad.

Love is patient, love is kind. It does not envy, it does not boast, it is not proud. It does not dishonor others, it is not self-seeking, it is not easily angered, it keeps no record of wrong. Love does not delight in evil but rejoices with the truth. It always protects, always trusts, always hopes, always preserves.

– 1 Corinthians 13: 4-7

Abstract

Series FACTS devices, such as a Variable Series Reactor (VSR), have the ability to continuously regulate the transmission line reactance so as to control power flow. This research work evaluates the benefits brought by VSRs in different aspects of power system and develops efficient planning models and algorithms to provide optimal investment plan for the VSRs.

First, an optimization approach capable of finding both optimal locations and settings of VSRs under a specific operating condition is developed. The tool implements a full ac model as well as detailed models for different power system components.

Second, an optimization tool which can optimally allocate VSRs to improve the load margin in a transmission network considering a multi-scenario framework including base case and some critical contingencies is proposed. Starting from a mixed integer nonlinear programming (MINLP) model, a reformulation technique is leveraged to transform the MINLP model into a mixed integer linear programming (MILP) model so that it is computationally tractable for large scale power systems. Detailed numerical simulations on the practical Northwest US power network demonstrate the proposed technique and the capability of VSRs.

Third, the VSR is introduced in the Transmission Expansion Planning (TEP) problem. A security constrained multi-stage TEP with the VSR is formulated as an MILP model. To reduce the computational burden for a practical large scale system, a decomposition approach is proposed. Simulation results demonstrate the

effectiveness of the proposed approach and show that the appropriately allocated VSRs allow reduced planning costs.

Fourth, in order to investigate the economic benefits brought by VSR in contingencies, a planning model to allocate VSR considering different operating conditions and the $N-1$ contingencies is formulated. We consider a single target year planning. Three distinct load patterns which represent peak, normal and low load level are selected to accommodate the yearly load profile. The transmission contingencies can occur in any of the three load conditions. A two phase Benders decomposition is proposed to solved the large scale MILP model. Simulation results on the IEEE-118 bus system and the practical Polish system establish the efficient performance of the proposed algorithm.

Table of Contents

1 Introduction **1**

1.1 Background and Research Objectives 1

1.2 Summary of Contributions 3

2 Literature Review **5**

2.1 Basics of AC Power Transmission 5

2.2 Power Flow Control Approaches 6

2.2.1 Power Flow Control Devices 6

2.2.2 Transmission Line Switching 8

2.3 Allocation and Utilization of Power Flow Control Devices 9

2.4 Transmission Expansion Planning 12

3 Continuously Variable Series Reactor **15**

3.1 Basic Configuration and Principle of Operation 15

3.2 Lab Tests and Results 17

4 The Application of a Variable Series Reactor to Enhance Power System Loadability **20**

4.1 Static Model of VSR in AC Power Flow 21

4.2 Optimization Model 21

4.2.1 Objective Function 21

4.2.2 Equality Constraints 22

4.2.3 Inequality Constraints 24
4.3 Optimization Methodology 25
4.3.1 Algorithm 25
4.3.2 Flow Chart of the Optimization Tool 26
4.4 Case Studies 27
4.4.1 IEEE Sample Systems 28
4.4.2 Initialization 28
4.4.3 IEEE System Results 29
4.4.4 Practical Application 31
4.5 Conclusion 35

5 Transfer Capability Improvement with a Variable Series Reactor 37
5.1 Static Model of VSR in DC power flow 38
5.2 Reformulation Technique 39
5.2.1 Classical Formulation 39
5.2.2 Reformulation 40
5.3 Two Stage Optimization Model 42
5.3.1 Flow Chart of the Optimization Tool 42
5.3.2 Allocation Model 43
5.3.3 Operation Model 44
5.4 Case Studies 45
5.4.1 IEEE 30-Bus System 45
5.4.2 IEEE 118-Bus System 48
5.4.3 Northwest Power Network 50
5.5 Conclusion 54

6 Security Constrained Multi-Stage Transmission Expansion Planning Considering a Variable Series Reactor 56
6.1 Optimization Model 57
6.1.1 $N-1$ Security Constraints 57

6.1.2 Integrated Planning Formulation 58
6.1.3 Decomposition 61
6.2 Case Studies 64
6.2.1 IEEE 24-Bus System 64
6.2.2 Polish 2383-Bus System 69
6.2.3 Computational and Optimality Issues 71
6.3 Conclusion 71

7 Optimal Allocation of a Variable Series Reactor for Large Scale Systems via Benders Decomposition 73
7.1 Problem Formulation 74
7.1.1 Objective Function 74
7.1.2 Constraints 76
7.2 Solution Approach 77
7.2.1 Master Problem 78
7.2.2 Subproblem 79
7.2.3 Solution Procedure 80
7.3 Numerical Case Studies 83
7.3.1 IEEE 118-Bus System 84
7.3.2 Polish System 87
7.4 Conclusion 88

8 Conclusion and Future Work 90
8.1 Conclusion 90
8.2 Future Work 92
8.2.1 Minimizing Wind Power Spillage with a Variable Series Reactor 92
8.2.2 Combining the Variable Series Reactor with Other Power Flow Control Approaches 93
8.2.3 Emulation of CVSR on the CURENT Hardware Testbed . . . 93

Bibliography **94**

Appendices **111**

A Modified Jacobian Matrix for the Power Balance Equations **112**

Vita **114**

List of Tables

4.1 Specifications of IEEE Sample Systems and Model Scales 28
4.2 CVSR Placement of IEEE 30-Bus System With Different Starting Points 30
4.3 CVSR Placement of IEEE 2736-Bus System With Different Starting Points 30
4.4 CVSR Placement of Northwest System With Different Starting Points 34
4.5 CVSR Settings for Different Contingencies 35
4.6 Thermal Loading of the Main Transmission Paths From North to South in Contingency 1 36

5.1 Maximum Loadability and CVSR Locations of the Multi-scenario Case for the IEEE 30-Bus System 48
5.2 Maximum Loadability and CVSR Locations of the Multi-scenario Case for the IEEE 118-Bus System 49
5.3 CVSR Settings of Different Scenarios for IEEE 118-Bus System . . . 50
5.4 Maximum Loadability and CVSR Placements of Northwest Power Network for Different Scenarios 52
5.5 CVSR Settings of Different Scenarios for Northwest Power Network . 53

6.1 Single Stage TEP Results Comparison for the IEEE 24-Bus System Using Integrated Model 66
6.2 Single TEP Results Comparison for the IEEE 24-Bus System Using Decomposed Model 67

6.3 Multi-stage TEP Results Comparison for the IEEE-24 Bus System Using Integrated Model 68
6.4 Multi-stage TEP Results Comparison for the IEEE 24-Bus System Using Decomposed Model 69
6.5 TEP Results Comparison for the Polish System 70
6.6 TEP Results Comparison for the Polish System Using Decomposed Model Considering Different Number of Critical Contingencies 72

7.1 Comparison of the Investment Results for IEEE 118-Bus System . . . 85
7.2 Annual Planning Cost with and without TCSC for IEEE 118-Bus System 87
7.3 Annual Planning Cost with and without TCSC for the Polish System 88

List of Figures

2.1 Static model of a simple transmission line. 5

2.2 Overview of power flow control devices. 8

3.1 Basic configuration of CVSR. 16

3.2 Magnetization (B-H) curve of core material (AK H-1 steel). 16

3.3 Photo of the low voltage CVSR prototype. 17

3.4 Typical setup for lab testing of the prototype CVSR. 18

3.5 CVSR output reactance versus the DC bias current at different AC load levels. 18

4.1 Static representation of VSR in AC power flow. 21

4.2 Flow chart of the optimization tool. 27

4.3 System loadability versus k_f 29

5.1 Static representation of VSR in DCPF. 38

5.2 Flow chart for the optimization tool. 42

5.3 Loadability for the base case and contingencies with different number of CVSRs. 46

5.4 Maximum loadability versus the number of CVSRs of the multi-scenario case for the IEEE 30-bus system. 47

5.5 Thermal loading of five transmission corridors from North to South in contingency 1. 54

6.1 Flow chart of the iterative approach. 62

7.1 Flowchart of the solution approach. 81
7.2 Hourly generation cost for peak and normal load level. 85
7.3 Generation rescheduling under different contingencies for the peak load level. 86
7.4 Load shedding amount under different contingencies for peak load level. 87
7.5 Evolution of the proposed Benders algorithm. 89

Nomenclature

Indices

$i,\ j$	Index of buses.
n	Index of generators.
m	Index of loads.
k	Index of transmission elements.
c	Index of states; $c = 0$ indicates the base case; $c > 0$ is a contingency state.
b	Index of load blocks.
t	Index of time.
E	Index for an existing transmission line.
C	Index for a candidate transmission line.

Variables

P^g_{ncbt}, Q^g_{ncbt}	Active and reactive power generation of generator n for state c under load block b at time t.
P_{kcbt}, Q_{kcbt}	Active and reactive power flow of line k for state c under load block b at time t.

$\Delta P^d_{mcb}, \Delta Q^d_{mcb}$	Active and reactive load shedding amount of load m for state c under load level b.
$\Delta P^{g,up}_{ncb}, \Delta P^{g,dn}_{ncb}$	Active power generation adjustment up and down of generator n for state c under load level b.
V_i	Voltage magnitude at bus i.
θ_{icbt}	Voltage angle at bus i for state c under load level b at time t.
θ_{kcbt}	Voltage angle difference of branch k for state c under load level b at time t.
x^V_{kcbt}	Reactance of a VSR at branch k for state c under load level b at time t.
δ_{kt}	Binary variable associated with placing a VSR on branch k at time t.
α_{kt}	Binary variable assciated with line investment for branch k at time t.

Parameters

r_k, x_k	Resistance and reactance for branch k.
τ_{ij}	Tap ratio of transformer branch ij.
θ^{shift}_{ij}	Phase shift of transformer branch ij.
$P^{g,\min}_n, Q^{g,\min}_n$	Minimum active and reactive power output of generator n.
P^d_{mcbt}, Q^d_{mcbt}	Active and reactive power consumption of demand m for state c under load level b at time t.
$S^{\max}_{kcbt}$	Thermal limit of branch k at state c under load level b at time t.

$x_{k,V}^{\min}, x_{k,V}^{\max}$	Minimum and maximum reactance of the VSR at branch k.
$\theta_k^{\max}$	Maximum angle difference across branch k.
$\theta_i^{\max}, \theta_i^{\min}$	Maximum and minimum bus angle at bus i.
$V_i^{\max}, V_i^{\min}$	Maximum and minimum bus voltage magnitude at bus i.
N_{kcbt}	Binary parameter associated with the status of branch k at state c under load level b at time t.
$R_n^{g,up}, R_n^{g,dn}$	Ramp up and down limit for generator n.
a_n^g	Cost coefficient for generator n.
$a_n^{g,up}, a_n^{g,dn}$	Cost coefficient for generator n to increase and decrease active power.
a_{LS}	Cost coefficient for the load shedding.
A_h	Annual operating hours: 8760 h.
H_{bt}	Operating hours for load block b during time period t.
C_k^V	Investment cost of the VSR on line k.
C_k^L	Investment cost for branch k.
A_k^V	Annual investment cost for VSR.

Sets

$\mathcal{D}$	Set of loads.
$\mathcal{D}_i$	Set of loads located at bus i.
Ω_L	Set of transmission lines.
Ω_L^+	Set of candidate transmission lines.

Ω_V	Set of candidate transmission lines to install VSR.
Ω_c	Set of contingency states.
Ω_0	Set of base states.
Ω_L^i	Set of transmission lines connected to bus i.
Ω_b	Set of load levels.
Ω_t	Set of time periods.
$\mathcal{G}$	Set of on-line generators.
$\mathcal{G}_i$	Set of on-line generators located at bus i.
$\mathcal{G}_{re}$	Set of on-line generators allowed to rescheduling.
$\mathcal{B}$	Set of Buses.
$\mathcal{B}_{COI}$	Set of buses for the COI interface.
$\mathcal{B}_{NCOI}$	Set of buses for non-COI interface buses.

Chapter 1

Introduction

1.1 Background and Research Objectives

In recent years, due to the power market restructuring and the rapid introduction of renewable energy, the electric power industry is going through profound changes across technical, economic and organizational concerns. Traditionally, the electric power industry had a vertically integrated structure, in which the entire process of power generation, transmission and distribution was controlled by one electric utility. The electricity price was set by the regulators and customers had no choice of suppliers. In the deregulated market, the generation, transmission and distribution sectors become separate business entities. Some consumers were given more than one choice of electric suppliers, resulting in a competitive power market [1, 2]. Deregulation was introduced to bring in the following benefits:

- a reduction in the prices due to the competitive environment (ideally, the producer would sell at the marginal cost);
- multiple electricity retailers providing choices of new services for the customers to choose; and

- new innovative technologies to improve grid efficiency, reliability and power quality.

While deregulation has been able to deliver on some of these promises, it has also led to concerns with the transmission infrastructure, which was not designed for this new structure. Increasing electricity consumption, less predictable power flows and massive integration of renewable energy has caused the aging power grid to become more congested and under unusual stress. In today's environment, the transmission facilities are often operated close to their security limits, which results in compromised reliability and higher energy cost. In general, there exists two options to reduce congestion. The first option is through power system expansion by building new power plants and transmission lines to relieve congested areas. The second option involves installing power flow control equipment. The investment cost issues must be taken into consideration for both options; however, the difficulty in obtaining the right of way, political obstacles and long construction times are major hurdles for new transmission lines and upgrades. Given these considerations and improvements in power flow control devices, better utilization of existing power system capacities by installing new equipment is increasingly attractive [3, 4, 5].

Flexible AC transmission systems (FACTS) are a technology for controlling power flow and enhancing the utilization of existing transmission network [2, 6, 7, 8]. Specific types of series FACTS devices, which are named as Variable Series Reactor (VSR), have the ability to efficiently regulate the power flow through the adjustment of the transmission line reactance. Typical examples of VSR are Thyristor Controlled Series Compensator (TCSC), Distributed Series Reactor (DSR) and smart wire [5, 9, 10]. One major factor that prevents the wide deployment of VSRs is the installation cost. Accordingly, the Advanced Research Projects Agency-Energy (ARPA-E) initiated a program, named the Green Electricity Network Integration (GENI) [11], to call for different approaches that can be utilized to enhance the power flow control across the U.S. power grid. A hardware device called continuously variable series

reactor (CVSR), which is designed and developed by Oak Ridge National Laboratory (ORNL), was one project under GENI [12, 13]. Due to its simple and the low rating of the control circuit, the cost is significantly decreased. It is anticipated that more VSR-like devices with far cheaper price will be commercially available soon for the transmission network across the US. Hence, the development of efficient algorithms that are capable of finding the optimal locations of VSR is needed.

The objective of this research work is to develop new tools and algorithms which can provide guidance to utilities and system operators on how to utilize the VSR to make better use of the existing transmission infrastructure. The developed tools are expected be able to carry out both off-line planning and on-line operation functions. The planning function gives the system planners information regarding where to allocate the VSR and the on-line operation function provides operators information about the optimal settings for the VSR under different scenarios. The proposed models and algorithms are all tested on practical large scale system to ensure that the developed methods are scalable and directly applicable in the power industry.

1.2 Summary of Contributions

The main contributions of this dissertation are summarized as follows:

- an optimization approach is developed for integrating potentially large numbers of the VSR into a power system to enhance the system loadability and eliminate transmission line congestion. The proposed approach is computationally efficient for both the on-line analysis and off-line planning function. In the model, a full AC power flow model is used. Sequential quadratic programming (SQP) is adopted to solve the optimization model. To evaluate the quality of the solutions, two commonly used starting points are selected to initialize the optimization model.

- a planning and operation optimization model is proposed to optimally allocate VSR considering multiple operating conditions including base case and contingencies. Originally, the planning model is a mixed integer nonlinear programming (MINLP) model, which is difficult to be solved by commercial solvers. Reformulation is used to transform the MINLP model into a mixed integer linear programming (MILP) model while ensuring global optimality. The detailed numerical simulation results considering IEEE sample systems and a practical Northwest US power network establish the performance of the proposed technique.

- a security constrained multi-stage Transmission Expansion Planning (TEP) with VSRs is formulated. In addition, an iterative approach is developed to decompose the model into the planning master problem and a security check subproblem so that it is computationally tractable for practical sized systems. This is critical as the model size increases dramatically with the number of stages, load blocks and contingencies.

- a planning model to allocate VSR in the transmission network considering different load patterns and contingencies as well as coupling constraints between base and contingency conditions is proposed. We implement a two phase Benders decomposition approach to solve the planning model which shows high performance even for a practical large scale network considering hundreds of operating states.

Chapter 2

Literature Review

2.1 Basics of AC Power Transmission

Consider a simple transmission line model with resistance and shunt susceptance ignored as shown in Fig. 2.1.

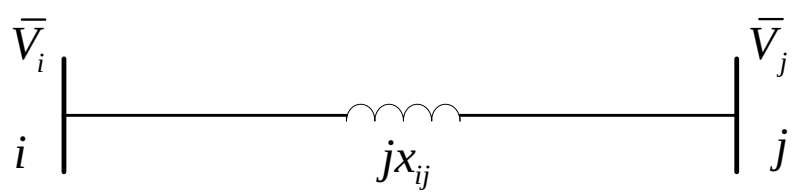

Figure 2.1: Static model of a simple transmission line.

The active power flow P_{ij} on this line is determined by the following well-known equation [14]:

$$P_{ij} = \frac{V_i V_j}{x_{ij}} \sin(\theta_i - \theta_j) \tag{2.1}$$

From (2.1), it can be seen that there are three possibilities to control the power flow on the line: 1) control either of the bus voltage magnitudes ($V_i,\ V_j$); 2) control the transmission line reactance (x_{ij}); or 3) control the bus angle difference across the line ($\theta_i - \theta_j$).

2.2 Power Flow Control Approaches

2.2.1 Power Flow Control Devices

The conventional mechanical switched devices, such as, an air-core series reactor, are one technology for changing the reactance [15, 16]. The advantage of the series reactor is its simple control since it only has two states, i.e., in or out. This characteristic also limits the flexibility. A different distribution load profile may require a different sized reactor. To add control flexibility, the phase shifting transformer (PST) has also been used [17, 18]. The PST has several tap changer set points that are used to vary the phase angle shift of the device [19]. Thus, it can efficiently change the power flow on the transmission line. All the mechanical switched devices share common drawbacks: switching is slow (from several seconds to minutes), frequent electromechanical switching shortens the equipment life and switching actions may cause stress on other equipment or on the system.

With the rapid development of power electronics technology, the appearance of Flexible AC Transmission System (FACTS) in the last two decades provides new opportunities for controlling the power flow. Compared with the conventional power flow control devices, the main difference brought by the FACTS is that the mechanical switching is replaced by power electronics switching [20]. The FACTS devices have two types of switching technology:

- Thyristor controlled switching;
- Power electronic converter based switching using Insulated Gate Bipolar Transistors (IGBT).

The thyristor based controllers have a typical switching speed of a few cycles of the system frequency. The power electronics converter can switch less than one cycle. The dramatic decrease in the switching speed from mechanical to electrical enables the FACTS devices also to be applied for dynamic control of the power system.

Depending on the connection of the devices, there are three types of FACTS:

Shunt Controller

The shunt FACTS controller mainly includes the static Var compensator (SVC) and static synchronous compensator (STATCOM). They are capable of exchanging reactive power with the power grid so that they are usually utilized for voltage regulation rather than power flow control. Moreover, they can also be used to improve the power system transient stability.

Series Controller

A series FACTS controller, such as, TCSC, has the ability to vary the transmission line reactance so it is suitable for power flow control. In addition, since the system oscillations are closely related to the system impedances, the TCSC controller can be designed to provide additional damping to the power system. The static synchronous series compensator (SSSC) is another type of series FACTS. Unlike TCSC, the SSSC uses power electronics converter based switching. It can insert a controlled voltage which is orthogonal to the line current and act as either an inductor or capacitor.

Combined Shunt & Series Controller

The dynamic power flow controller (DPFC) and unified power flow controller (UPFC) combine shunt and series devices. They allow the function of both the series and shunt devices and are able to provide full and fast controllability for the system. The UPFC is a back-to-back implementation of an SSSC unit and a STATCOM unit. The active and reactive power on the line can be controlled independently. However, the high installation cost limits use of the UPFC. The DPFC is a combination of a conventional PST with thyristor switched series capacitors (TSSC) and thyristor switched series reactor (TSSR). The response time of the DPFC is much faster than the PST and it is able to rapidly control the active and reactive power flow through a transmission line.

Fig. 2.2 overviews the conventional power flow control and primary FACTS devices [2].

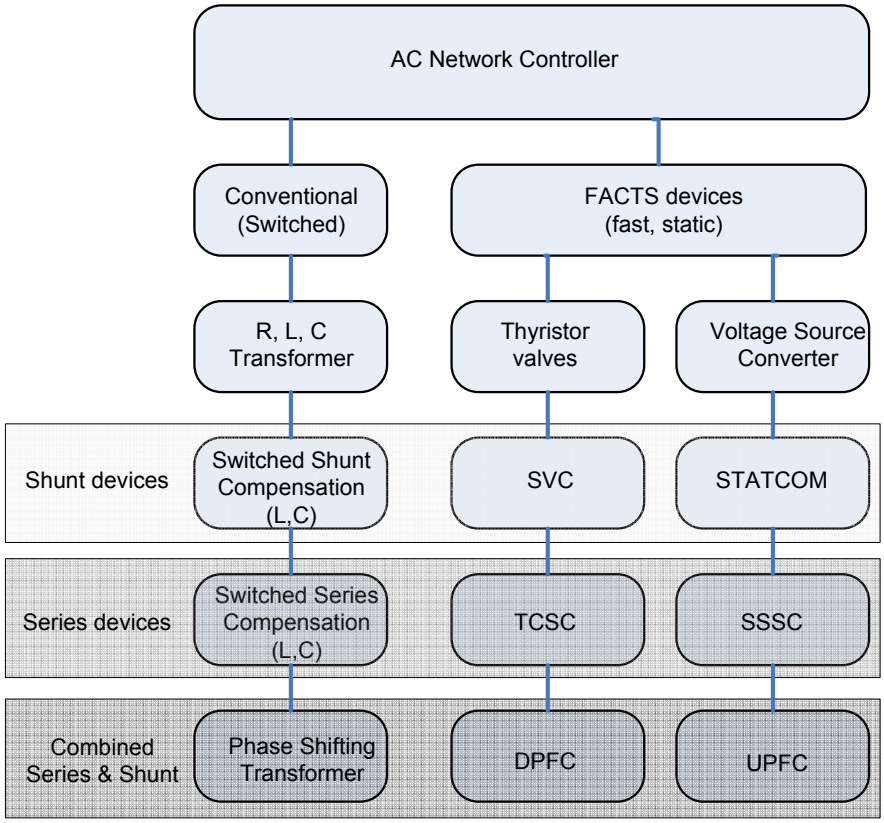

Figure 2.2: Overview of power flow control devices.

2.2.2 Transmission Line Switching

Switching of transmission lines consists of simply switching in and out lines and is another approach to control power flow. While there are obvious limitations to such a strategy in improving capacity utilization, transmission switching (TS) has been extensively studied since around 1980. In [21], TS was introduced to determine the best topology for overload reduction. The work in [22] used corrective switching to mitigate the transmission flow violations. The switching out of the transmission line was modeled by current injections at the line terminals in the base network. The same approach was applied to reduce the system loss in [23]. TS was also employed

to relieve the system violations after contingencies. In [24, 25], TS was embedded in the optimal power flow (OPF) problem to ensure a $N-1$ secure network. The TS algorithm based on a fast decoupled power flow with limited iteration count was discussed in [26] to mitigate both the overload and voltage violations following the contingencies. In [27], the TS served as the corrective action in the day-head security constrained unit commitment (SCUC) to reduce the possible contingency violations. To relieve the computational burden, the greedy algorithm was employed to generate a rank list for the candidate switching transmission lines.

These works demonstrate that TS can be utilized as an additional control action for system security, loss reduction, voltage stability and congestion management. In the market context, TS may provide additional economic benefits [28]. In [29], the operating cost savings by using TS was investigated. This work was extended in [30] to evaluate the changes in locational marginal price (LMP), load payments, congestion cost, generation revenues and flow gate prices introduced by optimal transmission switching. In [31], the security constraints were added to the TS optimization model in [29] to ensure economic savings can be achieved while maintaining an $N-1$ secure network. The objective was to minimize the expected generation cost for the base case and contingencies. In [32], TS was included as part of the SCUC to reduce operating costs. Benders Decomposition was adopted to decompose the optimization problem into one master problem and two subproblems. The master problem was a general unit commitment (UC) problem. The two subproblem included the TS feasibility check and transmission contingency check problems.

2.3 Allocation and Utilization of Power Flow Control Devices

Determining the best locations and settings of FACTS devices in a highly interconnected network is a complex task. Due to the nonlinear and non-convex nature

of the power flow equations, meta-heuristic methods such as genetic algorithm (GA) [33, 34, 35, 36], differential evolution (DE) [37, 38], particle swarm optimization (PSO) [39, 40] have all been proposed to find the optimal placement of FACTS devices. These techniques have the advantage of simple implementation; however, these techniques tend not to scale well and for solutions to be trapped in a local minimum. Beyond the poor scalability, repeatability of solutions prevent practical application for on-line analysis.

Sensitivity approaches are another class of methods for locating FACTS devices. In [41], a reactive power spot price index (QPSI) was developed to determine the best locations of SVC. The QPSI was a weighted index at each bus under different operating conditions, including base case and some critical contingencies. In [42], the optimal locations of TCSC were computed by using the sensitivity of the transfer capability with respect to the line reactance. This method was also used to allocate UPFCs. The work in [43] computed the sensitivity of different objectives, such as, real power flow and real power loss, to line reactance to optimally allocate TCSCs. The settings of TCSCs were determined by using GA. Reference [44] introduced an index called the single contingency sensitivity (SCS) which provided an indicator regarding the effectiveness of a given branch in relieving the congestions under all considered contingencies. After the locations of TCSC were selected based on ranking of SCS, an optimization problem was formulated to get the settings of TCSCs for each contingency.

With rapid advances in mathematical programming algorithms, these methods have garnered renewed interests and have been widely employed to locating FACTS devices. In [45], the power injection models of FACTS devices were proposed to be embedded into the power flow problem. By using the injection models, the original Jacobian matrix need not be modified so various types of FACTS devices can be easily integrated into the power flow equations. Researchers in [46] proposed a two level hybrid PSO/SQP algorithm to allocate SVC and TCSC. The upper level problem used a standard PSO to determine the locations and capacities of the FACTS devices

and the lower level was to determine the settings for normal state and contingencies by SQP. In [47], sequential optimal power flows were used to find optimal placement of TCSC. The approach was based on repeated OPF by varying TCSC locations and settings in a step by step manner. The optimal locations and settings of TCSC were the best results among these OPF results.

In [4], a mixed integer nonlinear programming (MINLP) was proposed to determine locations and settings for a TCSC to enhance the system loadability. Reference [48] proposed a mixed integer linear programming (MILP) model to locate a Thyristor Controlled Phase Shifting Transformer (TCPST). A two stage model was formulated. The objective function for the first stage was to maximize the loadability. In the second stage, the loadability achieved in the first stage was maintained while the objective was changed to minimizing the investment cost. In [49], based on the line flow equation proposed by [50], the locations and settings of TCSC were identified via MILP and MIQP. The same approaches were adopted in [51] and [52] to optimally allocate SVC and UPFC. To eliminate the quadratic terms in the constraints, one variable in the quadratic term was replaced by its hard limit. In addition, the phase angle constraint which is essential in the meshed network was not included in the planning model. Therefore, the planning model under this approach was only suitable for preliminary system design and required verification from a full AC model. The authors in [53] propose a mixed integer conic programming (MICP) to allocate SVC with the objective of reducing the network loss and improving the voltage profile. The load uncertainties are also considered by using a number of scenarios. In [54, 55], benefits of FACTS devices on the economic dispatch (ED) problem was investigated. The bilinear term of the product between the variable reactance and bus voltage angle was linearized by using the big-M method. The nonlinear programming model was reformulated to an MILP model which can be solved by commercial solvers to achieve the global optimums.

The authors in [56] implemented Benders decomposition to find the optimal placement of SVCs considering the base case and contingencies. In order to avoid

local minimum, a multiple restart algorithm was proposed. In [57, 58], Benders Decomposition was used to investigate the benefits of VSR devices in the Security Constrained Optimal Power Flow (SCOPF) problem. The master problem was to minimize the generation cost with the pre-located FACTS devices and the subproblem was used to check the feasibility for each contingency.

2.4 Transmission Expansion Planning

Transmission Expansion Planning (TEP) is a task that determines the best strategy to add new transmission lines to the existing power network in order to satisfy the growth of electricity demand and generation over a specified planning horizon. In the contemporary power system, due to the power market restructuring and massive integration of renewable energy, it is critical to have a rationally planned power system that is not only capable of serving the increasing load reliably and efficiently but also economically [59]. Depending on the model, TEP can be classified as either a single-stage or multi-stage model. For a single-stage TEP, additional lines are planned only for the target planning year; while for the multi-stage TEP, several different planning horizons with distinct load and generation patterns are considered together. Multi-stage TEP not only decides *where* to build the new transmission line, but also determines *when* to build the new line [60, 61].

The modeling and solution techniques for the traditional TEP problem have been studied extensively. Mathematical programming is a major category of the solution methods. At the transmission level, the DC power flow model is capable of providing a good approximation and linear methods can be applied. In [62, 63], the TEP in DC network model was formulated as an MILP problem and solved by a commercial optimization solver. A disjunctive factor was introduced to eliminate the product between continuous and binary variables. Given the non-convex nature of the power system, the exact AC network model for the TEP problem is generally a non-convex MINLP problem. This type of model is challenging for existing commercial solvers.

Therefore, several relaxed or approximated AC models for the TEP problem have been proposed.

In [64, 65], the nonlinear AC power flow equations were linearized around the operating point based on Taylor series to achieve the linear model for the AC TEP. The quadratic constraints, such as, the active and reactive power losses, the MVA limit for the transmission line were approximated by using piecewise linearization. In [66], the lift and project [67] technique was adopted to lift the TEP problem into higher dimensional space and project the relaxed solution onto the original space. In [68], the line flow based power flow equations [50] were employed to give a convex second order cone model for the AC TEP. The voltage magnitude was assumed to be equal to one and the non-convex constraint for the voltage drop across a transmission line was omitted. The AC or relaxed AC TEP models provide a relatively more accurate representation of the network and can include the reactive power planning (RPP) into the TEP problem. However, to the best of the authors' knowledge, the AC TEP models were only applied to small or medium scale systems. Meta-heuristic methods, such as, genetic algorithms [69], greedy randomized search [70], particle swarm optimization [71] and differential evolution [72] have also been proposed to solve the TEP problem. These techniques have the advantage of easy and straightforward implementation; however, they suffer disadvantages of susceptibility to local optimum and slow computational speed for large practical systems.

Major hurdles for construction of new transmission lines are difficulties in obtaining the right-of-way, political resistance, long construction time and limited capital budget. These challenging issues have drawn interest in techniques for delaying upgrades. In [73], transmission switching (TS) was introduced to defer the construction of new transmission lines. Benders Decomposition was employed to solve the planning and operation problem alternately. In [74], the authors evaluated the economic benefits and increased flexibility by including the FACTS devices in the TEP. In [75], a single stage TEP model considering energy storage systems (ESS)

was presented. The total investment cost for the transmission lines can be reduced by appropriately placing the ESS in the system.

Chapter 3

Continuously Variable Series Reactor

In this chapter, the basic configuration and operating principles of the CVSR will be discussed. Lab test results based on a 480 V prototype will be presented. Note that most of the contents in this chapter follow from reference [12] and [76].

3.1 Basic Configuration and Principle of Operation

The concept of using saturation characteristics for circuit control was first introduced in the 1920s [77]. The application of the saturable-core reactor was mainly in the fields of low power electronic circuits, such as, magnetic amplifier [78, 79, 80]. The CVSR adopts the same concept of the magnetic amplifier and takes advantage of the mature and sophisticated technologies of power transformer design along with low voltage/current power electronics. The basic configuration of the CVSR is shown in Fig. 3.1.

The saturation of the power reactor magnetic core is controlled by a DC current source using low power electronics. A change in the DC current will result in the

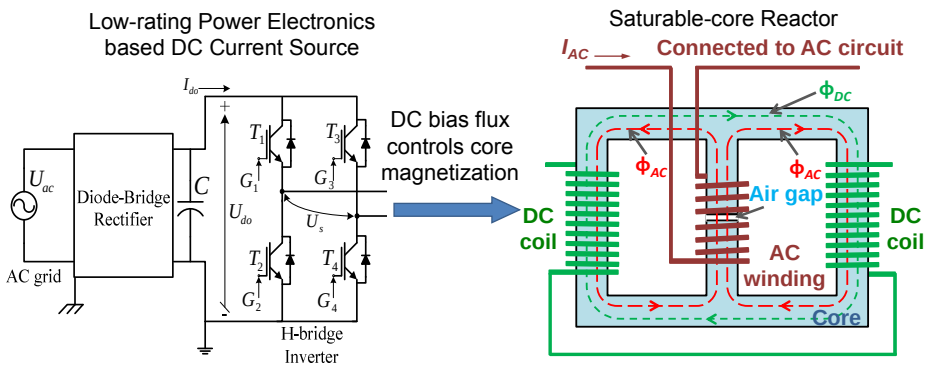

Figure 3.1: Basic configuration of CVSR.

change in the magnetic flux bias which changes the inductance of the AC circuit. Fig. 3.2 depicts a typical B-H curve for the magnetic core. When the magnetic core is deeply saturated (at large enough DC current) for the configuration shown, the minimum inductance is reached and when the core operates with minimal flux (zero DC current) the reactor reaches maximum inductance.

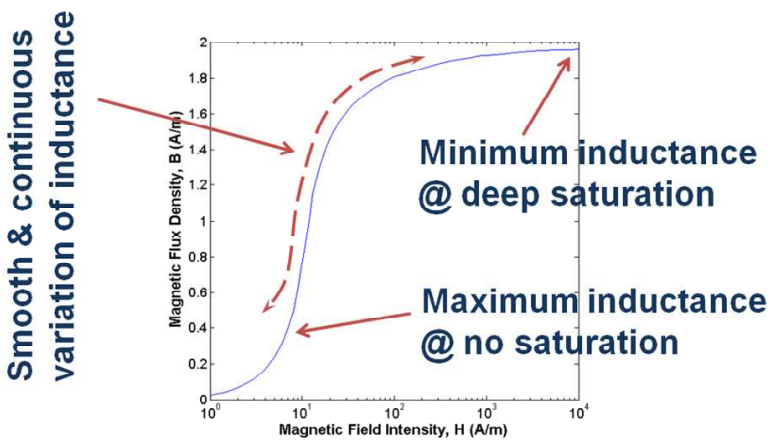

Figure 3.2: Magnetization (B-H) curve of core material (AK H-1 steel).

The full CVSR-based power flow controller design has the following characteristics:

- the device isolates sensitive power electronics from the higher grid voltage and AC currents requiring lower ratings for the power electronics (this is the major difference between the CVSR and the FACTS controller with similar capability);

- the control circuit uses a low power DC source and eliminates the need for extensive cooling;
- the windings and core can be arranged to minimize harmonics injected into power grid; and
- a continuously variable reactance can be achieved by controlling the magnetization of the core.

3.2 Lab Tests and Results

An R&D team led by Oak Ridge National Laboratory (ORNL) in partnership with the University of Tennessee, Knoxville and the SPX/Waukesha Electric Systems, Inc. has developed a three phase prototype device, which is rated at 480 V/200 A. For practical system application, a CVSR rated at 115 kV and 1500 A is undergoing factory testing.

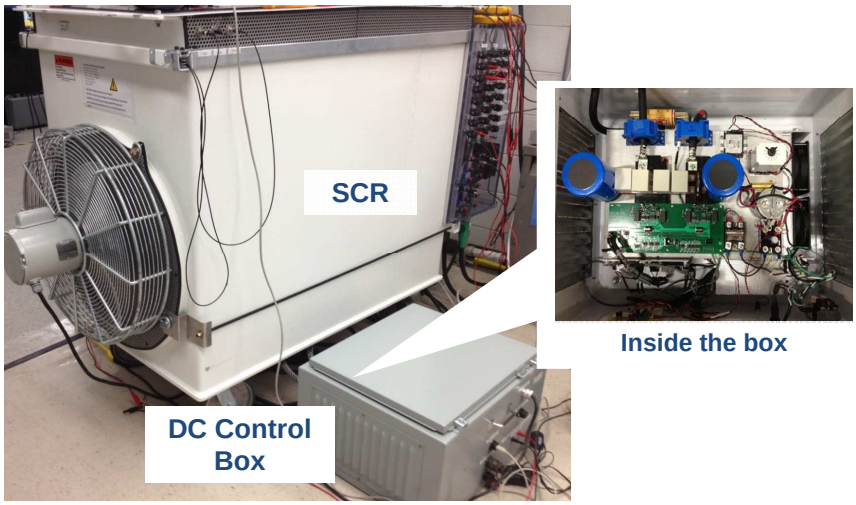

Figure 3.3: Photo of the low voltage CVSR prototype.

Fig. 3.3 shows a photo of the tested CVSR prototype. The reactor is inside the white box and the DC control box has a 600 A/600 V IGBT module based inverter with pulsewidth-modulated (PWM) control. This prototype is installed at

the Distributed Energy Communications and Control (DECC) Laboratory of ORNL. The setup of the prototype testing is given in Fig. 3.4.

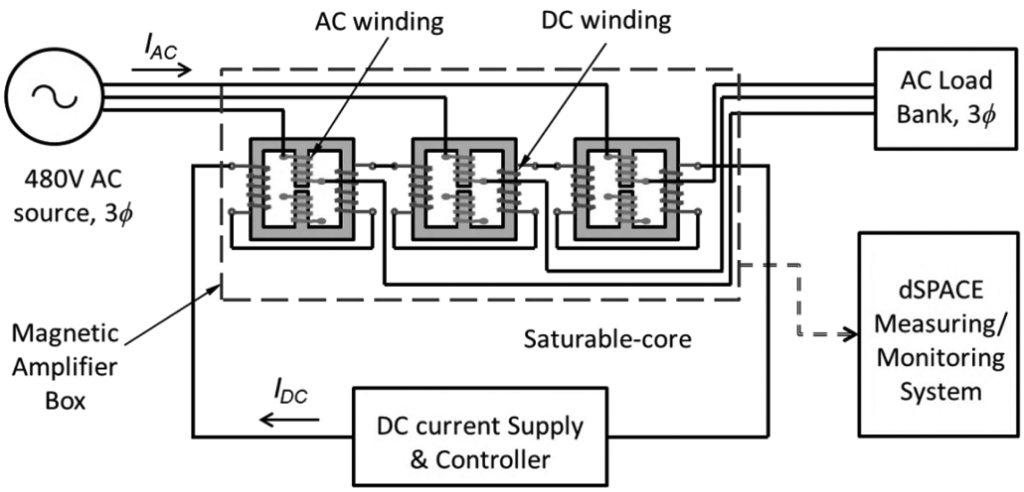

Figure 3.4: Typical setup for lab testing of the prototype CVSR.

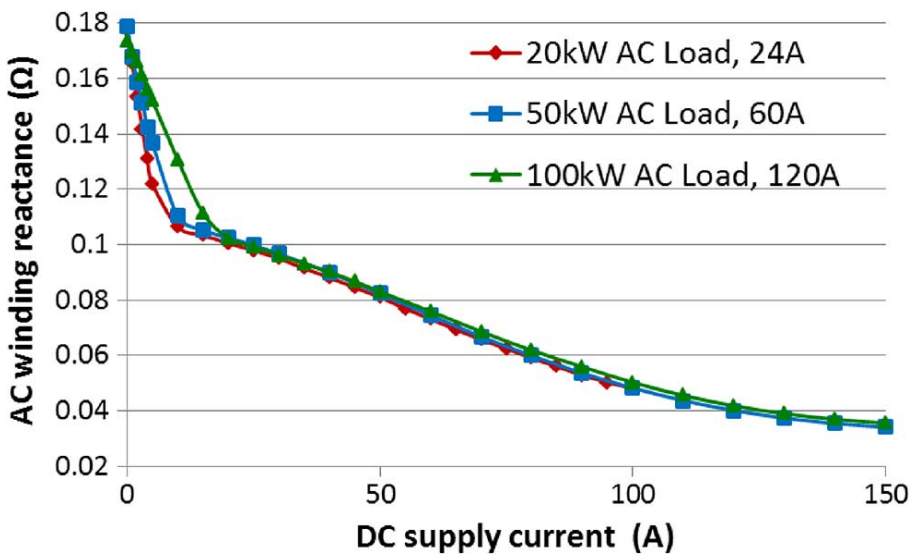

Figure 3.5: CVSR output reactance versus the DC bias current at different AC load levels.

During the testing, the AC load was varied from 20 kW to 100 kW. Fig. 3.5 shows the output reactance of CVSR versus the DC supply current under different AC load levels. It can be seen that when the DC bias current is changed from 0 A to 150

A, the output reactance of the CVSR varies from 0.18 Ω to 0.035 Ω, which is about 6:1 regulation of the reactance. Moreover even when the AC load current is low, the magnetic core is easily saturated. This can be seen from the rapid drop under light loading when the DC current is small. After the DC current is increased above 20 A, the three loading curves overlap with each other, which is due to the deeper saturation of the magnetic core. One drawback of the CVSR is response time, which is about 10 times longer than a TCSC. This has no effect for the static applications but may be limiting, or must be compensated appropriately, in dynamic applications.

Chapter 4

The Application of a Variable Series Reactor to Enhance Power System Loadability

The main contribution of this chapter is to develop an optimization tool for integrating large numbers of the VSRs into a power system to enhance the system loadability and eliminate transmission line congestion. The proposed tool is capable of carrying out both on-line analysis and off-line planning functions. The tool benefits from the maturity of nonlinear programming (NLP) solvers and implements a full AC model as well as a detailed model for different power system components.

The remaining sections of this chapter are organized as follows. In Section 4.1, a static model of VSR in AC power flow is presented. Section 4.2 illustrates the detailed models of the power system components and the optimization model. A short description regarding sequential quadratic programming (SQP) and the flow chart of the developed optimization tool are presented in Section 4.3. In Section 4.4, two IEEE sample systems and a large subsystem of the WECC are selected for the case studies. Finally, the conclusions are given in Section 4.5.

4.1 Static Model of VSR in AC Power Flow

The static model of VSR can be represented by a variable inductive reactance with the parasitic resistance ignored as given in Fig. 4.1. The inserted reactance effectively changes the overall impedance of the branch.

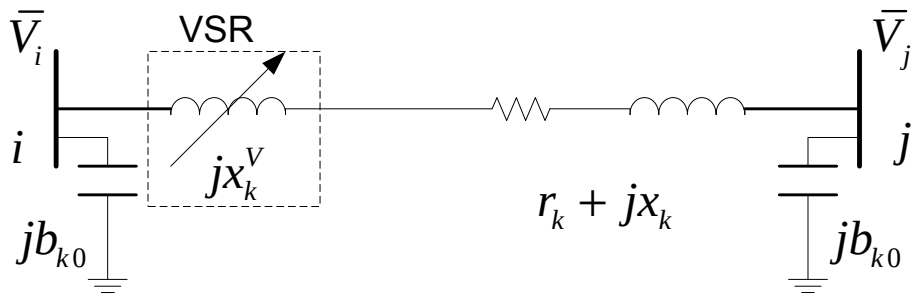

Figure 4.1: Static representation of VSR in AC power flow.

4.2 Optimization Model

4.2.1 Objective Function

The loadability or load margin reflects the percentage of the load that can be increased in the power system without violating system constraints. Generally, loadability can be considered to be associated with the following three issues [56]:

- voltage related limits, including bus voltage magnitude, generator reactive power and stability (collapse point); and
- equipment thermal limits.

Loadability provides useful information about closeness to system limits as a form of a security margin for a given operating condition. The objective function is chosen here as a good proxy for maximizing capacity utilization. Specifically:

$$\max \quad \mu \tag{4.1}$$

4.2.2 Equality Constraints

Transmission Line

Transmission lines are modeled by the standard π model. The overall impedance of the transmission line with VSR is

$$z_{ij} = r_{ij} + j(x_{ij} + x_{ij}^V), \quad (i,j) \in \Omega_V \tag{4.2}$$

The resulting conductance and susceptance are

$$g_{ij} = \frac{r_{ij}}{r_{ij}^2 + (x_{ij} + x_{ij}^V)^2}, \quad (i,j) \in \Omega_V \tag{4.3}$$

$$b_{ij} = -\frac{(x_{ij} + x_{ij}^V)}{r_{ij}^2 + (x_{ij} + x_{ij}^V)^2}, \quad (i,j) \in \Omega_V \tag{4.4}$$

Define $\boldsymbol{y} = [\boldsymbol{\theta}\ \boldsymbol{V}\ \boldsymbol{x^V}]^T$. The active and reactive power flows from bus i to bus j are

$$P_{ij}(\boldsymbol{y}) = g_{ij}V_i^2 - V_iV_j(g_{ij}\cos(\theta_i - \theta_j) + b_{ij}\sin(\theta_i - \theta_j)),\ (i,j) \in \Omega_L \tag{4.5}$$

$$Q_{ij}(\boldsymbol{y}) = -V_i^2(b_{ij0} + b_{ij}) - V_iV_j(g_{ij}\sin(\theta_i - \theta_j) - b_{ij}\cos(\theta_i - \theta_j)),\ (i,j) \in \Omega_L \tag{4.6}$$

Transformer

The transformer is located at the $from$ end of the branch. Taking the leakage inductance and conductance into consideration, the active and reactive power flows

from bus i to bus j are

$$
\begin{aligned}
P_{ij}(\boldsymbol{y}) =& (g_{ij} + g_{ij}^{Mag})\frac{V_i^2}{\tau_{ij}^2} - \frac{V_i V_j}{\tau_{ij}}(g_{ij}\cos(\theta_i - \theta_j - \theta_{ij}^{shift}) \\
&+ b_{ij}\sin(\theta_i - \theta_j - \theta_{ij}^{shift})), \qquad (i,j) \in \Omega_T \qquad (4.7) \\
Q_{ij}(\boldsymbol{y}) =& -\frac{V_i^2}{\tau_{ij}^2}(b_{ij0} + b_{ij} + b_{ij}^{Mag}) \\
&- \frac{V_i V_j}{\tau_{ij}}(g_{ij}\sin(\theta_i - \theta_j - \theta_{ij}^{shift}) \\
&- b_{ij}\cos(\theta_i - \theta_j - \theta_{ij}^{shift})), \qquad (i,j) \in \Omega_T \qquad (4.8)
\end{aligned}
$$

For the same branch, the active and reactive power flow from bus j to bus i are

$$
\begin{aligned}
P_{ji}(\boldsymbol{y}) =& g_{ij}V_j^2 - \frac{V_i V_j}{\tau_{ij}}(g_{ij}\cos(\theta_j - \theta_i + \theta_{ij}^{shift}) \\
&+ b_{ij}\sin(\theta_j - \theta_i + \theta_{ij}^{shift})), \qquad (i,j) \in \Omega_T \qquad (4.9) \\
Q_{ji}(\boldsymbol{y}) =& -V_j^2(b_{ij0} + b_{ij}) - \frac{V_i V_j}{\tau_{ij}}(g_{ij}\sin(\theta_j - \theta_i + \theta_{ij}^{shift}) \\
&- b_{ij}\cos(\theta_j - \theta_i + \theta_{ij}^{shift})), \qquad (i,j) \in \Omega_T \qquad (4.10)
\end{aligned}
$$

Power Flow Equations

The active and reactive power balance at each bus are given by

$$
P_i^g - \mu \cdot P_i^d - g_i V_i^2 = \sum_{j \in \mathcal{B}_i} P_{ij}(\boldsymbol{y}), \quad i \in \mathcal{B} \qquad (4.11)
$$

$$
Q_i^g - \mu \cdot Q_i^d + b_i V_i^2 = \sum_{j \in \mathcal{B}_i} Q_{ij}(\boldsymbol{y}), \quad i \in \mathcal{B} \qquad (4.12)
$$

where

$$P_i^g = \sum_{n \in \mathcal{G}_i} P_n^g, \quad i \in \mathcal{B} \tag{4.13}$$

$$Q_i^g = \sum_{n \in \mathcal{G}_i} Q_n^g, \quad i \in \mathcal{B} \tag{4.14}$$

$$P_i^d = \sum_{m \in \mathcal{D}_i} P_m^d, \quad i \in \mathcal{B} \tag{4.15}$$

$$Q_i^d = \sum_{m \in \mathcal{D}_i} Q_d^d, \quad i \in \mathcal{B} \tag{4.16}$$

4.2.3 Inequality Constraints

Physical Limits

Bus voltage magnitudes must be within their operating limits to ensure the voltage stability [81, 82, 83, 84]:

$$V_i^{\min} \leq V_i \leq V_i^{\max}, \quad i \in \mathcal{B} \tag{4.17}$$

The power generation is limited by the capacity of the generators

$$P_n^{g,\min} \leq P_n^g \leq P_n^{g,\max}, \quad n \in \mathcal{G} \tag{4.18}$$

$$Q_n^{g,\min} \leq Q_n^g \leq Q_n^{g,\max}, \quad n \in \mathcal{G} \tag{4.19}$$

Based on the ratings, the output reactance of VSR should be within their operating limits

$$x_{ij}^{V,\min} \leq x_{ij}^V \leq x_{ij}^{V,\max}, \quad (i,j) \in \Omega_V \tag{4.20}$$

The power flow through all the branches in the network should not exceed the thermal limits

$$\sqrt{P_{ij}^2(\boldsymbol{y}) + Q_{ij}^2(\boldsymbol{y})} \leq S_{ij}^{\max}, \quad (i,j) \in \Omega_L \cup \Omega_T \tag{4.21}$$

Total Reactance Limit

In order to limit the number of VSRs that can be installed in the system, the following constraint is introduced:

$$\sum x_{ij}^{V} \leq k_f \sum x_{ij}^{V,\max}, \quad (i,j) \in \Omega_V \tag{4.22}$$

When $k_f = 0$, no VSR is allowed to be installed in the system; whereas if $k_f = 1$, the number of VSRs that can be installed in the system is equal to the number of candidate locations. By varying k_f, the amount of reactance inserted by the VSRs is changed, which effectively controls the maximum number of VSRs in the system.

4.3 Optimization Methodology

4.3.1 Algorithm

The full optimization model is solved by using sequential quadratic programming (SQP) [85], which is effective in dealing with this constrained optimization problem. This technique combines the advantages of the Newton method with standard quadratic programming (QP). In each major iteration of SQP, one corresponding sub-QP problem is solved to obtain the search direction of the optimization variable and the new value of Lagrangian multiplier for the next iteration. At each iteration k, the objective function of the sub-QP problem is approximately formulated by its second-order Taylor expansion and the equality and inequality constraints are linearized by their first-order Taylor expansion at a regular point $\boldsymbol{w^k}$. In general, the nonlinear constrained optimization problem can be written as:

$$\begin{aligned} \textbf{minimize} \quad & f(\boldsymbol{w}) \\ \textbf{subject to} \quad & \boldsymbol{g}(\boldsymbol{w}) = 0 \\ & \boldsymbol{h}(\boldsymbol{w}) \leq 0 \end{aligned} \tag{4.23}$$

The Lagrangian of the problem is given by:

$$\mathcal{L}(\boldsymbol{w}, \boldsymbol{\lambda}, \boldsymbol{\beta}) = f(\boldsymbol{w}) + \boldsymbol{\lambda}^T \boldsymbol{g}(\boldsymbol{w}) + \boldsymbol{\beta}^T \boldsymbol{h}(\boldsymbol{w}) \tag{4.24}$$

The QP subproblem at iteration k can be formulated as:

$$\begin{aligned} \textbf{minimize} \quad & \nabla \boldsymbol{f}(\boldsymbol{w^k})^T \Delta \boldsymbol{w} + \frac{1}{2} \Delta \boldsymbol{w}^T \boldsymbol{W^k} \Delta \boldsymbol{w} \\ \textbf{subject to} \quad & \boldsymbol{g}(\boldsymbol{w^k}) + \nabla \boldsymbol{g}(\boldsymbol{w^k})^T \Delta \boldsymbol{w} = 0 \\ & \boldsymbol{h}(\boldsymbol{w^k}) + \nabla \boldsymbol{h}(\boldsymbol{w^k})^T \Delta \boldsymbol{w} \leq 0 \end{aligned} \tag{4.25}$$

where $\boldsymbol{W^k}$ is the Hessian of the Lagrangian at iteration k:

$$\boldsymbol{W^k} = \nabla^2 \mathcal{L}(\boldsymbol{w^k}, \boldsymbol{\lambda^k}, \boldsymbol{\beta^k}) \tag{4.26}$$

In practice, the Hessian matrix of the Lagrangian need not to be calculated at each iteration; instead, it is approximated and updated by using the quasi-Newton method [86]. The modified Jacobian matrix of the power balance equations are given in the Appendix.

4.3.2 Flow Chart of the Optimization Tool

A complete framework of the proposed optimization tool is described in Fig. 4.2. The candidate VSR locations can be selected based on voltage level, physical installation limitations, or other concerns. Depending on the application, the tool has several different objective functions available, including maximizing load margin, minimizing loss, and minimizing generation cost. The default objective function is to maximize load margin.

In a practical power system, the system operators focus on ensuring no overloads after outages and meeting other operational standards. Determining the maximum loadability under an outage condition with the power flow control device is more

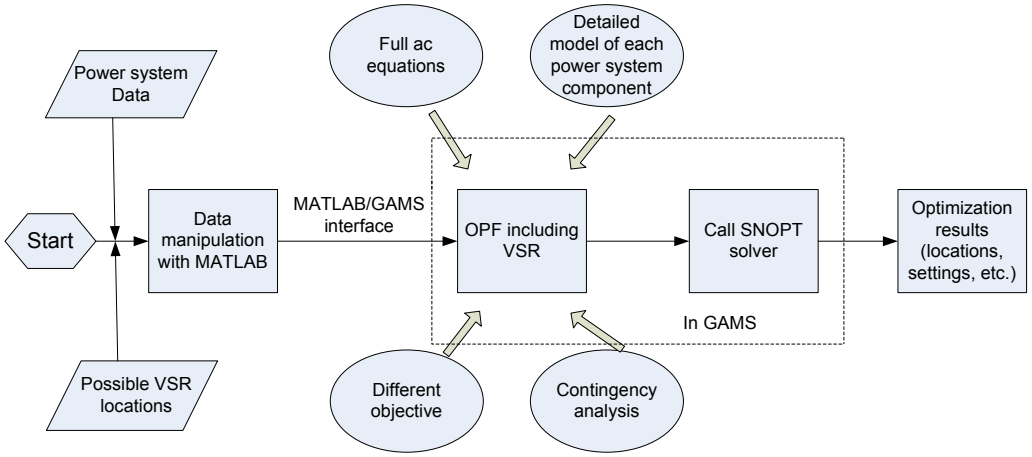

Figure 4.2: Flow chart of the optimization tool.

important than under no outage conditions. Hence, the contingency analysis is included in the optimization. It should be noted that the formulation in this chapter mainly shows that installing several VSRs into the power system can reduce the congestion and possible load shedding after a specific contingency. The issue with respect to determining the VSRs locations when considering a series of contingencies together will be addressed in Chapter 5.

4.4 Case Studies

The proposed optimization tool is applied to the IEEE 30-bus, 2736-bus power systems and a subsystem of the WECC. The data for the IEEE sample systems are from MATPOWER software [87]. The computer used for simulations has an Inter Core(TM) i5-2400M CPU @ 2.30 GHz with 4.00 GB of RAM. The developed tool makes use of the NLP solver SNOPT (Large Scale SQP) [86] under GAMS [88].

The Continuously Variable Series Reactor (CVSR) is selected for the case studies. The modulation percentage of CVSR is allowed to vary from 0% to 20% of its corresponding branch reactance.

$$0 \leq x_{ij}^{V} \leq 0.2x_{ij}, \quad (i,j) \in \Omega_V \tag{4.27}$$

4.4.1 IEEE Sample Systems

A description of IEEE 30-bus and 2736-bus systems are given in Table 4.1. For the IEEE sample systems, we mainly focus on the off-line planning function of the optimization. It is assumed that every branch except the transformer branches are candidate locations to install the CVSR.

Table 4.1: Specifications of IEEE Sample Systems and Model Scales

Systems	30- bus system	2736- bus system
Number of branches	41	3,504
Total active load (MW)	354.25	18,075
Max active power generation (MW)	485	20,247
Total reactive load (MVar)	126.2	5,339.5
Max reactive power generation (MVar)	188	11,450
Number of variables	109	9,642
Equality constraints	61	5,473
Inequality constraints	256	22,787

4.4.2 Initialization

Given that the full optimization model is a non-convex problem, a general NLP solver cannot guarantee the solution will be globally optimal. As one way to evaluate the solutions, we consider both "hot-start" and "cold-start" initializations to investigate possible problems with local minima. This also provides some insight on the time savings with different initializations when multiple optimization problems are run by a planner under similar conditions. In the hot start model, a solved ac power flow base point is available. This model is often used in the applications where the network topology is relatively stable, such as, LMP-based market calculations or real-time security constrained economic dispatch (SCED). In the cold-start model, no reliably

solved ac base case is assumed available. The cold start model is typically used in long term planning studies [89, 90].

4.4.3 IEEE System Results

Fig. 4.3 shows the variation of system loadability versus k_f. It is clear that the system loadability increases as more reactance is allowed to be installed into the system. However, the system loadability tends to level off as k_f increases which indicates that most of the improvement in system loadability arises from the first few devices located along critical paths. It should be also noted that by setting $k_f = 1$ in constraint (4.22), the algorithm ends up with a large number of CVSR locations since no penalty is given to the total inserted reactance.

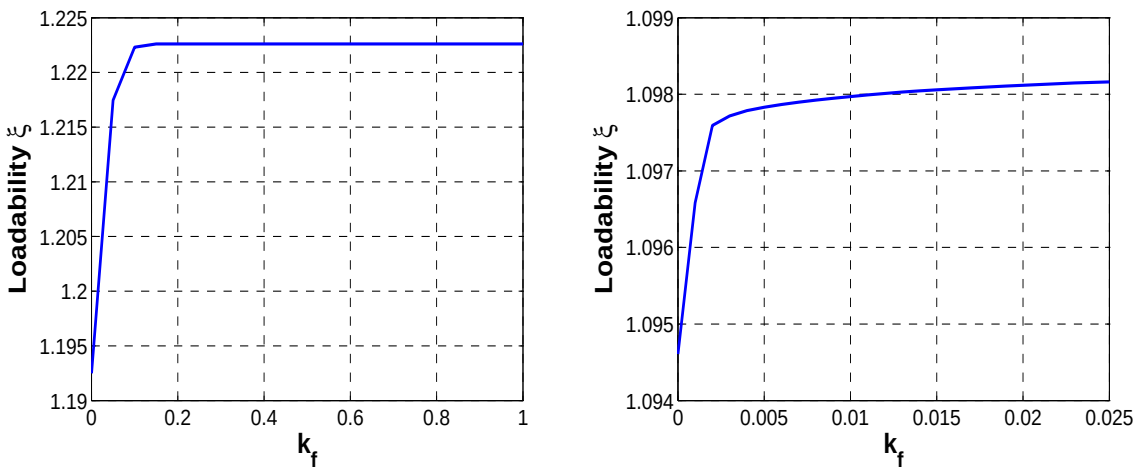

(a) IEEE 30-bus **(b)** IEEE 2736-bus

Figure 4.3: System loadability versus k_f

Table 4.2 and 4.3 show the CVSR placement for the two sample systems with different starting points. Note μ_0 is the maximum loadability that the system can achieve without any CVSR; μ^* is the maximum loadability for the system when k_f in constraint (4.22) is equal to 1, i.e., maximum possible loadability the system can achieve. It can be seen that there is some room for improving the system loadability

without CVSR, which is mainly due to the generation rescheduling. In the IEEE 30-bus system, the system loadability increases by 21.8% with 3 CVSRs. This accounts for 83.3% of the total improvement. When 6 CVSRs are installed into the system, 96.7% of the total improvement can be achieved. For the IEEE 2736-bus system, 50% of the total improvement can be gained by 3 CVSRs and 75% of the enhancement can be achieved by 7 CVSRs.

Table 4.2: CVSR Placement of IEEE 30-Bus System With Different Starting Points

k_f	Start point	Branch #	Time (s)	μ	μ_0	μ^*
0.05	Hot start	1,3,6	0.015	1.218	1.193	1.223
	Cold start	1,3,6	0.015	1.218	1.193	1.223
0.1	Hot start	1,3,5,6 18,35	0.031	1.222	1.193	1.223
	Cold start	1,3,5,6 18,35	0.031	1.222	1.193	1.223

Table 4.3: CVSR Placement of IEEE 2736-Bus System With Different Starting Points

k_f	Start point	Branch #	Time (s)	μ	μ_0	μ^*
$1e^{-3}$	Hot start	394,2238,2252	32.73	1.0966	1.0946	1.0985
	Cold start	394,2238,2252	54.90	1.0966	1.0946	1.0985
$2e^{-3}$	Hot start	99,394,1079 1818,1819 2238,2252	43.82	1.0976	1.0946	1.0985
	Cold start	99,394,1079 1818,1819 2238,2252	79.51	1.0976	1.0946	1.0985

For both the hot start and the cold start, the optimization tool gives the same maximum loadability as well as the placement strategies for the CVSR. The computation times vary for different starting points, especially for the larger system with, as expected, the hot start converging faster.

4.4.4 Practical Application

The proposed optimization tool is applied to a portion of the WECC system in the Northwest area.

Network Description

The power network model for the Northwest area contains 4016 nodes and about 4700 branches. The overall power transfer direction is from North to South since the Northwest system delivers a large amount of power to California via the California Oregon Intertie (COI) and the DC tie. According to [91], the COI is usually not fully utilized at its capacity (4800 MW) due to various system constraints. The optimization task here is to maximize the power transferred on the COI by appropriately installing several CVSRs in the Northwest power network.

Modification of Optimization Model

The bus "Malin" and "Captain Jack" in the Northwest system are the starting buses of the COI [91], these two buses are denoted as the load center buses. We use the built in "equivalencing" function in PowerWorld [92] to make the active and reactive power transferred on the COI equivalent to two constant loads located at these buses. In order to maximize the loadability associated with the the load center buses, the power balance equations (4.11) and (4.12) should be modified as below:

$$P_i^g - \mu \cdot P_i^d - g_i V_i^2 = \sum_{j \in \mathcal{B}_i} P_{ij}, \quad i \in \mathcal{B}_{COI} \tag{4.28}$$

$$Q_i^g - \mu \cdot Q_i^d + b_i V_i^2 = \sum_{j \in \mathcal{B}_i} Q_{ij}, \quad i \in \mathcal{B}_{COI} \tag{4.29}$$

$$P_i^g - P_i^d - g_i V_i^2 = \sum_{j \in \mathcal{B}_i} P_{ij}, \quad i \in \mathcal{B}_{NCOI} \tag{4.30}$$

$$Q_i^g - Q_i^d + b_i V_i^2 = \sum_{j \in \mathcal{B}_i} Q_{ij}, \quad i \in \mathcal{B}_{NCOI} \tag{4.31}$$

The voltage magnitudes of generator buses with voltage control should be fixed at their regulated values. To prevent the numerical difficulties introduced by a strict equality, we allow the controlled bus voltage to vary within a small range. Constraint (4.17) is modified as:

$$\max\{0.97V_i^{reg}, V_i^{\min}\} \leq V_i \leq \min\{1.03V_i^{reg}, V_i^{\max}\}, \quad i \in \mathcal{B}_{reg} \tag{4.32}$$

$$V_i^{\min} \leq V_i \leq V_i^{\max}, \qquad i \in \mathcal{B}_{ureg} \tag{4.33}$$

A practical power system subjected to a certain contingency often requires generator rescheduling. However, not all generators can participate in the rescheduling process. The rescheduling generators usually have higher ramp rate and serve no base load [59]. In the Northwest US power system, only 20% of the total number of generators are allowed to reschedule, the generation of the other generators are fixed to their pre-scheduled values. To demonstrate some limited possibility of rescheduling in coordination with the CVSRs, the constraint (4.18) and (4.19) are modified as:

$$P_n^{g,\min} \leq P_n^g \leq P_n^{g,\max}, \quad n \in \mathcal{G}_{re} \tag{4.34}$$

$$Q_n^{g,\min} \leq Q_n^g \leq Q_n^{g,\max}, \quad n \in \mathcal{G}_{re} \tag{4.35}$$

$$P_n^g = P_n^{g,sch}, \qquad n \in \mathcal{G}_{fix} \tag{4.36}$$

$$Q_n^g = Q_{gn}^{g,sch}, \qquad n \in \mathcal{G}_{fix} \tag{4.37}$$

Based on a prototype device that is planned to be installed, we assume that the only CVSRs rated at 115 kV can be installed into the system. The maximum output reactance of this 115 kV CVSR is around 5.2 Ω, which corresponds to 0.0393 p.u. Constraint (4.20) is modified as:

$$0 \leq x_{ij}^V \leq 0.0393\ p.u., \quad (i,j) \in \Omega_V \tag{4.38}$$

Off-line Planning

We analyze 94 possible contingencies in the Northwest network. In this dissertation, the results of three worst contingencies for this planning case are presented.

- Contingency 1: Loss of a 500 kV transmission line from north to south.
- Contingency 2: Loss of two 230 kV transmission lines from north to south.
- Contingency 3: Loss of two 500 kV transmission lines from north to south.

For contingency 1 and contingency 3, 637 115 kV transmission lines owned by two utilities in the Northwest are considered as possible locations to install CVSR. Three more utilities with another 475 115 kV lines participate in contingency 2, so the number of possible branches to install CVSR is 1112. We consider two types of a hot start as the starting points. In hot start I, the starting point is from the load flow solution of the base case. The starting point for hot start II is the load flow solution of the post contingency system. In these simulation cases, we allow the maximum reactance inserted in the system to be $5x_{ij}^{V,\max} = 0.1965\ p.u.$

Table 4.4 lists the placement strategies of the CVSR with different initialization. It can be seen that most of the CVSR locations are the same when using different starting points. The difference is due to the large and relatively "flat" optimization space. That is at the margin where a slight improvement if the objective is obtained, many different locations of CVSR are similar. However, the key locations which are essential in enhancing the system loadability always remain the same. The computation time provides similar information as the sample systems. The model with cold start can require as much as 10 times the computations of the hot start model. For contingency 1, about 15% of the power cannot be transferred to California by just rescheduling. With the installation of 10 CVSRs, the amount of unserved power reduces to 4.5%. In contingency 2, there is 3.4% power curtailment on the COI with only rescheduling. By installing 8 CVSRs, no power curtailment is needed. Moreover, there is even some room for increasing the power on the COI. Similar

results are obtained for contingency 3. Thus, the better utilization of the COI can be achieved by installing several CVSRs.

Table 4.4: CVSR Placement of Northwest System With Different Starting Points

Cont.	Start point	Branch #	Time (s)	ξ	ξ_0	ξ^*
1	Hot start I	576,577,779,1177,2721 2941,3009,3033,3103,4127	63.6	0.9553	0.8509	0.9740
	Hot start II	576,577,779,1177,2721 2941,3009,3033,3103,4127	57.0	0.9553	0.8509	0.9718
	Cold start	576,577,779,1177,2721,2797 2941,3009,3033,3034,3103,4127	116.4	0.9552	0.8509	0.9700
2	Hot start I	593,599,844,2819 2858,2884,3176,3583	43.8	1.1012	0.9661	1.1060
	Hot start II	593,599,844,2819 2858,2884,3176,3583	58.0	1.1012	0.9661	1.1055
	Cold start	203,593,599,844 926,2665,2858,3176	290.2	1.1013	0.9661	1.1062
3	Hot start I	63,389,719,844,1298 2497,2667,2858,3009,3176	44.9	1.0085	0.8491	1.0159
	Hot start II	389,719,844,1298 2497,2858,3009,3176	51.7	1.0085	0.8491	1.0156
	Cold start	63,389,719,844,1298 2496,2497,2858,3009,3176	473.9	1.0084	0.8491	1.0162

On-line Analysis

To consider the on-line analysis function of the optimization tool, we fix the CVSR locations to 4 branches: 2497, 2819, 2941, 3009. This is based on both the planning study in the above section and the suggestions of the utility engineer. In addition, there is no limit on the total reactance inserted into the system, i.e., constraint (4.22) is removed. We use both types of the hot start as the starting points, which would be available from the Energy Management System (EMS). Both starting points give exactly the same solution with a similar computation time. The results of the model by using hot start I are reported here. Table 4.5 shows the CVSR parameter settings, computation time and loadability for each contingency. It can be seen that

the loadability for contingency 1 and 2 improves a lot with just 3 and 2 CVSRs respectively. For the contingency 3 with the least improvement, there is still about 2.5% increase of power available on the COI. The computation time is fast enough for utilities to do the on-line scheduling following a contingency.

Table 4.5: CVSR Settings for Different Contingencies

Cont.	x_{CVSR} $(p.u.)$				Time (s)	ξ
	2497	2819	2941	3009		
1	0	0.0393	0.0393	0.0063	37.02	0.9477
2	0	0.0393	0	0.0277	25.12	1.0942
3	0.0393	0.0393	0	0.0393	30.61	0.8741

In Table 4.6, the thermal burdens on the main transmission paths from North to South following contingency 1 are given. Due to the loss of the 500 kV transmission line from North to South, the other paths need to share the power which is initially transferred by the outage line before the contingency. Thus, it can be seen that the thermal burdens for all the paths are increasing after the contingency and branch 3009 and 2246 are congested. With only rescheduling, the congestion can be eliminated but the power transferred to the south should be reduced, which can be seen by the decreasing thermal loading for the transmission paths when no CVSR is in the system. This also explains the low loadability obtained by the system without any CVSR. The installation of the CVSR can redistribute the power flow and push more power from North to South through paths which still have transfer capability. In this case, except for the fully loaded branch 3009, all the other main paths from North to South will have the loading increase. Thus, the loadability is enhanced and more power can be transferred to the COI.

4.5 Conclusion

In this chapter, an optimization is developed for finding the locations and settings of VSR assuming numerous devices that could be installed due to their low cost. The

Table 4.6: Thermal Loading of the Main Transmission Paths From North to South in Contingency 1

Voltage level	115 kV		230 kV			500 kV
Branch #	2456	3009	842	2246	2415	78
Before Cont.	62.6%	86.3%	30.2%	73.1%	65.9%	38.8%
After Cont.	84.7%	107%	55.4%	104%	94.8%	60.3%
Without CVSR	78.1%	100%	47.2%	95.9%	88.3%	54.0%
With CVSR	80.9%	100%	50.5%	99.3%	91.7%	57.3%

optimization benefits from the maturity of the SQP algorithm and the formulation is applicable for both off-line planning and on-line analysis functions. Taking two IEEE sample systems and a subsystem of the WECC as test systems, the simulation results show that the system loadability and maximum power transfer capability can be significantly improved by several well located VSRs. The high computational efficiency and accuracy of the optimization tool enable its direct application for large systems analysis.

Chapter 5

Transfer Capability Improvement with a Variable Series Reactor

This chapter addresses the optimal placement of VSR in a transmission network in order to maximize the load margin while considering a multi-scenario framework including base case and contingencies. The optimization model begins with a MINLP model. The MINLP model, especially for those with non-convex constraints, are quite difficult to solve by the existing MINLP solvers. Even if the MINLP model is solvable, the solution is not guaranteed to be global optimal or the size of the model can be quite limited. A reformulation technique is proposed to transform the original MINLP model into an MILP model so that the model is computationally tractable for large scale systems.

The contributions of this chapter are summarized as below:

- A reformulation technique is proposed to transform the MINLP model into MILP model that ensures the global optimality.
- An efficient planning/operation tool is proposed to allocate VSR with diverse scenarios across a base case and critical contingencies.

- The detailed numerical simulation results considering IEEE sample test systems and a practical Northwest US power network establish the performance of the proposed technique.

The remaining sections are organized as follows. In Section 5.1, the static model of VSR in DC power flow is presented. Section 5.2 illustrates details about the optimization model and the reformulation technique. The description of the optimization tool is given in Section 5.3. In Section 5.4, two IEEE sample systems and a Northwest US power network are selected for the case studies. Finally, the conclusions are given in Section 5.5.

5.1 Static Model of VSR in DC power flow

The static model of VSR in DC power flow can be represented by an variable inductive reactance with the parasitic resistance ignored as given in Fig. 5.1.

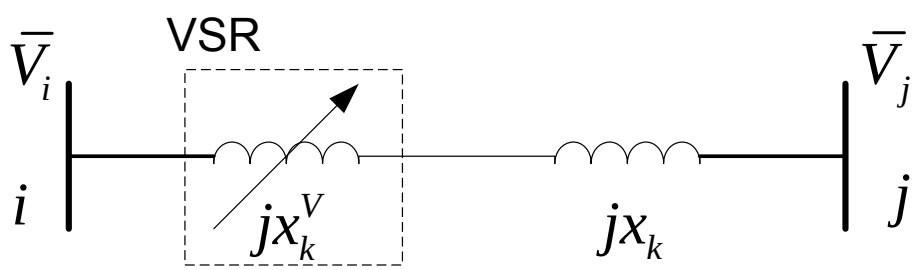

Figure 5.1: Static representation of VSR in DCPF.

The total susceptance of the transmission line can be represented as:

$$b'_k = -\frac{1}{x_k + x_k^V} = -(b_k + b_k^V) \tag{5.1}$$

where

$$b_k = \frac{1}{x_k} \tag{5.2}$$

$$b_k^V = -\frac{x_k^V}{x_k(x_k + x_k^V)} \tag{5.3}$$

The active power flow on the line installed with VSR can be expressed as:

$$P_k = (b_k + b_k^V) \cdot \theta_k \tag{5.4}$$

$$b_{k,V}^{\min} \leq b_k^V \leq b_{k,V}^{\max} \tag{5.5}$$

5.2 Reformulation Technique

5.2.1 Classical Formulation

This optimization problem can be directly formulated as an MINLP model.

Objective Function

The loadability factor (load margin) is an indicator of the load that can be increased in the power system without violating system constraints. It provides useful information about the security margin under a given operating condition. When the loadability factor is only applied to a specific load center, it could also be interpreted as the available transfer capability (ATC). The objective function employed in this paper is to maximize the loadability:

$$\max \quad \mu \tag{5.6}$$

Constraints

The complete constraints of the MINLP model are:

$$P_k = b_{k0}\theta_k, \quad k \in \Omega_L \backslash \Omega_V \tag{5.7}$$

$$P_k = (b_{k0} + \delta_k b_k^V)\theta_k, \quad k \in \Omega_V \tag{5.8}$$

$$P_i^g - \mu \cdot P_i^d = \sum_{k \in \Omega_L^i} P_k, \quad i \in \mathcal{B} \tag{5.9}$$

$$P_i^g = \sum_{n \in \mathcal{G}_i} P_n^g, \quad i \in \mathcal{B} \tag{5.10}$$

$$P_i^d = \sum_{m \in \mathcal{D}_i} P_m^d, \quad i \in \mathcal{B} \tag{5.11}$$

$$-S_k^{\max} \leq P_k \leq S_k^{\max}, \quad k \in \Omega_L \tag{5.12}$$

$$P_n^{g,\min} \leq P_n^g \leq P_n^{g,\max}, \quad n \in \mathcal{G} \tag{5.13}$$

$$b_{k,V}^{\min} \leq b_k^V \leq b_{k,V}^{\max}, \quad k \in \Omega_V \tag{5.14}$$

$$\sum_{k \in \Omega_V} \delta_k \leq N_V, \quad k \in \Omega_V \tag{5.15}$$

The constraints (5.7)-(5.8) denote the active power flow on normal transmission lines and transmission lines installed with VSRs respectively. A binary variable δ_k is introduced in (5.8) to define the location of VSR, i.e., if $\delta_k = 1$, a VSR is placed on line k. The constraint (5.9) represents the power balance at each bus and (5.10)-(5.11) provide the power injection and consumption at each bus. The physical limits of the system are denoted by the constraints (5.12)-(5.14). The constraint (5.15) is used to limit the number of VSRs.

5.2.2 Reformulation

It can be seen that the only nonlinearity lies in the trilinear term $\delta_k b_k^V \theta_k$ from (5.8). To eliminate the nonlinearity, we introduce a new variable w_k which is defined as:

$$w_k = \delta_k b_k^V \theta_k, \quad k \in \Omega_V \tag{5.16}$$

The constraint (5.8) is the modified to:

$$P_k = b_k \theta_k + w_k, \quad k \in \Omega_V \tag{5.17}$$

We multiply each side of the constraint (5.14) with δ_k and combine with (5.16) to yield:

$$\delta_k b_{k,V}^{\min} \leq \frac{w_k}{\theta_k} = \delta_k b_k^V \leq \delta_k b_{k,V}^{\max}, \quad k \in \Omega_V \tag{5.18}$$

Depending on the sign of θ_k, the inequality (5.18) can be written as:

$$\begin{cases} \delta_k \theta_k b_{k,V}^{\min} \leq w_k \leq \delta_k \theta_k b_{k,V}^{\max}, \text{ if } \theta_k > 0 \\ w_k = 0, \qquad\qquad\qquad\qquad \text{ if } \theta_k = 0 \\ \delta_k \theta_k b_{k,V}^{\max} \leq w_k \leq \delta_k \theta_k b_{k,V}^{\min}, \text{ if } \theta_k < 0 \end{cases} \tag{5.19}$$

The "if" constraints can be formulated by introducing an additional binary variable y_k and the big-M complementary constraints [55, 93]:

$$-M_k y_k + \delta_k \theta_k b_{k,V}^{\min} \leq w_k \leq \delta_k \theta_k b_{k,V}^{\max} + M_k y_k, \; k \in \Omega_V \tag{5.20}$$

$$-M_k(1 - y_k) + \delta_k \theta_k b_{k,V}^{\max} \leq w_k \leq \delta_k \theta_k b_{k,V}^{\min} + M_k(1 - y_k), \; k \in \Omega_V \tag{5.21}$$

Only one of these two constraints will be active during the optimization and the other one is a redundant constraint which is always satisfied. For example, if $\theta_k > 0$, y_k will be equal to zero so the constraint (5.20) would be active. The constraint (5.21) will become redundant because of the sufficiently large number M_k. M_k should be chosen appropriately as a too large value can cause numerical problem.

In constraints (5.20) and (5.21), there still exists a bilinear term $\delta_k \theta_k$ which is the product between a binary variable and a continuous variable. We introduce another variable z_k and use the standard linearization method [94] to find:

$$-\delta_k \theta_k^{\max} \leq z_k \leq \delta_k \theta_k^{\max}, \quad k \in \Omega_V \tag{5.22}$$

$$\theta_k - (1 - \delta_k)\theta_k^{\max} \leq z_k \leq \theta_k + (1 - \delta_k)\theta_k^{\max}, \quad k \in \Omega_V \tag{5.23}$$

Then the constraint (5.20) and (5.21) can be written as:

$$-M_k y_k + z_k b_{k,V}^{\min} \leq w_k \leq z_k b_{k,V}^{\max} + M_k y_k, \quad k \in \Omega_V \tag{5.24}$$

$$-M_k(1-y_k) + z_k b_{k,V}^{\max} \leq w_k \leq z_k b_{k,V}^{\min} + M_k(1-y_k), \quad k \in \Omega_V \tag{5.25}$$

The original MINLP model has now been transformed into an MILP model. The full MILP model involves maximizing (5.6) subjecting to (5.7), (5.9)-(5.13), (5.15), (5.17), and (5.22)-(5.25).

5.3 Two Stage Optimization Model

5.3.1 Flow Chart of the Optimization Tool

The flow chart of the proposed optimization tool is shown in Fig. 5.2. The input for the allocation model is the power system data, possible VSR locations and the contingency list. In stage one, the allocation model is used to find the optimal locations for the VSR considering a series of operating states including base case and contingencies. With the determined locations, the operation model in stage two is utilized to set the reactance of VSRs for each operating state.

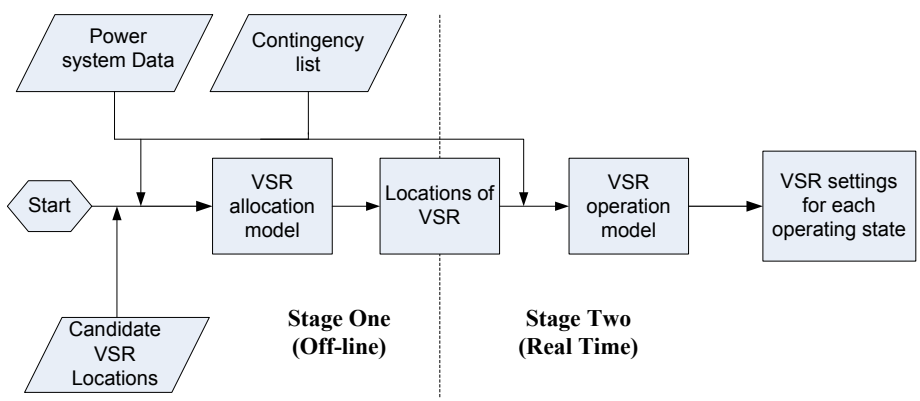

Figure 5.2: Flow chart for the optimization tool.

5.3.2 Allocation Model

The $N-1$ criterion indicates that the power network should be capable of handling any single element loss in the system. In practice, it would be more interesting and more important for the system operators to determine the maximal load margin with the loss of transmission elements. Note that considering a complete N-1 contingency increases the computational burden and is not necessary in a practical system. The selection of the contingency can be based on the experience of the system operators or some contingency screening algorithm [95]. In this paper, we consider the transmission $N-1$ contingencies. A binary parameter N_{kc} is introduced to represent the corresponding status with respect to the line k in state c [59]. $N_{kc}=1$ indicates that line k is in service in state c; otherwise it is in outage.

The MILP model given in Section 5.2.2 is expanded to consider multiple operating states together and formulated as:

$$\{\max \quad \sum_{c\in\Omega_c} \rho_c \mu_c \tag{5.26}$$

subject to:

$$P_{kc} - b_k\theta_{kc} + M_k'^{(}1 - N_{kc}) \geq 0, k \in \Omega_L \backslash \Omega_V \tag{5.27}$$

$$P_{kc} - b_k\theta_{kc} - M_k'^{(}1 - N_{kc}) \leq 0, k \in \Omega_L \backslash \Omega_V \tag{5.28}$$

$$P_{kc} - b_k\theta_{kc} - w_{kc} + M_k'^{(}1 - N_{kc}) \geq 0, k \in \Omega_V \tag{5.29}$$

$$P_{kc} - b_k\theta_{kc} - w_{kc} - M_k'^{(}1 - N_{kc}) \leq 0, k \in \Omega_V \tag{5.30}$$

$$-M_k y_{kc} + z_{kc} b_{k,V}^{\min} \leq w_{kc} \leq z_{kc} b_{k,V}^{\max} + M_k y_{kc}, k \in \Omega_V \tag{5.31}$$

$$-M_k(1-y_{kc}) + z_{kc} b_{k,V}^{\max} \leq w_{kc} \leq z_{kc} b_{k,V}^{\min} + M_k(1-y_{kc}), k \in \Omega_V \tag{5.32}$$

$$-N_{kc}\delta_k\theta_{kc}^{\max} \leq z_{kc} \leq N_{kc}\delta_k\theta_{kc}^{\max}, k \in \Omega_V \tag{5.33}$$

$$N_{kc}(\theta_{kc} - (1-\delta_k)\theta_{kc}^{\max}) \leq z_{kc} \leq N_{kc}(\theta_{kc} + (1-\delta_k)\theta_{kc}^{\max}), k \in \Omega_V \tag{5.34}$$

$$P_{ic}^{g} - \mu_c \cdot P_{ic}^{d} = \sum_{k \in \Omega_L^i} P_{kc} \tag{5.35}$$

$$P_{ic}^{g} = \sum_{n \in \mathcal{G}_i} P_{nc}^{g} \tag{5.36}$$

$$P_{ic}^{d} = \sum_{m \in \mathcal{D}_i} P_{mc}^{d} \tag{5.37}$$

$$-N_{kc}S_{kc}^{\max} \leq P_{kc} \leq N_{kc}S_{kc}^{\max}, k \in \Omega_L \tag{5.38}$$

$$P_{nc}^{g,\min} \leq P_{nc}^{g} \leq P_{nc}^{g,\max} \tag{5.39}$$

$$\sum_{k \in \Omega_V} \delta_k \leq N_V, k \in \Omega_V \tag{5.40}$$

$$\}\forall c \in \Omega_c, i \in \mathcal{B}, n \in \mathcal{G}$$

The ρ_c in the objective function (5.26) can be interpreted either as the probability associated with the occurrence of each state c or as a weighting factor associated with the importance of each state c. The constraints (5.27)-(5.30) indicate the following: if line k is in service in state c, i.e., $N_{kc} = 1$, the line flow equations are forced to hold; otherwise, if line k is in outage in state c, the sufficiently large constant M_k' guarantees that the constraints are always satisfied regardless of the bus angle difference. M_k' is selected to be $|b_k\pi|$ in this dissertation. Constraints (5.31)-(5.34) ensure that the line flow change introduced by the VSR should be zero if the line installed with VSR is in outage, i.e., $w_{kc} = 0$ when $N_{kc} = 0$. Constraint (5.38) guarantees that the line flow is forced to be zero if the line is not in service. The VSR placement variable δ_k does not depend on the state unlike the other variables.

5.3.3 Operation Model

The operation model is utilized to determine the optimal settings of the installed VSRs to maximize the load margin for each operating state. The operation model is base on some minor modifications to the optimization model from (5.26) to (5.40):

- The objective function (5.26) is modified to be maximize the loadability for a specific state c.
- δ_k is kept but with a different interpretation: the operating status ("ON" or "OFF") of VSR.
- Constraint (5.40) is removed.

It should be noted that the number of binary variables indicating the status of VSR in the operation model is equal to the number of installed VSRs in the system, which is far less than the number of candidate locations. Therefore, the computation burden for the operation model is low and enables real time applications.

5.4 Case Studies

The proposed planning/operation tool is applied to the IEEE 30-bus, 118-bus power systems and a practical Northwest US power network. The data for the IEEE sample systems are from MATPOWER software [87]. The computer used for all the simulations has an Inter Core(TM) i5-2400M CPU @ 2.30 GHz with 4.00 GB of RAM. The YALMIP [96] toolbox in MATLAB is selected to implement the MILP problem, and the CPLEX solver [97] is used to solve.

The CVSR is selected for the case studies. The output reactance of CVSR is allowed to vary from 5% to 20% of its corresponding branch reactance:

$$0.05x_k \leq x_k^V \leq 0.2x_k,\ k \in \Omega_V \tag{5.41}$$

5.4.1 IEEE 30-Bus System

The IEEE 30-bus test system has 30 buses, 37 transmission lines, 4 transformers and 6 generators. The total active load is 283.4 MW and the maximum active power generation is 485 MW. The thermal limit for each branch is decreased to 75% of its

original value to cause system congestion. In this system, we assume that all the transmission line branches are candidate locations to install the CVSR so the number of possible locations is 37.

For this test system, we mainly focus on the planning function of the tool. The first task is to simulate each state (base case and contingencies) of the system independently. We consider the complete transmission $N-1$ contingency list except for those that would cause islanding (i.e., line outages for 9-11, 12-13 and 25-26 are not considered). The loadability for each state with different number of CVSRs is shown in Fig. 5.3.

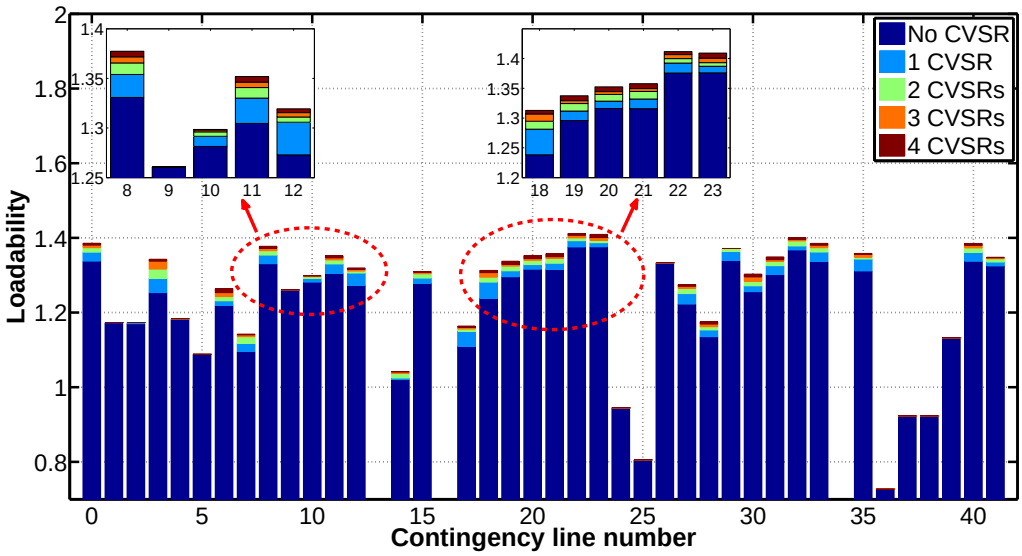

Figure 5.3: Loadability for the base case and contingencies with different number of CVSRs.

The contingency line number zero indicates the base case. From Fig. 5.3, the following observations can be made:

- Without any CVSR, there is some room to enhance the loadability. This is due to the generator rescheduling.
- The installation of CVSR helps to improve the loadability for most of the states. For example, the maximum loadability for the base case without any CVSRs is

1.34. By installing 4 CVSRs into the system, the maximum loadability increases to 1.39.

- Some contingency states have higher loadability than the base case. This result is to be expected because the switching of one or several lines is another approach to relieve the congestion [31, 98].

After simulating each transmission contingency individually, we found that the number of contingencies that the CVSR could help to enhance the loadability is 29. We simulate the multi-scenario cases considering the base case and these 29 contingencies. The probability ρ_c for the base case to be 80% and the remaining 20% probability is distributed equally across the 29 contingencies. Fig. 5.4 shows the maximum loading margin versus the number of CVSRs.

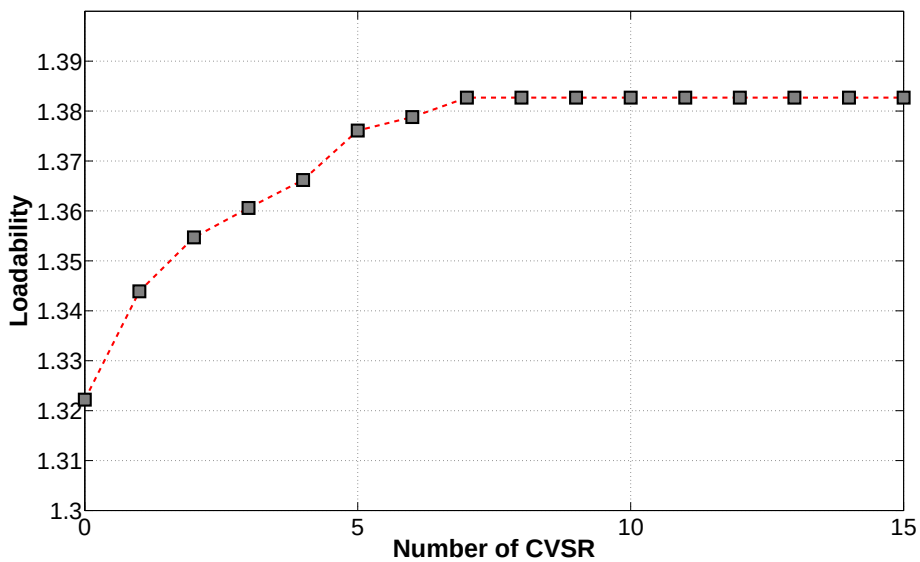

Figure 5.4: Maximum loadability versus the number of CVSRs of the multi-scenario case for the IEEE 30-bus system.

From Fig. 5.4, it can be seen that the maximum loadability increases as the number of CVSRs increases. When seven or more CVSRs are allowed to be installed, the loadability tends to level off and approaches its maximum value of 1.38. It should be noted that most of the enhancement in loadability is from a few well located

CVSRs. The installation of 3 CVSRs accounts for 63.5% of the total improvement in loadability and 72.7% of the total enhancement can be achieved by 4 CVSRs.

Table 5.1: Maximum Loadability and CVSR Locations of the Multi-scenario Case for the IEEE 30-Bus System

N_{CVSR}	Branch $(i-j)$	Objective	Time (s)
0	N/A	1.3222	0.1887
1	(12-15)	1.3439	41.66
2	(1-2),(12-15)	1.3547	41.98
3	(1-2),(2-4),(12-15)	1.3606	73.59
4	(1-2),(2-4),(2-6),(12-15)	1.3662	91.83

Table 5.1 summarizes the simulation results for the multi-scenario case when the number of CVSRs varies from 0 to 4. The computation time increases as the number of allowable CVSRs increases. This result is to be expected since larger N_V would expand the feasible region for the branch and cut algorithm. Note also that when $N_V = 0$, the MILP problem is reduced to an LP problem and the computation time is less than 0.2 sec.

5.4.2 IEEE 118-Bus System

The IEEE 118-bus system has 118 buses, 177 transmission lines, 9 transformers and 54 generators. The total active load is 4242 MW and the total generation capacity is 9966 MW. In this system, we assume that the number of possible locations for CVSR is 38 and the output reactance of CVSR is still allowed to vary from 5% to 20% of its corresponding branch reactance. The selection of the candidate locations of the CVSR is based on the congestion severity of each transmission line in the base operating condition.

Allocation

We consider the worst 30 contingencies for this test system so the number of states is 31. In addition, we assume equal weighting factor for each state in the objective

function (5.26), i.e., $\rho_c = 1/31$. The maximum loadability and CVSR locations are summarized in Table 5.2.

Table 5.2: Maximum Loadability and CVSR Locations of the Multi-scenario Case for the IEEE 118-Bus System

N_{CVSR}	Branch $(i-j)$	Objective	Time (min)
0	N/A	1.1928	0.0076
1	(16-17)	1.1983	1.63
2	(14-15),(16-17)	1.2035	2.32
3	(14-15),(16-17),(45-46)	1.2063	3.50
4	(14-15),(16-17) (25-27),(45-46)	1.2085	5.42
5	(14-15),(16-17) (25-27),(33-37),(45-46)	1.2105	5.65

Table 5.2 provides leads to similar conclusions as Table 5.1. Without any CVSRs, a 19.28% gain of loadability is achieved by rescheduling. This improves to 21.05% with the installation of 5 CVSRs. The computation time is 5.65 minutes for the case with $N_V = 5$, which is acceptable for the off-line allocation problem.

Operations

We fix the CVSRs to the 5 locations given in Table 5.2. The simulation results for the base case and 4 contingencies with lowest initial loadability are given in Table 5.3.

Table 5.3 shows the contingency line for each state. Note that the zero reactance output indicates the CVSR status is "OFF". The loadability (μ_0) without any CVSRs and the loadability (μ) with CVSRs are given in the table. It can be seen that different states will result in different operation status of CVSRs. The base case requires that all the 5 CVSRs should be turned on while only 3 CVSRs should be on for contingency 2. Moreover, the output reactance of CVSR also varies for different states. The CVSR on line 25-27 gives 0.0326 p.u. output reactance for the contingency 1 while the contingency 2 requires the output reactance to be 0.0235 p.u.. The computation time for all the cases is within 0.3 seconds, which is suitable for real time operations.

Table 5.3: CVSR Settings of Different Scenarios for IEEE 118-Bus System

Case		Base case	Cont. 1	Cont. 2	Cont. 3	Cont. 4
Cont. line $i-j$		N/A	60-61	8-5	5-11	4-11
x_k^V $(p.u.)$	14-15	0.0390	0.0390	0.0390	0.0390	0.0390
	16-17	0.0360	0	0.0360	0.0360	0.0360
	25-27	0.0326	0.0326	0.0235	0.0326	0.0326
	33-37	0.0284	0.0284	0	0.0284	0.0284
	45-46	0.0074	0.0271	0	0	0
μ_0		1.2373	0.9636	1.0734	1.1068	1.1206
μ		1.2579	0.9657	1.0929	1.1169	1.1361
Time (s)		0.2158	0.2687	0.2245	0.2273	0.2405

5.4.3 Northwest Power Network

Network Description

The Northwest US power network is a portion of the WECC system. It contains 4016 buses, 4707 branches and 416 generators. In the summer peak load pattern, a large amount of power is transferred from North to South via the California Oregon Intertie (COI) and the DC Intertie. Due to some system constraints, the full transmission capacity of COI may not be utilized [91]. The usable capacity decreases further after certain critical contingencies. The objective here is to maximize the available transfer capability (ATC) on the COI by installing several CVSRs considering these contingencies.

Modifications to Optimization Model

The "Malin" and "Captain Jack" are used as the interface buses for the COI [91]. The external system is reduced using the model reduction function in PowerWorld [92] so that the active power transferred on the COI is equivalent to the active load on these interface buses. The objective function is to maximize the load margin corresponding

to the equivalent load so the constraint (5.35) is modified to:

$$P_{ic}^{g} - \mu_c P_{ic}^{d} = \sum_{k \in \Omega_L^i} P_{kc},\ i \in \mathcal{B}_{COI}, c \in \Omega_c \tag{5.42}$$

$$P_{ic}^{g} - P_{ic}^{d} = \sum_{k \in \Omega_L^i} P_{kc},\ i \in \mathcal{B}_{NCOI}, c \in \Omega_c \tag{5.43}$$

In practice, generation rescheduling is often required following a severe contingency but the number of generators which can participate in the rescheduling process is limited. These generators usually have higher ramp rates and serve the non base load [59]. In the Northwest network, based on the guidance from Bonneville Power Administration (BPA), only 123 out of 416 generators were allowed to reschedule generation within their ramping limits following a contingency. For all the other generators, the power output is fixed. The constraint (5.39) is modified accordingly to:

$$P_{nc}^{g,\min} \leq P_{n0}^{g} + \Delta P_{nc}^{g,up} - \Delta P_{nc}^{g,dn} \leq P_{nc}^{g,\max},\ n \in \mathcal{G}_{re}, c \in \Omega_c \tag{5.44}$$

$$0 \leq \Delta P_{nc}^{g,up} \leq R_{nc}^{g,up},\ n \in \mathcal{G}_{re} \tag{5.45}$$

$$0 \leq \Delta P_{nc}^{g,dn} \leq R_{nc}^{g,dn},\ n \in \mathcal{G}_{re} \tag{5.46}$$

$$P_{nc}^{g} = P_{n0}^{g},\ n \in \mathcal{G}_{fix}, c \in \Omega_c \tag{5.47}$$

A prototype device, which is scheduled to be installed into the Northwest system, is rated at 115 kV with a minimum and maximum output reactance to be 1.2 Ω and 5.2 Ω respectively. In terms of per unit we have:

$$0.0091 \text{ p.u.} \leq x_k^V \leq 0.0393 \text{ p.u.}, k \in \Omega_V \tag{5.48}$$

We only consider 115 kV lines as possible locations for the CVSR.

Allocation

We consider 7 contingencies suggested by BPA. These contingencies all involve the loss of one or two transmission corridors from North to South. For the multi-scenario case, based on the importance of each contingency, we assign the weighting factors of contingency 1, 6 and 7 to be 0.2 and all the remaining contingencies are weighted as 0.1. Based on the congestion severity of the 115 kV transmission lines, the number of CVSR candidate locations is selected to be 50 and we allow up to 6 devices to be installed into the system.

Table 5.4: Maximum Loadability and CVSR Placements of Northwest Power Network for Different Scenarios

Case	Located branch #	μ_0	μ	Time (min)
Cont. 1	1177, 2721, 2941 2797, 3009, 4127	0.8118	1.0588	0.42
Cont. 2	44, 351, 926 1119, 2293, 2446	1.0881	1.0887	0.20
Cont. 3	926, 1119, 2276 2293, 2452, 2497	1.0809	1.0813	0.12
Cont. 4	44, 351, 377 926, 2276, 2293	1.0553	1.0559	0.11
Cont. 5	44, 351, 926 1119, 2276, 2293	1.1037	1.1043	0.12
Cont. 6	351, 389, 719 926, 1119, 2276	0.8355	1.0530	0.44
Cont. 7	351, 926, 2276 2293, 2446, 3176	0.7952	1.0976	0.40
Multi-scenario case	43, 389, 719 2276, 2941, 3009	0.9213	1.0741	17.53

The CVSR placement strategy for each scenario and multi-scenario case is given in Table 5.4. It can be seen that the load margins after contingency 1, 6 and 7 are all below one without any CVSRs. The results indicate that there will be some reduction in transfer needed on COI if only rescheduling. With 6 CVSRs installed into the system, the load margins for these three contingencies are above one. Moreover, there is some room to further increase the active power on the COI. For contingency 2-5, the

load margins with just rescheduling are above 1. There will be some improvements for the loadability with 6 CVSRs. However, the improvements are not as significant as that for contingency 1, 6 and 7.

From Table 5.4, it can be seen that most of the CVSR locations in the multi-scenario case can also be found in the locations for each contingency. The multi-scenario case will select those CVSR locations that are capable of improving the loadability for as many contingencies as possible. The computation time for each individual scenario is within 30 seconds. For the multi-scenario case, the computation time increases to 17.5 minutes. Still, this is acceptable for the off-line allocation studies in a large system.

Operations

From the allocation study results, we fix the CVSR locations to branch 43, 289, 719, 2276, 2941 and 3009. Table 5.5 gives the CVSR settings for contingency 1, 6 and 7. It can be seen that the maximum loadability achieved in Table 5.5 is slightly smaller than the loadability shown in Table 5.4. The result is expected since the CVSR locations for the multi-scenario case are used. For contingency 1, 4 out of the 6 CVSRs should be turned on, which will increase the loadability from 0.81 to 1.06. Similar results can also be found for contingencies 6 and 7. The computation time for each contingency is around 2.5 seconds.

Table 5.5: CVSR Settings of Different Scenarios for Northwest Power Network

Case		Cont. 1	Cont. 6	Cont. 7
x_k^V $(p.u.)$	43	0	0	0.0091
	389	0.0393	0.0393	0
	719	0.0393	0.0220	0
	2276	0	0.0393	0.0393
	2941	0.0393	0	0
	3009	0.0125	0	0.0175
μ_0		0.8118	0.8355	0.7952
μ		1.0571	1.0526	1.0971
Time (s)		2.55	2.16	2.07

Fig. 5.5 shows the thermal loading of 5 transmission paths from North to South before and after contingency 1. This contingency involves losing a 500 kV transmission line from North to South. After this contingency, if the same amount of active power as the normal operating condition ($\mu = 1$) is transferred on COI, branch 3009 and 2246 will be congested - indicated by the red bar. Generation rescheduling is able to eliminate the congestion but at the expense of reduced transfer on the COI ($\mu = 0.81$) - indicated by the decreased thermal loading in the black bar. The green bar shows that the CVSRs on the 115 kV lines increase the thermal loadings for the paths which still have spare transmission capacities. The result is more power can be transferred on the COI ($\mu = 1.06$).

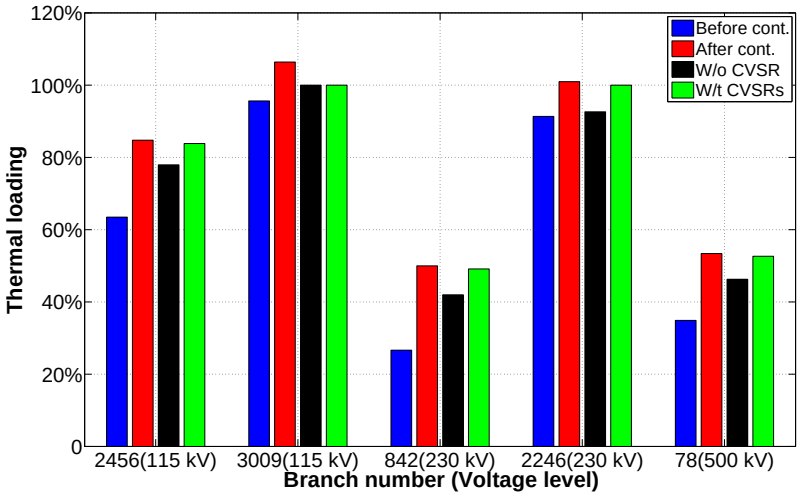

Figure 5.5: Thermal loading of five transmission corridors from North to South in contingency 1.

5.5 Conclusion

In this chapter, a planning and operation framework is developed to find the optimal locations of VSR considering a multi-scenario framework across the base case and select contingencies. The original MINLP model is transformed to a MILP model using a reformulation technique. The detailed simulation results on IEEE sample

systems and a practical Northwest system show that the system load margin can be greatly enhanced with several well located VSRs. The computation time of the developed tool is fast enough for both planning and operation studies.

Chapter 6

Security Constrained Multi-Stage Transmission Expansion Planning Considering a Variable Series Reactor

This chapter presents an MILP model for the multi-stage TEP considering VSRs, while satisfying $N-1$ security constraints. Three load blocks are selected to accommodate the load profile of each stage and the considered transmission contingencies can occur in any of the load blocks. Several benefits can be anticipated by introducing the VSR into TEP: 1) VSRs are conducive to improving the utilization of the existing network, which leads to deferment or even avoidance of new transmission lines; 2) VSRs can change the power flow pattern and increase the use of power generation from lower cost generators, which reduces the total operating cost; 3) VSRs add flexibility to the system and can provide additional corrective actions following contingencies.

The main contributions of this chapter are summarized below:

- A security constrained multi-stage TEP with VSRs is formulated.

- An iterative approach is developed to decompose the model into the planning master problem and the security check sub-problem so that it is computationally tractable for practical sized systems. This is critical as the model size increases dramatically with the number of stages, load blocks and contingencies.

Due to the heuristic method used in the iterative approach, the solution obtained by the decomposition model is not guaranteed to be globally optimal. However, it provides a high level picture of how the network can be rationally planned including VSRs so it is useful from an engineering point of view. In addition, the decomposition approach makes an originally large scale MINLP model tractable.

The remainder of this chapter is organized as follows. Section 6.1 presents detailed information about the optimization model and the iterative approach. Simulation results are given in Section 6.2 on the IEEE 24-bus and a more practical Polish system. Conclusions are given in Section 6.3.

The main contents of this chapter can also be found in [99].

6.1 Optimization Model

6.1.1 $N-1$ Security Constraints

Power grid security is the primary concern for the system operations and planning and it cannot be compromised. According to the NERC planning standards [100], a rationally planned power system should have the capability of maintaining an $N-1$ secure network. We introduce the same parameter N_{kc} as in Chapter 5 to model the transmission line $N-1$ contingencies.

For most planning problems, a complete set of $N-1$ contingencies is not needed and just results in excessive computations as the number of branches is large in a practical system. For the TEP problem, a complete $N-1$ contingency is not needed since the addition of some new transmission lines in one area will mainly affect the

power flow pattern in the nearby areas. The selection of the contingencies can be based on experimental data or a contingency screening algorithms [59, 95].

6.1.2 Integrated Planning Formulation

Integrated planning indicates that all the planning stages, load blocks and security constraints are included in one planning problem. With the reformulation technique proposed in Chapter 5, the complete model can be formulated as (6.1)-(6.18).

Objective Function

The objective employed for the TEP problem minimizes the total cost, which includes both the investment and operating cost. Assuming a fixed load demand (price inelastic), minimizing operating cost is equivalent to minimizing generation cost. The objective function is:

$$\min \sum_{t\in TPL}\sum_{k\in\Omega_L^+}\frac{C_k^L(\alpha_{kt}-\alpha_{k,t-1})}{(1+d)^{t-1}}+\sum_{t\in TPL}\sum_{k\in\Omega_V}\frac{C_k^V(\delta_{kt}-\delta_{k,t-1})}{(1+d)^{t-1}} + \sum_{t\in TPL}\sum_{b\in\Omega_b}\sum_{n\in\mathcal{G}}\frac{H_{bt}C_n^g P_{n0bt}^g}{(1+d)^{t-1}} \tag{6.1}$$

TPL represents the total planning horizon. The first two terms represent the one time investment cost for the new transmission lines and the installed VSRs. The third term is the generation cost across the operating horizon. Three distinct load patterns which represent peak, normal and low load condition are selected to accommodate the load profile in each stage. Here the generation cost is just an estimated cost. However, if the detailed load duration curve for each year is given, a relatively more accurate generation cost model can be formulated. All the cost terms are discounted to the present value by using the discount factor d. In this work, d is selected to be 5%.

Constraints

The active power flow through the existing transmission lines is:

$$P^E_{kcbt} - b_k\theta_{kcbt} + M'_k(1 - N_{kcbt}) \geq 0, k \in \Omega_L \backslash \Omega_V \tag{6.2}$$

$$P^E_{kcbt} - b_k\theta_{kcbt} - M'_k(1 - N_{kcbt}) \leq 0, k \in \Omega_L \backslash \Omega_V \tag{6.3}$$

$$P^E_{kcbt} - b_k\theta_{kcbt} - w_{kcbt} + M'_k(1 - N_{kcbt}) \geq 0, k \in \Omega_V \tag{6.4}$$

$$P^E_{kcbt} - b_k\theta_{kcbt} - w_{kctb} - M'_k(1 - N_{kcbt}) \leq 0, k \in \Omega_V \tag{6.5}$$

Constraints (6.2)-(6.5) hold $\forall c \in \Omega_c, b \in \Omega_b, t \in \Omega_t$.

Constraints (6.2) and (6.3) denote the active power on the lines without VSRs while constraints (6.4) and (6.5) represent the active power flow on the candidate lines to install VSRs. If the line is in service, i.e. $N_{kcbt} = 1$, the line flow equations are enforced. A large disjunctive factor M'_k is introduced to ensure these constraints are not restrictive when the transmission line is out of service. As the phase angle will not fall outside of the range $[-\pi/2\ \pi/2]$ if an appropriate slack bus is selected, M'_k is chosen to be $|b_k\pi|$.

Additional constraints introduced by the reformulation technique can be expanded to consider multiple states, load blocks and stages:

$$-M_k y_{kcbt} + z_{kcbt} b^{\min}_{k,V} \leq w_{kcbt} \leq z_{kcbt} b^{\max}_{k,V} + M_k y_{kcbt} \tag{6.6}$$

$$-M_k(1 - y_{kcbt}) + z_{kcbt} b^{\max}_{k,V} \leq w_{kcbt} \leq z_{kcbt} b^{\min}_{k,V} + M_k(1 - y_{kcbt}) \tag{6.7}$$

$$-N_{kcbt}\delta_{kt}\theta^{\max}_k \leq z_{kcbt} \leq N_{kcbt}\delta_{kt}\theta^{\max}_k \tag{6.8}$$

$$N_{kcbt}(\theta_{kcbt} - (1 - \delta_{kt})\theta^{\max}_k) \leq z_{kcbt} \leq N_{kcbt}(\theta_{kcbt} + (1 - \delta_{kt})\theta^{\max}_k) \tag{6.9}$$

Constraints (6.6)-(6.9) hold $\forall k \in \Omega_V, c \in \Omega_c, b \in \Omega_b, t \in \Omega_t$.

Constraints (6.6)-(6.9) guarantee that the line flow change w_{kcbt} introduced by the VSR is zero when line k with VSR is out of service in state c, load block b and at stage t.

The power flow through the candidate transmission lines is:

$$P^C_{kcbt} - b_k\theta_{kcbt} + M'_k(2 - N_{kcbt} - \alpha_{kt}) \geq 0 \tag{6.10}$$

$$P^C_{kcbt} - b_k\theta_{kcbt} - M'_k(2 - N_{kcbt} - \alpha_{kt}) \leq 0 \tag{6.11}$$

Constraints (6.10)-(6.11) hold $\forall k \in \Omega^+_L, c \in \Omega_c, b \in \Omega_b, t \in \Omega_t$.

In contrast with the existing transmission lines, a candidate transmission line has two situations where it is not connected: either it is not built or it has been built but is out of service.

The active power nodal balance at each bus is:

$$\sum_{n\in\mathcal{G}_i} P^g_{ncbt} - \sum_{m\in\mathcal{D}_i} P^d_{mcbt} = \sum_{k\in\Omega^i_L} P^E_{kcbt} + \sum_{k\in\Omega^i_L} P^C_{kcbt} \tag{6.12}$$

$$i \in \mathcal{B}, c \in \Omega_c, b \in \Omega_b, t \in \Omega_t$$

The system physical limits are represented by:

$$-N_{kcbt}S^{\max}_{kcbt} \leq P^E_{kcbt} \leq N_{kcbt}S^{\max}_{kcbt}, k \in \Omega_L \tag{6.13}$$

$$-\alpha_{kt}N_{kcbt}S^{\max}_{kcbt} \leq P^C_{kcbt} \leq \alpha_{kt}N_{kcbt}S^{\max}_{kcbt}, k \in \Omega^+_L \tag{6.14}$$

$$P^{g,\min}_{ncbt} \leq P^g_{ncbt} \leq P^{g,\max}_{ncbt}, n \in \mathcal{G} \tag{6.15}$$

$$P^g_{ncbt} = P^g_{n0bt},\ n \in \mathcal{G}_{fix}, c \in \Omega_c \backslash \Omega_0, b \in \Omega_b, t \in \Omega_t \tag{6.16}$$

Constraints (6.13)-(6.15) hold $\forall c \in \Omega_c, b \in \Omega_b, t \in \Omega_t$. Constraints (6.13) and (6.14) ensure that the power flow is zero if the line is not built or out of service; otherwise, the power flow on the line is limited by its thermal rating. Constraints (6.15) and (6.16) reflect that only a subset of the generators are allowed to re-dispatch after a contingency. The other generators which do not participate in the rescheduling are fixed at their base case power output.

The build decisions made in the current stage must be present on the later stage:

$$\alpha_{kt} \geq \alpha_{k,t-1}, \ k \in \Omega_L^+, t \in \Omega_t \tag{6.17}$$

$$\delta_{kt} \geq \delta_{k,t-1}, \ k \in \Omega_V, t \in \Omega_t \tag{6.18}$$

Note that α_{k0} and δ_{k0} are set to be zero.

6.1.3 Decomposition

In the integrated planning model, the constraints have four dimensions, i.e., power system element, state, load block and time. Hence, the size of the optimization model will grow dramatically with the system size and planning horizon. To reduce the computational burden for a large practical planning problem, the multiple stages are decomposed using forward planning [60, 63], in which the planning for each stage is solved successively while the building decisions from the previous stage are enforced on subsequent stages. Although forward planning may lead to a suboptimal plan, it greatly reduces the computational time with relatively minor degradation of the solution quality. This iterative approach is depicted in Fig. 6.1.

Essentially the majority of the $N-1$ security analysis will be performed iteratively at the sub-problem level. The process is as below:

1. Initialization of the stage number $N_s = 1$.

2. Run the single stage TEP with VSR model for the base case considering all the load blocks and several critical contingencies (CC). Obtain solutions and update the system with the new transmission lines and CVSRs.

3. Perform the remaining $N-1$ security analysis for the expanded system. If there are no violations, go to step 5); otherwise, identify the contingency leading to the worst violations. **Temporarily** remove the line from the system.

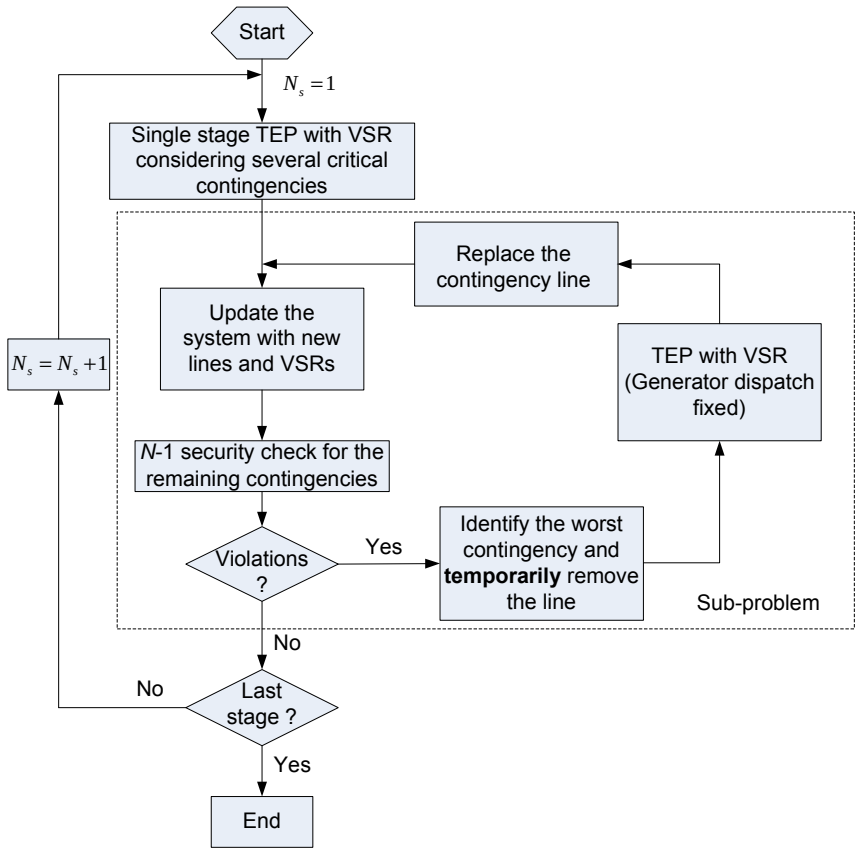

Figure 6.1: Flow chart of the iterative approach.

4. Run the TEP with VSR model. The generation dispatch is assumed to be unchanged. The purpose of this step is to find the optimal building plan (lines and VSRs) to resolve the worst contingency. Replace the contingency line and update the system with new lines and VSRs from this solution, go to step 3).

5. If the last stage is solved, then finished; otherwise, increase the stage number $N_s = N_s + 1$ and go to step 2).

Including several critical contingencies in the master problem is motivated by the idea that the critical contingencies have large impacts on the TEP results. However, considering more contingencies tends to increase the dimension of the master problem. The computational issues are discussed in Section 6.2.3. For a practical system, the

critical contingencies can be selected based on empirical data. In our test system, we rank the contingencies either in terms of circuit loading or the generation cost.

The two sections below detail the problem formulation of the master problem and sub-problem described above. Note that the constraints in Section 6.1.2 all pertain to a specific state c, load block b and stage t .

Master Problem

The planning master problem is to obtain the optimal building plan for the base case considering several critical contingencies. The optimization minimizes (6.1) subject to (6.2)-(6.18). Note that the solution from the previous stage is the input for the current stage, i.e., $\alpha_{k,t-1}$ and $\delta_{k,t-1}$ are known before solving stage t.

Sub-problem

After obtaining the solution for the master problem in stage t, the sub-problem performs $N-1$ security analysis for the expanded system. Here, P^g_{n0bt}, α_{kt} and δ_{kt} are all input values for the security sub-problem while P^g_{n0bt} is from the base case generation for each load block. In the iterative process of the sub-problem, new lines and CVSRs will be added to resolve the contingency, i.e., step 4), so α_{kt} and δ_{kt} need to be updated accordingly at each iteration.

The violations for the DC power flow model are only thermal limit violations. For the $N-1$ security check, we introduce four positive slack variables to represent possible violations of the existing and candidate transmission lines. For each contingency state c, the objective is to minimize the sum of these slack variables:

$$\min \sum_{k\in\Omega_L}(u^E_{k,1}+u^E_{k,2})+\sum_{k\in\Omega^+_L}(u^C_{k,1}+u^C_{k,2}) \tag{6.19}$$

The contingency with the maximum objective will be regarded as the worst contingency. If there is no violation, the objective for all the contingencies must

fall within a specified tolerance. The thermal limit constraints are:

$$-N_k(S_k^{\max} + u_{k,1}^E) \leq P_k^E \leq N_k(S_k^{\max} + u_{k,2}^E),\ k \in \Omega_L \tag{6.20}$$

$$-\alpha_k N_k(S_k^{\max} + u_{k,1}^C) \leq P_k^C \leq \alpha_k N_k(S_k^{\max} + u_{k,2}^C),\ k \in \Omega_L^+ \tag{6.21}$$

Constraints (6.20) and (6.21) enforce the power flow on the lines that are not connected to zero; however, these two constraints allow thermal violations on the lines in service. The remaining constraints include (6.2)-(6.12), (6.15)-(6.16).

6.2 Case Studies

The proposed planning model is applied to the IEEE 24-bus system and a more practical Polish 2383-bus system. The data for the IEEE 24-bus and the Polish 2383-bus system are included in the MATPOWER software [87]. For all the test systems, each stage is 5 years and all the selected lines and CVSRs are built at the beginning of each stage.

We select CVSR for the case studies. The investment cost for the CVSR is assumed to be \$10/kVA [12]. Based on the prototype that is going to be installed by Bonneville Power Administration (BPA), the maximum output reactance of the CVSR is allowed to be 20% of the corresponding line reactance:

$$0 \leq x_k^V \leq 0.2x_k,\ k \in \Omega_V \tag{6.22}$$

6.2.1 IEEE 24-Bus System

The IEEE 24-bus system has 29 transmission lines, 5 transformers, 32 generators and 21 loads. The thermal limits for all the transmission branches are decreased artificially to introduce congestion. For this test system, we assume only one candidate transmission line per existing line (i.e, exclude transformer upgrades) so the number of candidate transmission lines is 29. In addition, all the existing transmission

lines are possible locations to install a CVSR so the number of candidate locations for CVSR is also 29. Excluding one contingency (line 7-8) which splits the system into two parts, complete $N-1$ contingency constraints considering the existing branches are considered. Due to the absence of actual system expansion data, the investment for building new transmission lines is estimated by its length and cost per mile. The cost per mile for different voltage levels can be found in [101].

Single Stage Planning

We first consider the single stage planning for this test system. The selected lines and CVSRs are committed at the beginning of the stage and the operation cost is evaluated over the five years thereafter. The simulation results using integrated model are summarized in Table 6.1. From Table 6.1, it can be seen that the TEP without CVSRs requires building 3 transmission lines. When the CVSR is introduced in the TEP, only 2 transmission lines are needed for the considered stage. The construction of line 14-16 ($36.47M) is avoided by installing 3 low cost CVSRs ($13.5M) on line 11-14, 14-16 and 15-21. Thus, the investment cost decreases from $74.25M to $51.28M. Although the operating cost of the case with CVSR is $10M higher than the case without CVSR, the total saving for this five years plan is about $13 M. The computation time for the case without CVSR is 9.25 s and the time increases to 388.51 s for the case considering CVSR.

Table 6.2 shows the TEP results by using the decomposed model. To evaluate the impacts of the decomposition, two cases are simulated:

1. Considering one critical contingency (line 18-21) for the peak and normal load level in the master problem.

2. Considering two critical contingencies (line 18-21, 15-21) for the peak and normal load level in the master problem.

The critical contingencies are selected based on the circuit loading in the peak load level. As observed from Table 6.2, the investment plans for the TEP without

Table 6.1: Single Stage TEP Results Comparison for the IEEE 24-Bus System Using Integrated Model

	Case	
	w/o CVSR	w/t CVSR
Line	14-16 16-17 17-18	16-17 17-18
CVSR	-	11-14 14-16 15-21
Investment cost (M$)	74.25	51.28
Operating cost (M$)	1168.59	1178.91
Total cost (M$)	1242.84	1230.19
Computation Time (s)	9.25	388.51

CVSR are the same for these two cases, which are also identical as the results using integrated model. Nevertheless, the computational time using the decomposed model is only around 1.2 s. The investment plans for the TEP with CVSR are different for the two cases. For the case considering one critical contingency, 1 transmission line and 6 CVSRs are added. The cost in total is $1234.73M. The case considering two critical contingencies requires to build 2 transmission lines and 3 CVSRs, which are the same planning results as the integrated model. The computational time for the decomposed model considering two critical contingencies is 34.71 s. This time is 11 times faster than the integrated model.

Multi-stage Planning

We then consider a two stage planning for this test system. The load growth is estimated to be 25% in five years and this growth is distributed equally among the load buses. We first evaluate the impacts of $N-1$ contingency constraint on the TEP results. Table 6.3 summarizes the TEP results with CVSR and without CVSR for the cases that consider and do not consider $N-1$ contingency constraints. The number in the parenthesis indicate the installation year for the new lines and CVSRs.

Table 6.2: Single TEP Results Comparison for the IEEE 24-Bus System Using Decomposed Model

	One CC		Two CC	
	w/o CVSR	w/t CVSR	w/o CVSR	w/t CVSR
Line	14-16 16-17 17-18	16-17	14-16 16-17 17-18	16-17 17-18
CVSR	-	11-14 14-16 15-21 17-18 17-22 21-22	-	11-14 14-16 15-21
Investment cost (M$)	74.25	51.28	74.25	51.28
Operating cost (M$)	1168.59	1183.45	1168.59	1178.91
Total cost (M$)	1242.84	1234.73	1242.84	1230.19
Time (s)	1.15	31.47	1.26	34.71

It can be seen that the two cases lead to different network expansion plan. Without CVSR, 3 lines are built for the first stage and no line is needed for the second stage for the case do not consider $N-1$ security constraints. For the case considering $N-1$ security constraints, 2 transmission lines are committed for the first stage and 1 line is added for the second stage. Although the total number of installed transmission lines are the same for the two cases, one long transmission line (15-21) that costs $69.41M is needed for the case considering $N-1$ security constraint. The construction of this line significantly increases the investment cost for the case considering $N-1$ security constraints. Similar results can also be found in the TEP model with CVSR.

As observed from Table 6.3, for the case considering $N-1$ security constraints, 2 CVSRs on line 11-14 and 14-16 are installed in order to avoid the building of line 14-16. The total savings for this ten year plan is around $16.63M.

Table 6.3: Multi-stage TEP Results Comparison for the IEEE-24 Bus System Using Integrated Model

	Not consider $N-1$		Consider $N-1$	
	w/o CVSR	w/t CVSR	w/o CVSR	w/t CVSR
Lines	14-16 (1) 16-17 (1) 17-18 (1)	16-17 (1)	14-16 (1) 15-21 (1) 6-10 (6)	15-21 (1) 6-10 (6)
CVSR	-	11-14 (1) 14-16 (1) 15-21 (1)	-	11-14 (1) 14-16 (1)
Investment cost (M$)	74.25	37.78	114.76	87.29
Operating cost (M$)	3053.82	3069.82	3049.35	3060.19
Total cost (M$)	3128.07	3107.60	3164.11	3147.48
Time (s)	0.76	15.07	39.19	790.07

Table 6.4 shows the two stage TEP results by using the decomposed model. The same two critical contingencies (line 18-21, 15-21) are considered for the normal and peak load level in stage one and all the load levels in stage two. So the total number of operating states in the master problem is 7 in stage one and 9 in stage two. As observed from Table 6.4, the avoidance of building line 14-16 in stage one is achieved by installing 3 CVSRs on line 11-14, 14-16 and 15-21. In addition, the construction of line 18-21 in the second stage is avoided by installing 2 CVSRs on line 18-21 and 21-22. The total saving on the investment is $44.46M. When comparing the planning results from the integrated model with the results from the decomposed model, one long and expensive transmission line 15-21 ($69.41) is installed in stage one in the integrated model. This result arises since the forward planning is myopic and does not see the future benefits from the present reinforcement [60, 63]. However, the difference of the total cost between the decomposed model and the integrated model is $8.54M for the case considering CVSR, which is only 0.27% of the planning cost. The computation time of the decomposed model is far less than the integrated model. For the case

considering CVSR, the computation time is approximately 18 times faster using the decomposed model.

Table 6.4: Multi-stage TEP Results Comparison for the IEEE 24-Bus System Using Decomposed Model

	Case	
	w/o CVSR	w/t CVSR
Line	14-16 (1) 16-17 (1) 17-18 (1) 6-10 (6) 18-21 (6)	16-17 (1) 17-18 (1) 6-10 (6)
CVSR	-	11-14 (1) 14-16 (1) 15-21 (1) 18-21 (6) 21-22 (6)
Investment cost (M$)	111.68	67.22
Operating cost (M$)	3059.01	3088.80
Total cost (M$)	3170.68	3156.02
Computation Time (s)	2.98	45.13

6.2.2 Polish 2383-Bus System

The approach is also applied to a more practical Polish 2383-bus system. The system has 2895 existing branches, 327 generators and 1822 loads. Single stage planning model is used for this case study. Only a few transmission corridors have the potential for the construction with new lines because of the physical or regulatory constraints. It is assumed for this study that the number of candidate lines is 60. In addition, 80 existing transmission lines have been selected as candidate locations to install the CVSR. The selection criterion is the congestion severity of the transmission lines. The line investment cost is estimated by the approach given in Section 6.2.1. To obtain the contingency list, we first eliminate 643 contingencies that would cause islanding. Then we run the optimal power flow for each of the remaining transmission $N-1$ contingency and take the worst 100 contingencies in terms of the operating cost.

Moreover, the worst 6 contingencies are considered for the peak and normal load level in the master problem. Table 6.5 shows the TEP planning strategy for the case with CVSR and without CVSR by using the decomposed model.

Table 6.5: TEP Results Comparison for the Polish System

	Case	
	w/o CVSR	w/t CVSR
Line	437-220, 515-461 776-539, 1178-834 994-1289, 1417-1284 1632-1644, 1693-1632 1877-1875, 1932-1880 2328-2165, 2365-2261 2348-2379	437-220, 515-461 776-539, 1178-834 994-1289, 1417-1284 1877-1875, 1932-1880 2328-2165, 2365-2261 2348-2379
CVSR	-	310-6, 126-127 613-223, 477-310 939-1416, 1427-1249 1693-1632, 1693-1658
Investment cost (M$)	178.53	182.11
Operating cost (M$)	10474.49	10350.11
Total cost (M$)	10653.02	10532.22
Time (min)	39.23	111.97

As observed from Table 6.5, the TEP without CVSR requires building 13 transmission lines. The total investment cost for this planning strategy is $178.53M. For the TEP with CVSRs, 11 transmission lines and 8 CVSRs are selected. The investment cost increases by $3.58M compared to the case without CVSR. Nevertheless, the operating cost decreases significantly by $124.38M with the inclusion of CVSRs. The saving for this 5 year plan is $120.9M, which accounts for 1.13% of the total planning cost. It can also be seen from Table 6.5 that the operating cost takes up a large portion in the total cost for this practical large scale system. The CVSRs are intended to be installed in the appropriate transmission lines to reduce

congestion and the operating cost. For the peak load level, the hourly operating cost is $35,988 for the case without CVSRs. The cost is reduced to $35,383 when CVSR is introduced.

6.2.3 Computational and Optimality Issues

The computer used for all simulations has an Intel Core(TM) i5-2400M CPU @ 2.30 GHz with 4.00 GB of RAM. The MILP problem is modeled using the YALMIP [96] toolbox in MATLAB with the CPLEX solver [97] selected to solve the model. As mentioned in the introduction, a heuristic method is used for the decomposed model so the global optimality of the solution is not guaranteed. The impacts of decomposition by contingencies can be reduced by including more contingencies in the master problem. This will, however, increase the dimension of the master problem and result in larger computational time. So there is a compromise between solution quality and computational time. Table 6.6 compares the TEP results for the Polish system considering different number of critical contingencies. As can be observed from the table, TEP considering 6 critical contingencies in the master problem give better results than TEP considering 3 critical contingencies. Nevertheless, the computational time is higher for the case considering 6 contingencies. Note that each $N-1$ check subproblem takes around 1.2 s and is independent from each other. If the parallelization techniques are leveraged, the computational time in the subproblem can be significantly reduced and the total time will be largely determined by the master problem.

6.3 Conclusion

In this chapter, the VSR is investigated for improving transmission expansion planning. A security constrained multi-stage TEP model considering VSR is presented. A reformulation technique is leveraged to transform the MINLP model

Table 6.6: TEP Results Comparison for the Polish System Using Decomposed Model Considering Different Number of Critical Contingencies

	Three CC		Six CC	
	w/o CVSR	w/t CVSR	w/o CVSR	w/t CVSR
No. of Line	15	11	13	11
No. of CVSR	-	5	-	8
Investment cost (M$)	191.56	178.99	178.53	182.11
Operating cost (M$)	10466.28	10358.02	10474.49	10350.11
Total cost (M$)	10657.84	10537.01	10653.02	10532.22
Master problem (min)	2.55	48.68	11.34	63.30
Total Time (min)	38.59	94.33	39.23	111.97

into the MILP model so the model can be efficiently solved by commercial solvers. To relieve the computation burden for a practical large scale system, a decomposition approach is introduced to separate the problem into a planning master problem and security analysis sub-problem. Simulation results on two test systems show that if several VSRs are appropriately allocated in the system, the building of new transmission lines can be postponed or avoided. Moreover, the VSRs can change the power flow pattern, which is beneficial in reducing the operating cost. Finally, the installation of VSRs add flexibility to the power system operation and can serve as a corrective action to handle various contingencies.

Chapter 7

Optimal Allocation of a Variable Series Reactor for Large Scale Systems via Benders Decomposition

It has been shown in [102] that the VSR is capable of reducing the generation redispatching and load shedding cost following contingencies. Thus, a more useful investment strategy for the system planners can be achieved if the cost improvements allowed by VSRs considering contingencies are included in the planning process. The authors in [46] adopted the two level hybrid PSO/SQP algorithm to address this problem but the computation burden was large even for a small scale system.

This chapter proposes a new solution approach to optimally allocate VSR in large scale transmission networks considering the base case and a series of $N-1$ transmission contingencies. We consider a single target year for the planning. Three distinct load patterns which represent peak, normal and low load conditions are selected. The original planning model is a large scale mixed integer nonlinear programming (MINLP) model which is difficult to solve for practical systems. The

reformulation technique proposed in Chapter 4 is used to transform the MINLP model into an MILP model. To further relieve the computational burden, a two phase Benders Decomposition separates the problem into base case master problem and a series of subproblems for contingencies. The contributions of this chapter are twofold:

- developed a planning model to allocate VSR in the transmission network considering a multi-scenario framework and solve the model using mathematical programming rather than the heuristic or sensitivity methods so that the quality of the solution can be ensured; and
- implemented a two phase Benders decomposition for the planning problem which shows high performance even for a practical large scale network considering hundreds of operating conditions.

The remaining sections are organized as follows. The detailed optimization model is given in section 7.1. In section 7.2, the solution procedure based on Benders Decomposition is demonstrated. The IEEE 118-bus system and Polish 2383-bus system are selected for case studies in section 7.3. Finally, conclusions are given in section 7.4.

7.1 Problem Formulation

With the reformulation, the complete optimization model can be represented as a large scale MILP.

7.1.1 Objective Function

There are three components in the single target year planning cost: 1) operation cost under normal states; 2) operation cost under contingency states; 3) investment cost

for the VSR. The objective is then:

$$\min_{\Xi_{\mathrm{OM}}} \sum_{b\in\Omega_b}(\pi_{0b}C_{0b} + \sum_{c\in\Omega_c}\pi_{cb}C_{cb}) + \sum_{k\in\Omega_V} A_I\delta_k \tag{7.1}$$

In (7.1), C_{0b} is the operation cost for the normal state under load level b, which can be expressed as:

$$C_{0b} = \sum_{n\in\mathcal{G}} a_n^g P_{n0b}^g \tag{7.2}$$

Note that we assume the linear cost coefficients for the generators here. However, if the quadratic cost curve is required for the generators, the piecewise linearization can be used to linearize the curve [103, 104, 105, 106].

C_{cb} is the operation cost for the contingency state c under load level b, which includes three terms:

$$\begin{aligned} C_{cb} = &\sum_{n\in\mathcal{G}} a_n^g P_{ncb}^g + \sum_{m\in\Omega_D} a_{LS}\Delta P_{mcb}^d \\ &+ \sum_{n\in\mathcal{G}}(a_n^{g,up}\Delta P_{ncb}^{g,up} + a_n^{g,dn}\Delta P_{ncb}^{g,dn}) \end{aligned} \tag{7.3}$$

The first term is the generation cost under each contingency; the second term is the cost for involuntary load shedding; and the third term is the generator rescheduling cost, which indicates that any change from the base operating condition should have a payment to the agent involved [102]. Each operating state is associated with a duration time π_{cb}, the total operating hours for a target year is 8760:

$$\sum_{b\in\Omega_b}\pi_{0b} + \sum_{b\in\Omega_b}\sum_{c\in\Omega_c}\pi_{cb} = A_h \tag{7.4}$$

7.1.2 Constraints

The complete set of constraints are given below in (7.5) to (7.19).

$$P_{kcb} = N_{kcb} b_k \theta_{kcb},\ k \in \Omega_L \backslash \Omega_V \tag{7.5}$$

$$P_{kcb} = N_{kcb}(b_k \theta_{kcb} + w_{kcb}),\ k \in \Omega_V \tag{7.6}$$

$$-M_k y_{kcb} + z_{kcb} b_{k,V}^{\min} \leq w_{kcb} \leq z_{kcb} b_{k,V}^{\max} + M_k y_{kcb}, k \in \Omega_V \tag{7.7}$$

$$-M_k(1 - y_{kcb}) + z_{kcb} b_{k,V}^{\max} \leq w_{kcb} \leq z_{kcb} b_{k,V}^{\min} + M_k(1 - y_{kcb}),\ k \in \Omega_V \tag{7.8}$$

$$-\delta_k \theta_k^{\max} \leq z_{kcb} \leq \delta_k \theta_k^{\max},\ k \in \Omega_V \tag{7.9}$$

$$\theta_{kcb} - (1 - \delta_k)\theta_k^{\max} \leq z_{kcb} \leq \theta_{kcb} + (1 - \delta_k)\theta_k^{\max},\ k \in \Omega_V \tag{7.10}$$

$$\sum_{n \in \mathcal{G}_i} P_{ncb}^g - \sum_{m \in \mathcal{D}_i} (P_{mcb}^d - \Delta P_{mcb}^d) = \sum_{k \in \Omega_L^i} P_{kcb} \tag{7.11}$$

$$-S_{kcb}^{\max} \leq P_{kcb} \leq S_{kcb}^{\max},\ k \in \Omega_L \tag{7.12}$$

$$P_{ncb}^{g,\min} \leq P_{ncb}^g \leq P_{ncb}^{g,\max} \tag{7.13}$$

$$\theta_{ref} = 0 \tag{7.14}$$

$$P_{ncb}^g = P_{n0b}^g + \Delta P_{ncb}^{g,up} - \Delta P_{ncb}^{g,dn},\ n \in \mathcal{G}_{re} \tag{7.15}$$

$$0 \leq \Delta P_{ncb}^{g,up} \leq R_n^{g,up},\ n \in \mathcal{G}_{re} \tag{7.16}$$

$$0 \leq \Delta P_{ncb}^{g,dn} \leq R_n^{g,dn},\ n \in \mathcal{G}_{re} \tag{7.17}$$

$$P_{ncb}^g = P_{n0b}^g,\ n \in \mathcal{G} \backslash \mathcal{G}_{re} \tag{7.18}$$

$$0 \leq \Delta P_{mcb}^d \leq P_{mcb}^d \tag{7.19}$$

Constraints (7.5)-(7.14) hold $\forall c \in \Omega_c \cup \Omega_0, b \in \Omega_b, n \in \mathcal{G}, i \in \mathcal{B}$ and constraints (7.15)-(7.19) hold $\forall c \in \Omega_c, b \in \Omega_b, m \in \mathcal{D}$.

Constraints (7.5)-(7.14) are the operating constraints, including base case and contingencies. Specifically, constraint (7.5) is the power flow on the lines without VSR and constraint (7.6) represents the power flow on the candidate lines to install VSR. We introduce a binary parameter N_{kcb} to denote the corresponding status of the transmission element k in state c at load level b [59]. If $N_{kcb} = 1$, the line flow

equations are forced to hold; otherwise, if the line is in outage, the power flow on that line is forced to be zero. The reformulation considering multiple operating states and load level are denoted by constraints (7.7)-(7.10). Constraints (7.11) ensure the power balance at each bus. The thermal limits of the transmission lines and the active power limits of the generators are considered in (7.12) and (7.13). Note that the short term rating for the transmission line is used for the contingency states, which is 10% higher than the thermal limit under the base operating condition. Finally, constraint (7.14) sets the bus angle of the reference bus to zero.

Constraints (7.15)-(7.19) denote limits under the contingency states. Constraints (7.15)-(7.18) indicate that only a subset of generators are allowed to redispatch their generation during the contingencies and all the other generators should be fixed at their base operating condition. The load shedding amount should not exceed the existing load, which is given in (7.19).

The optimization variables of the complete planning model from (7.1)-(7.19) are the elements in set $\Xi_{\text{OM}} = \{\theta_{kcb}, P^g_{ncb}, \Delta P^d_{mcb}, \Delta P^{g,up}_{ncb}, \Delta P^{g,dn}_{ncb}, \delta_k, y_{kcb}, z_{kcb}, w_{kcb}\}$.

7.2 Solution Approach

The size of the MILP model formulated in Section 7.1 dramatically increases with the system size and the number of considered contingencies, which leads to excessive computations. In order to make the optimization model applicable to a practical large system, Benders Decomposition is used to decompose the original optimization model into a master problem and subproblem. The master problem deals with the base operating condition and the subproblem considers contingencies. The complicating variables between the master problem and subproblem are P^g_{n0b} and δ_k.

It should be noted that the prerequisite for Benders Decomposition is that the objective function of the considered problem projected on the subspace of the complicating variables has a convex envelope [107]. This is not the case in our model due to the existence of the binary flow direction variable y_{kcb} in the subproblem.

In [108], a modified Benders Decomposition (MBD) is developed for the security constrained unit commitment (SCUC) considering the quick-start units. The main idea is to construct a tighter LP subproblem based on the MILP subproblem and use the tighter LP to generate Benders cuts. We propose an alternative two phase approach in section 7.2.3. The simulation results obtained from the proposed approach and MBD are compared in section 7.3.

7.2.1 Master Problem

The master problem considers the base operating condition for the three load levels:

$$\min_{\Xi_{\mathrm{MP}}} \; Z_{down}^{(\nu)} = \sum_{b\in\Omega_b} \pi_{0b} C_{0b}^{(\nu)} + \sum_{k\in\Omega_V} A_I \delta_k^{(\nu)} + \alpha^{(\nu)} \tag{7.20}$$

subject to:

(7.5) – (7.14) and

$$\alpha^{(\nu)} \geq \alpha_{down} \tag{7.21}$$

$$\alpha^{(\nu)} \geq Z^{(l)} + \sum_{b\in\Omega_b}\sum_{n\in\mathcal{G}} \mu_{nb}^{(l)} (P_{n0b}^{g^{(\nu)}} - P_{n0b}^{g^{(l)}}) + \sum_{k\in\Omega_V} \beta_k^{(l)} (\delta_k^{(\nu)} - \delta_k^{(l)}), \; l = 1, \cdots, \nu - 1 \tag{7.22}$$

Constraints (7.20)-(7.22) hold $\forall c \in \Omega_0, b \in \Omega_b, n \in \mathcal{G}, i \in \mathcal{B}$.

The optimization variables of the master problem are those in the set $\Xi_{\mathrm{MP}} = \{\theta_{kcb}, P_{ncb}^{g}, \delta_k, y_{kcb}, z_{kcb}, w_{kcb}, \alpha\}$. Note that all the variables are subject to Benders iteration parameter ν. The first and second term in the objective function are the operating cost in the base case and the investment cost for the VSR. $\alpha^{(\nu)}$ denotes the total operating cost during the contingencies. To accelerate the convergence speed, constraint (7.21) puts a lower bound on $\alpha^{(\nu)}$. Constraint (7.22) represents the Benders cut, which will be generated once per iteration.

7.2.2 Subproblem

The subproblem for contingency state c and load level t is:

$$\min_{\Xi_{\text{SP}}} Z_{cb}^{(\nu)} = C_{cb}^{(\nu)} + \sum_{i \in \mathcal{B}} h_i (s_{icb,1}^{(\nu)} + s_{icb,2}^{(\nu)}) \tag{7.23}$$

subject to

$$(7.5) - (7.10), (7.12) - (7.19) \text{ and}$$

$$\sum_{n \in \mathcal{G}_i} P_{ncb}^{g^{(\nu)}} - \sum_{m \in \mathcal{D}_i} (P_{mcb}^{d} - \Delta P_{mcb}^{d^{(\nu)}}) + s_{icb,1}^{(\nu)} - s_{icb,2}^{(\nu)} = \sum_{k \in \Omega_L^i} P_{kcb}^{(\nu)} \tag{7.24}$$

$$s_{icb,1}^{(\nu)} \geq 0, \; s_{icb,2}^{(\nu)} \geq 0 \tag{7.25}$$

$$P_{n0b}^{g^{(\nu)}} = \hat{P}_{n0b}^{g} \quad : \mu_{ncb}^{(\nu)} \tag{7.26}$$

$$\delta_k^{(\nu)} = \hat{\delta}_k \quad : \beta_{kcb}^{(\nu)} \tag{7.27}$$

Constraints (7.23)-(7.27) hold $\forall c \in \Omega_c, b \in \Omega_b, n \in \mathcal{G}, i \in \mathcal{B}, m \in \mathcal{D}$.

The optimization variables of the subproblem are those in the set $\Xi_{\text{SP}} = \{\theta_{kcb}, P_{ncb}^{g}, \Delta P_{mcb}^{d}, \Delta P_{ncb}^{g,up}, P_{ncb}^{g,dn}, z_{kcb}, y_{kcb}, \delta_k, w_{kcb}, s_{icb,1}, s_{icb,2}\}$. The first term of the objective function is the operating cost in each contingency. Note that although load shedding is allowed in the contingency state, the subproblem can still be infeasible due to generator ramping constraints. Two slack variables $s_{icb,1}^{(\nu)}$ and $s_{icb,2}^{(\nu)}$ are introduced to ensure the subproblem is feasible with h_i a sufficiently large positive constant. The complicating variables are fixed at the value obtained from the master problem in constraints (7.26) and (7.27). $\mu_{ncb}^{(\nu)}$ and $\beta_{kcb}^{(\nu)}$ are the dual variables associated with these two constraints.

The sensitivity used to generate Benders cut is the weighted dual variable, which can be expressed as:

$$\mu_{nb}^{(\nu)} = \sum_{c \in \Omega_c} \pi_{cb} \mu_{ncb}^{(\nu)} \tag{7.28}$$

$$\beta_{k}^{(\nu)} = \sum_{c \in \Omega_c} \sum_{b \in \Omega_b} \pi_{cb} \beta_{kcb}^{(\nu)} \tag{7.29}$$

In the master problem, Z in the Benders cut constraint can be calculated as:

$$Z^{(\nu)} = \sum_{c \in \Omega_c} \sum_{b \in \Omega_b} \pi_{cb} Z_{cb}^{(\nu)} \tag{7.30}$$

With the solution of the subproblem, the upper bound of the objective function for the original problem is calculated as:

$$Z_{up}^{(\nu)} = Z^{(\nu)} + \sum_{b \in \Omega_b} \pi_{0b} \hat{C}_{0b} + \sum_{k \in \Omega_V} A_I \hat{\delta}_k \tag{7.31}$$

The last two terms in (7.31) are calculated using the fixed value of $\hat{P}_{n0b}^{g}$ and $\hat{\delta}_k$.

7.2.3 Solution Procedure

As mentioned at the beginning of this section, a two phase approach is proposed to solve the planning model. The flow chart of the optimization procedure is shown in Fig. 7.1. The detailed description of the proposed algorithm is given below:

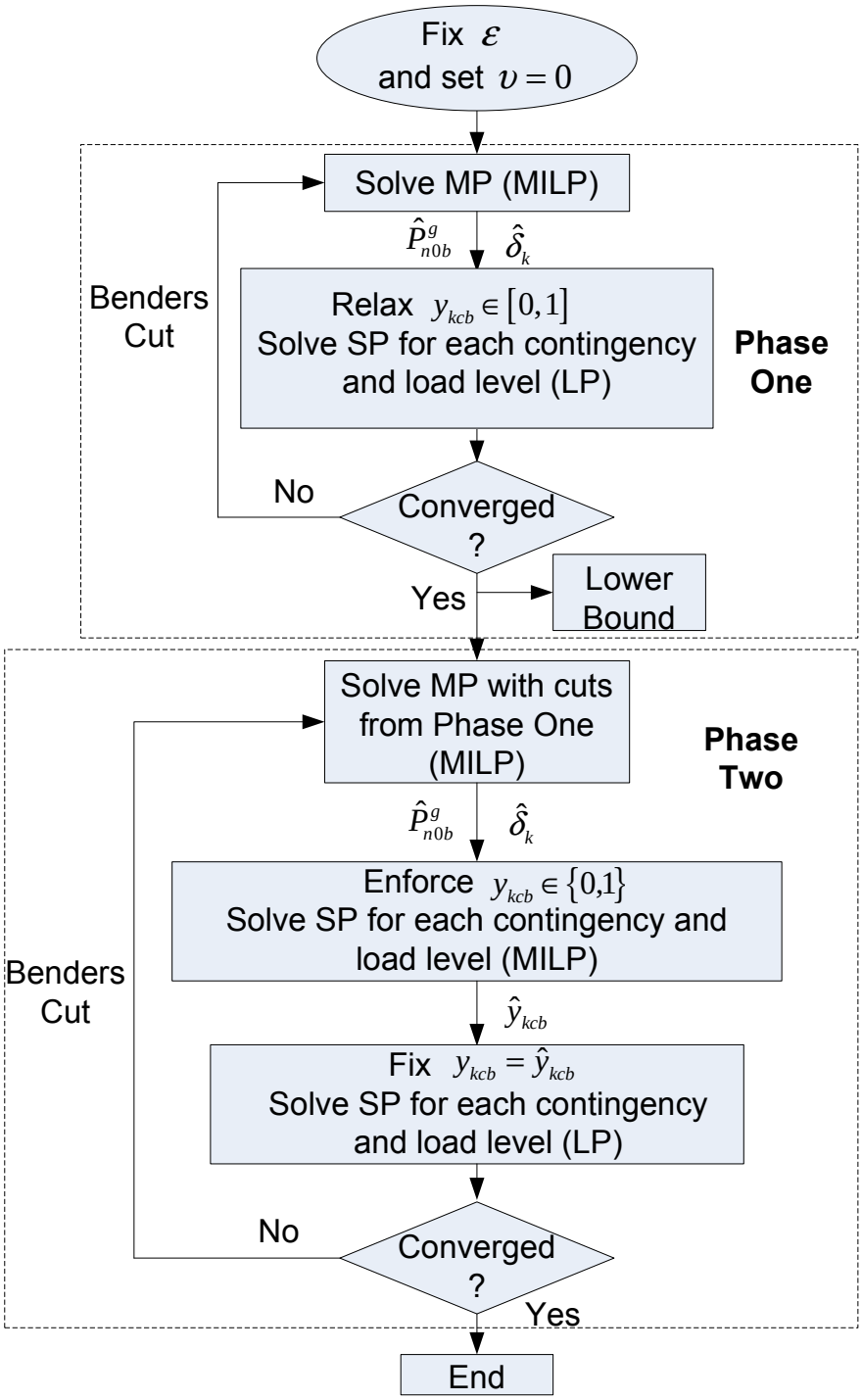

Figure 7.1: Flowchart of the solution approach.

1: **Initialization**: Set a small value ϵ to control the convergence and initiate the iteration counter $\nu = 0$.

2: **Phase one master problem solution**: Solve the master problem considering only the normal operating states. Note that for the first iteration, the master problem is solved without considering any Benders cut, e.g., constraint (7.22).

3: **Relaxed subproblem solution**: With P^{g}_{n0b} and δ_k obtained from the master problem, solve the subproblem as an LP by relaxing the flow direction variable y_{ncb} as a continuous variable in $[0, 1]$.

4: **Convergence check**: If $|Z^{(\nu)}_{up} - Z^{(\nu)}_{down}|/|Z^{(\nu)}_{down}| \leq \epsilon$, the optimal solution for the relaxed original problem is achieved and proceed to phase two. Otherwise, generate Benders cut and go to step 2). Set $\nu \leftarrow \nu + 1$.

5: **Phase two master problem solution**: Solve the master problem while keeping all the Benders cut generated from phase one.

6: **Unrelaxed subproblem solution**: Enforce the binary constraint for the flow direction y_{kcb}. Solve the unrelaxed subproblem into optimality and output the optimal solution $\hat{y}_{kcb}$.

7: **Sensitivities generation**: Fix $y_{kcb} = \hat{y}_{kcb}$. Solve the subproblem and obtain the dual variables associated with constraints (7.26) and (7.27).

8: **Convergence check**: If $|Z^{(\nu)}_{up} - Z^{(\nu)}_{down}|/|Z^{(\nu)}_{down}| \leq \epsilon$, the optimal solution is obtained. Otherwise, generate Benders cut and go to step 5). Set $\nu \leftarrow \nu + 1$.

The two phase approach is an efficient method to accelerate convergence of Benders Decomposition [109]. In phase one, we solve the master problem with the relaxed subproblem at optimality. All the Benders cuts generated in phase one are valid for the original problem. The reason is that the relaxed subproblem provides a lower bound on the original subproblem so that it will also generate a valid lower

bound for α [110]. In addition, the objective value obtained from phase one provides a lower bound for the original problem, which can be used to evaluate the quality of the final solution. In phase two, the generation of the Benders cut is heuristic because it involves fixing the binary variable y_{kcb}. Although it cannot ensure a global optimum, our case studies show that the solution obtained is very close to the lower bound of the original problem. Therefore, the solution is of high quality from an engineering point of view.

7.3 Numerical Case Studies

The IEEE 118-bus and the Polish 2383-bus system are selected to test the effectiveness of our planning model. The system data can be found in the MATPOWER package [87]. There is only one load pattern defined for these standard systems. For the IEEE 118-bus system, we treat the given load as the normal load level. The peak load level is 20% higher than the given load and the lower load level is 20% lower. For the Polish system, the given load data is the winter peak so we treat the normal load level and low load level as 80% and 60% of the given load, respectively. All simulations are performed on a personal computer with an Inter Core(TM) i5-2400M CPU @ 2.30 GHz and 4.00 GB of RAM. The problem is modeled by using the MATLAB toolbox YALMIP [96] with CPLEX [97] as the solver.

In this case study, we investigate the allocation strategy for one typical VSR: TCSC. The allowable compensation range of TCSC varies from -70% to +20% of the corresponding line reactance[47]. Thus, the physical limits for b_k^V are $-\frac{1}{6x_k} \leq b_k^V \leq \frac{7}{3x_k}$. M_k is selected as $|\frac{7}{3x_k}\theta_k^{\max}|$. The investment cost of the TCSC is dependent on its operating range. The annual investment cost A_I is converted from the total investment cost by using the interest rate and life span of the TCSC [34, 46]. In this work, the interest rate is selected to be 5% and the life span of TCSC is 5 years [47].

7.3.1 IEEE 118-Bus System

The IEEE-118 bus system has 118 buses, 177 transmission lines, 9 transformers and 19 generators. The total load at the peak level is 4930 MW and the generation capacity is 6466 MW. The thermal flow limits are decreased artificially to create congestion. In a real power system, it is unnecessary to consider every transmission line as the candidate location to install FACTS device due to some physical or economic limitations. A preliminary study based on the sensitivity approach in [42] is adopted to obtain the candidate locations for TCSC. In this case study, 30 transmission lines are selected as the candidate locations. In addition, 30 contingencies which significantly affect the planning cost are considered so the number of operating states is 93 for this test case.

Table 7.1 provides the comparison for the non-decomposed approach, the MBD approach and proposed Benders algorithm. The non-decomposed model indicates solving the complete model in Section 7.1 directly [111]. For the large scale optimization problem, it may take excessive time to get the solution within the default mipgap (0.01%) in CPLEX. For comparison purpose, we just seek a solution within a given computation time. As shown in the table, the total planning cost for the non-decomposed model is $1099.59M with an mipgap 1.47% after 3 hours. In addition, two TCSCs are selected to be installed in the system. The results for the MBD approach show that five TCSCs should be installed in the system and the total planning cost is $1090.03M . The computation time decreases significantly by using the MBD, which is only 315.86 s. The proposed Benders algorithm suggest to install six TCSCs in the system and the total planning cost is $1088.21M. The lower bound from phase one for this test system is $1087.20M, indicating that the solution obtained by the proposed approach is close enough to the global optimal solution. Compared with the computation time given by MBD, a further time reduction (70 s) can be achieved by using the proposed Benders algorithm.

Table 7.1: Comparison of the Investment Results for IEEE 118-Bus System

Approach	Non-decomposed [111]	MBD [108]	Proposed BD
TCSC Locations $(i-j)$	(26-30),(30-38)	(17-31),(20-21) (26-30),(22-23) (30-38)	(17-31),(20-21) (21-22),(26-30) (22-23),(30-38)
Investment [million $]	1.64	2.68	2.94
Total Cost [million $]	1099.59	1090.03	1088.21
CPU time	3.00 [hours]	315.86 [s]	244.81 [s]

Fig. 7.2 shows that hourly generation cost for each operating state under the peak and normal load level. The generation cost reduction can be observed for all the operating states by installing TCSCs into the network. The hourly generation cost for the base case during the peak load level is $167,653 per hour without any TCSC. This cost decreases to $156,907 per hour with the installation of six TCSCs. The cost reduction is mainly due to the congestion relief which enable more power to be delivered from the cheaper generators. It can also be seen that the generation cost reduction in the normal load level is not as much as that in the peak load level for all the operating states except for contingency (25-27).

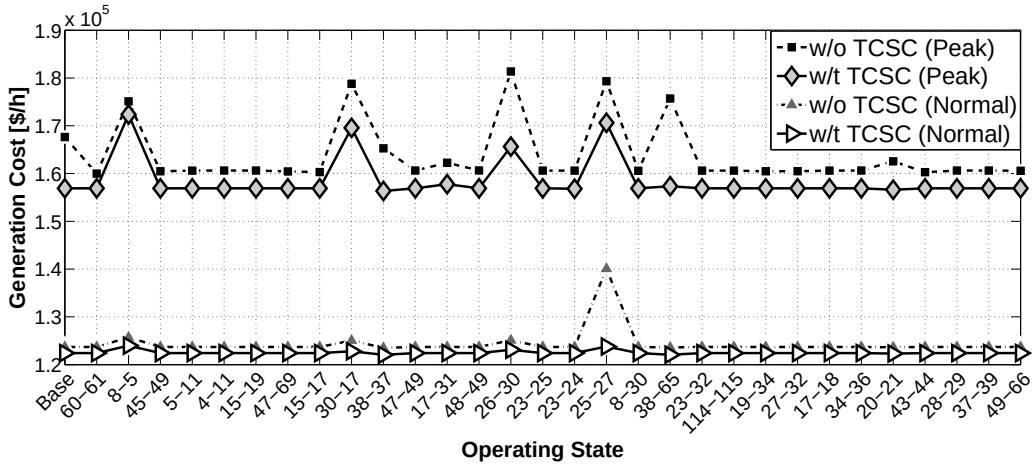

Figure 7.2: Hourly generation cost for peak and normal load level.

Fig. 7.3 provides generation rescheduling amount under different contingencies for the peak load level. Fig. 7.4 gives the load shedding amount in the peak load level for the five contingencies which involve load shedding. Note that there is no involuntary load shedding for all the operating states under normal and low load level. From Fig. 7.3, it can be seen that the amount of generation rescheduling decreases in the majority of operating states. The largest reduction occurs under contingency (8-5) where the amount of generation rescheduling decreases from 1200 MW to about 600 MW. In contingency (25-27), the rescheduling amount increases for about 300 MW with TCSC. However, about 60 MW load shedding can be avoided in that contingency as shown in Fig. 7.4. This indicates that the installation of TCSC enable cheaper ways, such as, rescheduling to resolve load shedding. As can be seen in Fig. 7.4, the load shedding for contingency (30-17), (38-37), (26-30) and (25-27) are eliminated with TCSC. For the most severe contingency (8-5), the load shedding decreases from 76.36 MW to 15.30 MW.

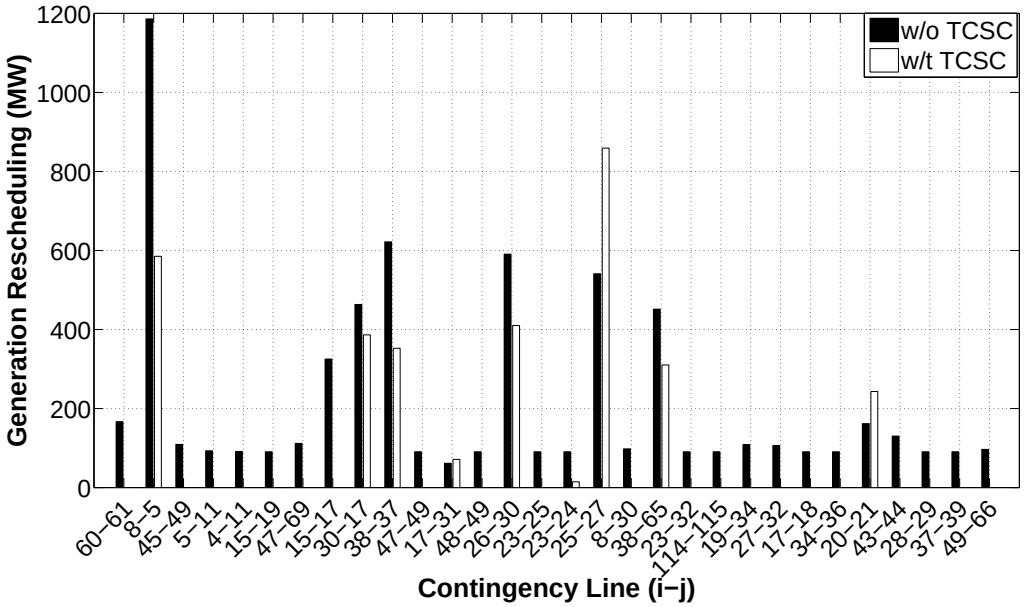

Figure 7.3: Generation rescheduling under different contingencies for the peak load level.

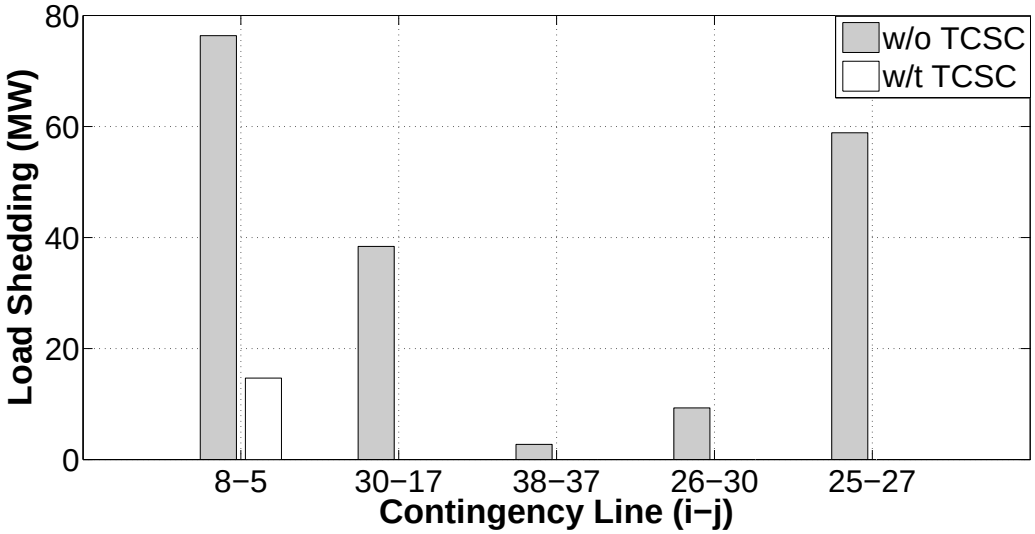

Figure 7.4: Load shedding amount under different contingencies for peak load level.

Table 7.2 compares the annual planning cost for the case with and without TCSC. We categorize the planning cost into four groups: 1) generation cost; 2) generation rescheduling cost; 3) load shedding cost; 4) Investment cost on TCSC. Except for the investment on TCSC, it can be seen that the cost decreases in all the categories with the installation of TCSCs. The annual reduction for the total planning cost is about \$36.58M, which is approximately 3.25% of the annual planning cost.

Table 7.2: Annual Planning Cost with and without TCSC for IEEE 118-Bus System

Cost Category	Annual Cost [million \$]	
	w/o TCSC	w/t TCSC
Generation cost in normal state	1048.31	1018.74
Generation cost in contingency	66.58	65.30
Rescheduling cost	1.09	0.54
Load shedding cost	8.81	0.70
Investment on TCSC	-	2.94
Total cost	1124.79	1088.21

7.3.2 Polish System

The Polish system includes 2,383 buses, 327 generators, 2,728 transmission lines and 168 transformers. The total load at the peak level is 20,465 MW and the generation

capacity is 29594 MW. Based on sensitivity method, we select 50 candidate locations to install TCSC. We consider 60 contingencies so the number of operating states for this test system is 183.

The planning model suggests 15 transmission lines to be installed with TCSCs. These lines are (29-13), (1342-1301), (1948-1649), (432-356), (920-821), (395-334), (7-4), (10-3), (493-306), (11-4), (152-66), (612-413), (1489-1431), (833-1230) and (1055-1079). Table 7.3 provides the comparison of the planning cost for the case with and without TCSC. The annual savings for the Polish system is about $64.5M.

Table 7.3: Annual Planning Cost with and without TCSC for the Polish System

Cost Category	Annual Cost [million $]	
	w/o TCSC	w/t TCSC
Generation cost in normal state	9527.18	9464.42
Generation cost in contingency	1299.87	1291.18
Rescheduling cost	6.28	4.83
Load shedding cost	9.59	5.55
Investment on TCSC	-	12.43
Total cost	10842.93	10778.41

Fig. 7.5 illustrates the iteration process of the proposed Benders algorithm. The convergence tolerance ϵ is selected to be 0.35%. It can be seen that after 5 iterations, the problem in phase one is converged with the lower bound to be $10774.27M. Then it takes another 5 iteration for the problem in phase two to be converged. The computation time for this practical large scale system is about 1.50 hours, which is fast enough for the considered planning problem. Note that the subproblem in the proposed algorithm is independent from each other so the computation time can be further reduced if parallel computing is implemented.

7.4 Conclusion

This chapter proposes a planning model to allocate VSR considering different operating conditions and critical $N-1$ contingencies. The original planning model is

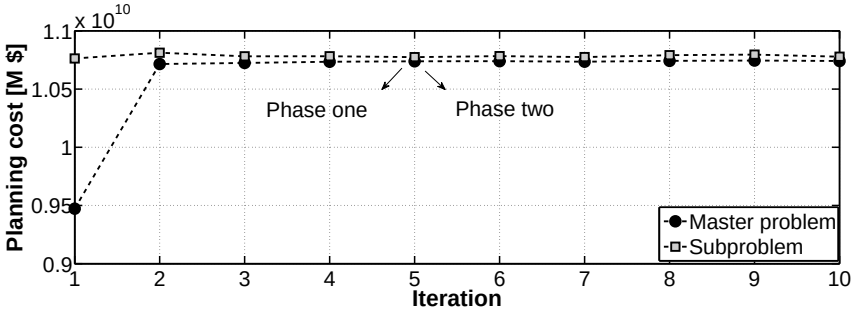

Figure 7.5: Evolution of the proposed Benders algorithm.

a large scale MINLP model. A reformulation is introduced to transform the MINLP model into a MILP model. To further reduce the computation burden, a two phase Benders decomposition is proposed. The solution obtained is not guaranteed to be a global optimum but analysis indicates the solution is near optimal. Case studies on the IEEE 118-bus and the Polish system demonstrate the performance of the proposed algorithm. The simulation results show that the generation cost for both the normal operating states and contingency states can be reduced with the installation of VSR. In addition, the cost reductions can be observed in the generation rescheduling and involuntary load shedding following contingencies.

Chapter 8

Conclusion and Future Work

8.1 Conclusion

The electric power system has undergone considerable changes over the last decades. First, there is an increase in distributed smaller generation, which is often from renewable energy sources [112, 113]. Due to the intermittent nature of the renewable sources, the power injections as well as the power flows in the system have become more variable and less predictable by the system operators. Second, the power market trades has resulted in a significant increase in the variability of long distance transactions. These transactions can lead to additional stress on the system. Third, as the traditional vertically integrated power companies are separated into generator companies, transmission system operators (TSO), distributed system operators (DSO) and retailers, operators have reduced control over the loads and generation but active control of the transmission can help compensate.

In order to respond to these changes, this work investigates application of an Variable Series Reactor (VSR) for power flow control. Chapter 3 introduces a recently proposed VSR-like device called Continuously Variable Series Reactor (CVSR). It is a simple, cost effective device which can be used to modulate the transmission line reactance. The basic configuration and operating principle are presented in Chapter

3. A CVSR prototype which is rated at 480 V has already been developed and tested in ORNL. The lab test results are discussed in Section 3.2.

In Chapter 4, to evaluate the capability of the VSR in the power system, an optimization approach is developed for finding the locations and settings of VSR assuming numerous devices could be installed in a single system. The optimization approach benefits from the maturity of the SQP algorithm and the formulation is applicable for both off-line planning and on-line analysis functions.Two IEEE sample systems and a subsystem of the WECC system is analyzed and shows that the system loadability and maximum transfer capability can be significantly improved by several well located VSRs, especially under line outage conditions.

A drawback of the approach proposed in Chapter 4 is that the locations of the VSR are obtained based on a specific operating condition. If the operation condition is changed, the algorithm should be re-run to obtain a new VSR placement strategy. These two allocations of VSR could be quite different. Accordingly, a planning/operation tool is proposed in Chapter 5 to find optimal locations of the VSR considering multi-scenarios, including the base case and critical contingencies. The original MINLP model is transformed to an MILP model using the proposed reformulation technique. The computation time is sufficiently fast for both planning and operation studies.

In Chapter 6, the VSR is introduced into the Transmission Expansion Planning (TEP) problem. The security constrained multi-stage TEP with the consideration of CVSR is formulated as a large scale MILP model. To relieve the computational burden for the practical large scale network, a decomposition approach is proposed to separate the complete model into master planning problem and security check subproblem. The simulation results demonstrate that the total planning cost can be reduced if several VSRs are placed appropriately in the transmission network.

To investigate the economic benefits of VSRs in the contingencies, Chapter 7 proposes a planning model to address the optimal investment of VSRs. A single target year with three distinct load patterns is considered and the transmission

$N-1$ contingencies have a probability to occur in any of the three load levels. The coupling constraints between the base operating condition and the contingency are also incorporated in the planning model. A two phase Benders decomposition algorithm is used to solve the large scale MILP model. The simulation results on IEEE 118-bus and the Polish system show that the VSRs are capable of decreasing the generation cost in both the base operating condition and contingencies. Moreover, the cost reductions can also be observed in the generation rescheduling and load shedding during the contingencies.

8.2 Future Work

Based on the work to date, two directions for further work are suggested.

8.2.1 Minimizing Wind Power Spillage with a Variable Series Reactor

Wind power has become the largest portion of the newly added renewable power generation in the United States since 2000. Wind generation has reached over 61 GW installed capacity in 2013 and it is expected to supply 20% and 30% of end-use electricity demand by 2030 and 2050, respectively [114]. The increasing penetration of wind generation not only brings great opportunities but also new challenges to the operation of the power grid [115, 116]. One of the major challenges is to integrate wind generation without compromising the reliability and efficiency of the power system. The integration issue is largely caused by the variability of the wind and the limited transmission capacity in the existing grid [117, 118, 119]. For example, when large amount of output from a wind farm coincides with the load valley (load falloff in the evening), some of the wind turbines may have to be shut down in certain parts of the power system if insufficient transmission capacity is available. As shown in this dissertation, VSR has the ability to enhance the utilization of the existing network and

improve the operation flexibility. Hence, it can be utilized to help integrating the wind power to the transmission network. To incorporate the intermittent characteristics of wind power, a stochastic or robust optimization model should be introduced. In addition, the bilevel optimization model [120, 121] can be leveraged to obtain the investment decision within electricity market environment.

8.2.2 Combining the Variable Series Reactor with Other Power Flow Control Approaches

As shown in Chapter 2, there are other power flow control approaches such as Phase Shifting Transformer (PST) and Transmission Switching (TS). It may be interesting to combine the VSR with other power flow control approaches and investigate the operational benefits brought by bringing multiple techniques together.

8.2.3 Emulation of CVSR on the CURENT Hardware Testbed

The Hardware Testbed (HTB) in the CURENT research center is a scaled Hardware Universal Grid Emulator (HUGE) which allows testing and demonstration of key technologies on monitoring, control, actuation and visualization [122, 123]. Several emulators have already been integrated in the system such as the synchronous generator emulator [124, 125], transmission line emulator [126], induction motor emulator [127], solar power emulator [128, 129] and wind turbine emulator [130]. It would be interesting to design a suitable emulator for the CVSR to evaluate its power flow control function in real time.

Bibliography

[1] S. Stoft, *Power System Economics: Designing Market for Electricity.* New York, NY, USA: Wiley-IEEE Press, 2002. 1

[2] X. Zhang, C. Rehtanz, and B. Pal, *Flexible AC Transmission Systems: Modelling and Control.* London, UK: Springer, 1999. 1, 2, 8

[3] T. T. Lie and W. Deng, "Optimal flexible AC transmission systems (FACTS) devices allocation," *Electrical Power Energy Syst.*, vol. 19, no. 2, pp. 125–134, Feb. 1997. 2

[4] A. K. Sharma, "Optimal number and location of TCSC and loadability enhancement in deregulated electricity markets using MINLP," *International Journal of Emerging Electric Power Syst.*, vol. 5, no. 1, pp. 1–15, Mar. 2006. 2, 11

[5] C. Schaffner and G. Andersson, "Performance of a TCSC for congestion relief," in *Proc. IEEE Power Tech.*, St. Pertersburg, Russia, Jun. 27–30, 2005. 2

[6] N. G. Hingorani and L. Gyugyi, *Understanding FACTS: Concepts and Technology of Flexible AC Transmission System.* New York, NY, USA: Wiley-IEEE Press, 1999. 2

[7] L. Gyugyi, C. D. Schauder, and K. Sen, "Static synchronous series compensator: A solid approach to the series compensation of transmission lines," *IEEE Trans. Power Del.*, vol. 12, no. 1, pp. 406–413, Jan. 1997. 2

[8] Y. Xiao, Y. H. Song, C. C. Liu, and Y. Z. Sun, "Available transfer capability enhancement using FACTS devices," *IEEE Trans. Power Syst.*, vol. 18, no. 1, pp. 305–312, Feb. 2003. 2

[9] D. M. Divan, W. E. Brumsickle, R. S. Schneider, B. Kranz, R. W. Gascoigne, D. T. Bradshaw, M. R. Ingram, and I. S. Grant, "A distributed static series compensator system for realizing active power flow control on existing power lines," *IEEE Trans. Power Del.*, vol. 1, no. 22, pp. 642–649, Jan. 2007. 2

[10] Smart Wires. [Online]. Available: http://www.smartwires.com/technology/. 2

[11] Green Electricity Network Integration. [Online]. Available: http://arpa-e.energy.gov/?q=arpa-e-programs/geni. 2

[12] A. Dimitrovski, Z. Li, and B. Ozpineci, "Magnetic amplifier-based power flow controller," *IEEE Trans. Power Del.*, vol. 30, no. 4, pp. 1708–1714, Aug. 2015. 3, 15, 64

[13] S. Zheng, J. Wang, F. Yang, F. Wang, L. M. Tolbert, and D. J. Costinett, "A dc controller for continuous variable series reactors (CVSRs)," in *Energy Conversion Congress and Exposition (ECCE)*, 2015, pp. 5786–5793. 3

[14] P. Kundur, *Power System Stability and Control.* New York, NY, USA: McGraw-Hill, 1994. 5

[15] G. Wolf, J. Skliutas, G. Drobnjak, and M. D. Costa, "Alternative method of power flow control using air core series reactors," in *Proc. IEEE Power Eng. Soc. Gen. Meeting*, vol. 2, Jul. 2003, pp. 574–580. 6

[16] K. Papp, G. Christiner, H. Popelka, and M. Schwan, "High voltage series reactors for load flow control," *Elektrotechnik und Informationstechnik*, vol. 121, no. 12, pp. 455–460, Dec. 2004. 6

[17] R. Baker, G. Guth, W. Egli, and P. Eglin, "Control algorithm for a static phase shifting transformer to enhance transient and dynamic stability of large power systems," *IEEE Trans. Power App. Syst.*, vol. PAS-101, no. 9, pp. 3532–3542, Sep. 1982. 6

[18] R. D. Youssef, "Phase-shifting transformers in load flow and short-circuit analysis: modeling and control," *IET Gener., Transm., Distrib.*, vol. 140, no. 4, pp. 331–336, Jul. 1993. 6

[19] N. Johansson, "Aspects on dynamic power flow controllers and related devices for increased flexibility in electric power systems," Ph.D. dissertation, Royal Institute of Technology, Stockholm, 2011. [Online]. Available: http://www.diva-portal.org/smash/get/diva2:435280/FULLTEXT02. 6

[20] G. Yang, "Applying advanced methods to power system planning studies," Ph.D. dissertation, Univ. of Queensland, Brisbane, Aug. 2008. [Online]. Available: http://espace.library.uq.edu.au/view/UQ:159218. 6

[21] H. J. Koglin and H. Müller, "Corrective switching: a new dimension in optimal load flow," *Int. Journal of Electrical Power & Energy Systems*, vol. 4, no. 2, pp. 142–149, Apr. 1982. 8

[22] R. Bacher and H. Glavittsch, "Network topology optimization with security constraints," *IEEE Trans. Power Syst.*, vol. 1, no. 4, pp. 103–111, Nov. 1986. 8

[23] R. Bacher and H. Glavitsch, "Loss reduction by network switching," *IEEE Trans. Power Syst.*, vol. 3, no. 2, pp. 447–454, May 1988. 8

[24] G. Schnyder and H. Glavitsch, "Integrated security control using an optimal power flow and switching concepts," *IEEE Trans. Power Syst.*, vol. 3, no. 2, pp. 782–790, May 1988. 9

[25] ——, "Security enhancement using an optimal switching power flow," *IEEE Trans. Power Syst.*, vol. 5, no. 2, pp. 674–681, May 1990. 9

[26] W. Shao and V. Vittal, "Corrective switching algorithm for relieving overloads and voltage violations," *IEEE Trans. Power Syst.*, vol. 20, no. 4, pp. 1877–1885, Nov. 2005. 9

[27] M. A. Khorsand and K. W. Hedman, "Day-ahead corrective transmission topology control," in *Proc. IEEE Power Eng. Soc. Gen. Meeting*, National Harbor, MD, USA, Jul. 27–31, 2014, pp. 1–5. 9

[28] R. P. O'Neill, R. Baldick, U. Helman, M. H. Rothkopf, and W. Stewart, "Dispatchable transmission in RTO market," *IEEE Trans. Power Syst.*, vol. 20, no. 1, pp. 171–179, Feb. 2005. 9

[29] E. B. Fisher, R. P. O'Neill, and M. C. Ferris, "Optimal transmission switching," *IEEE Trans. Power Syst.*, vol. 23, no. 3, pp. 1346–1355, Aug. 2008. 9

[30] K. W. Hedman, R. P. O'Neill, E. B. Fisher, and S. S. Oren, "Optimal transmission switching-sensitivity analysis and extensions," *IEEE Trans. Power Syst.*, vol. 23, no. 3, pp. 1469–1479, Aug. 2008. 9

[31] ——, "Optimal transmission switching with contingency analysis," *IEEE Trans. Power Syst.*, vol. 24, no. 3, pp. 1577–1586, Aug. 2009. 9, 47

[32] A. Khodaei and M. Shahidehpour, "Transmission switching in security-constrained unit commitment," *IEEE Trans. Power Syst.*, vol. 25, no. 4, pp. 1937–1945, Nov. 2010. 9

[33] N. Yorino, E. E. El-Araby, H. Sasaki, and S. Harada, "A new formulation for FACTS allocation for security enhancement against voltage collapse," *IEEE Trans. Power Syst.*, vol. 18, no. 1, pp. 3–10, Feb. 2003. 10

[34] L. J. Cai, I. Erlich, and G. Stamtsis, "Optimal choice and allocation of FACTS devices in deregulated electricity market using genetic algorithms," in *Proc. IEEE PES Power Syst. Conf. Expo.*, vol. 1, Oct. 2004, pp. 201–207. 10, 83

[35] S. Gerbex, R. Cherkaoui, and A. J. Germond, "Optimal location of multi-type FACTS devices in a power system by means of genetic algorithm," *IEEE Trans. Power Syst.*, vol. 16, no. 3, pp. 537–543, Aug. 2001. 10

[36] A. Alabduljabbar and J. V. Milanovic, "Robust allocation of FACTS devices for improved techno-economic operation of power systems," in *Proc. of the 7th IASTED International Conference on Power and Energy Systems*, Palma de Mallorca, Aug. 29–31, 2007, pp. 444–449. 10

[37] G. I. Rashed, Y. Sun, and H. I. Shaheen, "Optimal TCSC placement in a power system by means of differential evolution algorithm considering loss minimization," in *Proc. 2011 6th IEEE Conference on Industrial Electronics and Applications (ICIEA)*, Jun. 2011, pp. 2209–2215. 10

[38] P. Jirapong and W. Ongsakul, "Optimal placement of multi-type FACTS devices for total transfer capability enhancement using hybrid evolutionary algorithm," *Electric Power Components and Systems*, vol. 35, no. 9, pp. 981–1005, Sep. 2007. 10

[39] M. Saravanan, S. M. R. Slochanal, R. Venkatesh, and J. P. S. Abrahamh, "Application of PSO technique for optimal location of FACTS devices considering system loadability and cost of installation," *Elect. Power Syst. Res.*, vol. 77, no. 3, pp. 276–283, Mar. 2007. 10

[40] S. Panda and N. P. Padhy, "Optimal location and controller design of STATCOM for power system stability improvement using pso," *Journal of the Franklin Institute*, vol. 345, no. 2, pp. 166–181, Mar. 2008. 10

[41] J. G. Singh, S. N. Singh, and S. C. Srivastava, "An approach for optimal placement of static var compensators based on reactive power spot price," *IEEE Trans. Power Syst.*, vol. 22, no. 4, pp. 2021–2029, Nov. 2007. 10

[42] T. Orfanogianni and R. Bacher, "Steady-state optimization in power systems with series FACTS devices," *IEEE Trans. Power Syst.*, vol. 18, no. 1, pp. 19–26, Feb. 2003. 10, 84

[43] A. Samimi and P. Naderi, "A new method for optimal placement of TCSC based on sensitivity and congestion management," *Smart Grid and Renewable Energy*, vol. 3, no. 1, pp. 10–16, Feb. 2012. 10

[44] Y. Lu and A. Abur, "Static security enhancement via optimal utilization of thyristor-controlled series capacitors," *IEEE Trans. Power Syst.*, vol. 17, no. 2, pp. 324–329, May 2002. 10

[45] Y. Xiao, Y. H. Song, and Y. Z. Sun, "Power flow control approach to power systems with embedded FACTS devices," *IEEE Trans. Power Syst.*, vol. 17, no. 4, pp. 943–950, Nov. 2002. 10

[46] R. S. Wibowo, N. Yorino, M. Eghbal, Y. Zoka, and Y. Sasaki, "FACTS devices allocation with control coordination considering congestion relief and voltage stability," *IEEE Trans. Power Syst.*, vol. 26, no. 4, pp. 2302–2310, Nov. 2011. 10, 73, 83

[47] P. K. Tiwari and Y. R. Sood, "An efficient approach for optimal allocation and parameters determination of TCSC with investment cost recovery under competitive power market," *IEEE Trans. Power Syst.*, vol. 28, no. 3, pp. 2475–2484, Aug. 2013. 11, 83

[48] F. G. M. Lima, F. D. Galiana, I. Kockar, and J. Munoz, "Phase shifter placement in large-scale system via mixed integer linear programming," *IEEE Trans. Power Syst.*, vol. 18, no. 3, pp. 1029–1034, Aug. 2003. 11

[49] G. Yang, G. Hovland, R. Majumder, and Z. Dong, "TCSC allocation based on line flow based equations via mixed-integer programming," *IEEE Trans. Power Syst.*, vol. 22, no. 4, pp. 2262–2269, Nov. 2007. 11

[50] M. E. Baran and F. F. Wu, "Optimal sizing of capacitors placed on a radial distribution system," *IEEE Trans. Power Del.*, vol. 4, no. 1, pp. 735–743, Jan. 1989. 11, 13

[51] R. W. Chang and T. K. Saha, "Maximizing power system loadability by optimal allocation of SVC using mixed integer linear programming," in *Proc. IEEE*

Power Eng. Soc. Gen. Meeting, Minneapolis, MN, USA, Jul. 25–29, 2010, pp. 1–7. 11

[52] R. W. Chang, T. Kuo, and T. K. Saha, "Mixed-integer method for optimal upfc placement based on line flow-based equations," in *Proc. 20th Australasian Universities Power Engineering Conf. (AUPEC)*, Christchurch, New Zealand, Dec. 5–8, 2010, pp. 1–6. 11

[53] X. Zhang, D. Shi, Z. Wang, J. Huang, X. Wang, G. Liu, and K. Tomsovic, "Optimal allocation of static var compensator via mixed integer conic programming," in *IEEE Power and Energy Society General Meeting*, Chicago, IL, USA, Jul. 16–20, 2017, pp. 1–5. 11

[54] T. Ding, R. Bo, F. Li, and H. Sun, "Optimal power flow with the consideration of flexible transmission line impedance," *IEEE Trans. Power Syst.*, vol. 31, no. 2, pp. 1655–1656, Mar. 2016. 11

[55] M. S. Ardakani and K. W. Hedman, "A fast LP approach for enhanced utilization of variable impedance based FACTS devices," *IEEE Trans. Power Syst.*, vol. 31, no. 3, pp. 2204–2213, May 2016. 11, 41

[56] R. Minguez, F. Milano, R. Zarate-Minano, and A. J. Conejo, "Optimal network placement of SVC devices," *IEEE Trans. Power Syst.*, vol. 22, no. 4, pp. 1851–1860, Nov. 2007. 11, 21

[57] R. S. Wibowo, T. P. Fathurrodli, O. Penangsang, and A. Soeprijanto, "Security constrained optimal power flow with facts devices using bender decomposition," in *Proc. TENCON 2014-2014 IEEE Region 10 Conference*, Oct. 2014, pp. 1–5. 12

[58] J. Mohammadi, G. Hug, and S. Kar, "A benders decomposition approach to corrective security constrained opf with power flow control devices," in *Proc. IEEE PES General Meeting*, Jul. 2013, pp. 1–6. 12

[59] H. Zhang, V. Vittal, G. T. Heydt, and J. Quintero, "A mixed-integer linear programming approach for multi-stage security-constrained transmission expansion planning," *IEEE Trans. Power Syst.*, vol. 27, no. 2, pp. 1125–1133, May 2012. 12, 32, 43, 51, 58, 76

[60] R. A. Jabr, "Optimization of AC transmission system planning," *IEEE Trans. Power Syst.*, vol. 28, no. 3, pp. 2779–2787, Aug. 2013. 12, 61, 68

[61] G. C. Oliveira, S. Binato, M. Pereira, and L. M. Thomé, "Multi-stage transmission expansion planning considering multiple dispatches and contingency criterion," in *Anais do Congresso Brasileiro de Automática 2004*, Gramado, RS, Brazil, Sep. 21–24, 2004, paper 505. 12

[62] N. Alguacil, A. L. Motto, and A. J. Conejo, "Transmission expansion planning: A mixed-integer LP approach," *IEEE Trans. Power Syst.*, vol. 18, no. 3, pp. 1070–1077, Aug. 2003. 12

[63] G. Vinasco, M. J. Rider, and R. Romero, "A strategy to solve the multistage transmission expansion planning problem," *IEEE Trans. Power Syst.*, vol. 26, no. 4, pp. 2574–2576, Nov. 2011. 12, 61, 68

[64] H. Zhang, G. T. Heydt, V. Vittal, and J. Quintero, "An improved network model for transmission expansion planning considering reactive power and network losses," *IEEE Trans. Power Syst.*, vol. 27, no. 3, pp. 3471–3479, Aug. 2013. 13

[65] T. Akbari and M. T. Bina, "A linearized formulation of AC multi-year transmission expansion planning: A mixed-integer linear programming approach," *Elect. Power Syst. Res.*, vol. 114, pp. 93–100, Sep. 2014. 13

[66] J. A. Taylor and F. S. Hover, "Linear relaxations for transmission expansion planning," *IEEE Trans. Power Syst.*, vol. 26, no. 4, pp. 2533–2538, Nov. 2011. 13

[67] J. B. Lasserre, "Polynomial programming: LP-relaxations also converge," *SIAM J. Optim.*, vol. 15, no. 2, pp. 383–393, 2005. 13

[68] J. A. Taylor and F. S. Hover, "Conic AC transmission system planning," *IEEE Trans. Power Syst.*, vol. 28, no. 2, pp. 952–959, May 2013. 13

[69] A. H. Escobar, R. A. Gallego, and R. Romero, "Multi-stage and coordinated planning of the expansion of transmission systems," *IEEE Trans. Power Syst.*, vol. 19, no. 2, pp. 735–744, May 2004. 13

[70] S. Binato, G. C. D. Oliveira, and J. L. D. Araújo, "A greedy randomized adaptive search procedure for transmission expansion planning," *IEEE Trans. Power Syst.*, vol. 16, no. 2, pp. 247–253, May 2001. 13

[71] Y. Jin, H. Cheng, J. Yan, and L. Zhang, "New discrete method for particle swarm optimization and its application in transmission network expansion planning," *Elect. Power Syst. Res.*, vol. 77, no. 3, pp. 227–233, Mar. 2007. 13

[72] J. Zhao, Z. Dong, P. Lindsay, and K. Wong, "Flexible transmission expansion planning with uncertainties in an electricity market," *IEEE Trans. Power Syst.*, vol. 24, no. 1, pp. 479–488, Feb. 2009. 13

[73] A. Khodaei, M. Shahidehpour, and S. Kamalinia, "Transmission switching in expansion planning," *IEEE Trans. Power Syst.*, vol. 25, no. 3, pp. 1722–1733, Aug. 2010. 13

[74] G. Blanco, F. Olsina, F. Garcés, and C. Rehtanz, "Real option valuation of FACTS investment based on the least square Monte Carlo method," *IEEE Trans. Power Syst.*, vol. 26, no. 3, pp. 1389–1398, Aug. 2011. 13

[75] F. Zhang, Z. Hu, and Y. Song, "Mixed-integer linear model for transmission expansion planning with line losses and energy storage systems," *IET Gener., Transm., Distrib.*, vol. 7, no. 8, pp. 919–928, Apr. 2013. 13

[76] A. Dimitrovski, Z. Li, and B. Ozpineci, "Application of saturable-core reactors (SCR) in power systems," in *2014 IEEE PES T&D Conf. and Expo.*, Chicago, IL, USA, Apr. 14–17, 2014, pp. 1–5. 15

[77] A. Boyajian, "Theory of D-C. excited iron-core reactors and regulators," *AIEE Trans.*, vol. XLIII, pp. 919–936, 1924. 15

[78] H. S. Kirschbaum and E. L. Harder, "A balanced amplifier using biased saturable core reactors," *AIEE Trans.*, vol. 66, no. 1, pp. 273–278, 1957. 15

[79] R. A. Ramey, "On the mechanics of magnetic amplifier operation," *AIEE Trans.*, vol. 70, no. 2, pp. 1214–1223, Jul. 1951. 15

[80] W. A. Geyger, *Magnetic-amplifier Circuits*. New York: McGraw-Hill, 1957. 15

[81] F. Hu, K. Sun, A. Del Rosso, E. Farantatos, and N. Bhatt, "Measurement-based real-time voltage stability monitoring for load areas," *IEEE Transactions on Power Systems*, vol. 31, no. 4, pp. 2787–2798, Sep. 2016. 24

[82] F. Hu, L. Yang, J. Wang, Y. Ma, K. Sun, L. M. Tolbert, and F. Wang, "Measurement-based voltage stability assessment and control on curent hardware test bed system," in *IEEE Power and Energy Society General Meeting*, Boston, MA, USA, Jul. 17–21, 2016, pp. 1–5. 24

[83] H. Yuan and F. Li, "Hybrid voltage stability assessment (vsa) for n- 1 contingency," *Electric Power Systems Research*, vol. 122, pp. 65–75, May 2015. 24

[84] ——, "A comparative study of measurement-based thevenin equivalents identification methods," in *North American Power Symposium (NAPS), 2016*, Pullman, WA, USA, Sep. 7–9, 2014, pp. 1–6. 24

[85] J. Nocedal and S. J. Wright, *Numerical Optimization.* New York, NY, USA: Springer, 1999. 25

[86] F. E. Gill, W. Murray, and M. A. Saunders, "SNOPT: An SQP algorithm for large-scale constrained optimization," *SIAM Journal on Optimization*, vol. 12, no. 4, pp. 979–1006, Apr. 2002. 26, 27

[87] R. D. Zimmerman, C. E. Murillo-Sanchez, and R. J. Thomas, "MATPOWER: Steady-state operations, planning and analysis tools for power system research and education," *IEEE Trans. Power Syst.*, vol. 26, no. 1, pp. 12–19, Feb. 2011. 27, 45, 64, 83, 113

[88] A. Brooke, D. Kendrick, A. Meeraus, R. Raman, and R. E. Rosenthal, *GAMS, A User's Guide.* Washington DC, USA: GAMS Development Corp., 1998. 27

[89] T. J. Overbye, X. Cheng, and Y. Sun, "A comparison of the AC and DC power flow models for LMP calculations," in *Proc. of the 37th Annual Hawaii International Conference on System Sciences*, Jun. 5–8, 2004. 29

[90] B. Stott, J. Jardim, and O. Alsac, "DC power flow revisited," *IEEE Trans. Power Syst.*, vol. 24, no. 3, pp. 1290–1300, Aug. 2009. 29

[91] COI utilization report. [Online]. Available: http://www.oatioasis.com/WASN/WASNdocs/COI-Utilization-Report-S.Anners.pdf. 31, 50

[92] PowerWorld. [Online]. Available: http://www.powerworld.com. 31, 50

[93] T. Ding, R. Bo, W. Gu, and H. Sun, "Big-M based MIQP method for economic dispatch with disjoint prohibited zones," *IEEE Trans. Power Syst.*, vol. 29, no. 2, pp. 976–977, Mar. 2014. 41

[94] W. P. Adams and R. J. Forrester, "Linear forms of nonlinear expressions: New insights on old ideas," *Operations Research Letters*, vol. 35, no. 4, pp. 510–518, Jul. 2007. 41

[95] C. M. Davis and T. J. Overbye, "Multiple element contingency screening," *IEEE Trans. Power Syst.*, vol. 26, no. 3, pp. 1294–1301, Aug. 2011. 43, 58

[96] J. Löfberg, "YALMIP: A toolbox for modeling and optimization in matlab," in *Proc. CACSD Conf.*, Taipei, Taiwan, Jul. 2004, pp. 284–289. 45, 71, 83

[97] (2014) IBM ILOG CPLEX V 12.6. [Online]. Available: http://www.ibm.com/software/commerce/optimization/cplex-optimizer/. 45, 71, 83

[98] M. Khanabadi, H. Ghasemi, and M. Doostizadeh, "Optimal transmission switching considering voltage security and N-1 contingency analysis," *IEEE Trans. Power Syst.*, vol. 28, no. 1, pp. 542–550, Feb. 2013. 47

[99] X. Zhang, K. Tomsovic, and A. Dimitrovski, "Security constrained multistage transmission expansion planning considering a continuously variable series reactor," *IEEE Trans. Power Syst.*, 2017. [Online]. Available: http://ieeexplore.ieee.org/document/7859423/. 57

[100] (2005) NERC System Performance Under Normal Condions. [Online]. Available: http://www.nerc.com/files/tpl-001-0.pdf. 57

[101] (2014) Capital Costs for Transmission and Substations: Updated Recommendations for WECC Transmission Expansion Planning. [Online]. Available: https://www.wecc.biz/Reliability/2014_TEPPC_Transmission_CapCost_Report_B+V.pdf. 65

[102] R. Z. Miñano, A. J. Conejo, and F. Milano, "OPF-based security redispatching including FACTS devices," *IET Gener., Transm., Distrib.*, vol. 2, no. 6, pp. 821–833, Nov. 2008. 73, 75

[103] G. Liu, M. Starke, B. Xiao, X. Zhang, and K. Tomsovic, "Microgrid optimal scheduling with chance-constrained islanding capability," *Electric Power Systems Research*, vol. 145, pp. 197–206, Apr. 2017. 75

[104] G. Liu, M. Starke, X. Zhang, and K. Tomsovic, "A milp-based distribution optimal power flow model for microgrid operation," in *IEEE Power and Energy Society General Meeting*, Boston, MA, USA, Jul. 17–21, 2016, pp. 1–5. 75

[105] G. Liu, M. Starke, B. Xiao, X. Zhang, and K. Tomsovic, "Community microgrid scheduling considering building thermal dynamics," in *IEEE Power and Energy Society General Meeting*, Chicago, IL, USA, Jul. 16–20, 2017, pp. 1–5. 75

[106] ——, "A new distributed optimization for community microgrids scheduling," in *Proceedings of the 50th Hawaii International Conference on System Sciences*, 2017. 75

[107] A. J. Conejo, E. Castillo, R. Minguez, and R. Garcia-Bertrand, *Decomposition techniques in mathematical programming: engineering and science applications*. Heidelberg, Germany: Springer Science & Business Media, 2006. 77

[108] B. Hu and L. Wu, "Robust SCUC considering continuous/discrete uncertainties and quick-start units: a two-stage robust optimization with mixed integer recourse," *IEEE Trans. Power Syst.*, vol. 31, no. 2, pp. 1407–1419, Mar. 2016. 78, 85

[109] N. Papadakos, "Integrated airline scheduling," *Computers & Operations Research*, vol. 36, no. 1, pp. 176–195, 2009. 82

[110] Q. P. Zheng, J. Wang, P. M. Pardalos, and Y. Guan, "A decomposition approach to the two-stage stochastic unit commitment problem," *Annals of Operations Research*, vol. 210, no. 1, pp. 387–410, 2013. 83

[111] X. Zhang, K. Tomsovic, and A. Dimitrovski, "Optimal investment on series FACTS device considering contingencies," in *North American Power Symposium (NAPS), 2016*, Denver, CO, USA, Sep. 18–20, 2016, pp. 1–6. 84, 85

[112] Y. Zhu, J. Yao, and D. Wu, "Comparative study of two stages and single stage topologies for grid-tie photovoltaic generation by pscad/emtdc," in *Advanced Power System Automation and Protection (APAP), 2011 International Conference on*, vol. 2. IEEE, 2011, pp. 1304–1309. 90

[113] Y. Zhu, R. Azim, H. A. Saleem, K. Sun, D. Shi, and R. Sharma, "Microgrid security assessment and islanding control by support vector machine," in *IEEE Power and Energy Society General Meeting*, Denver, CO, USA, Jul. 26–30, 2056, pp. 1–5. 90

[114] (2015) Wind Vision: A New Era for Wind Power in the United States. [Online]. Available: http://www.energy.gov/sites/prod/files/WindVision_Report_final.pdf. 92

[115] C. Huang, F. Li, and Z. Jin, "Maximum power point tracking strategy for large-scale wind generation systems considering wind turbine dynamics," *IEEE Transactions on Industrial Electronics*, vol. 62, no. 4, pp. 2530–2539, Apr. 2015. 92

[116] C. Huang, F. Li, T. Ding, Z. Jin, and X. Ma, "Second-order cone programming-based optimal control strategy for wind energy conversion systems over complete operating regions," *IEEE Transactions on Sustainable Energy*, vol. 6, no. 1, pp. 263–271, Jan. 2015. 92

[117] J. Lawhorn, D. Osborn, J. Caspary, B. M. Nickell, D. Larson, W. Lasher, and M. E. Rahman, "The view from the top," *IEEE Power and Energy Magazine*, vol. 7, no. 6, pp. 76–88, 2009. 92

[118] M. Milligan, K. Porter, E. DeMeo, P. Denholm, H. Holttinen, B. Kirby, N. Miller, A. Mills, M. O'Malley, M. Schuerger *et al.*, "Wind power myths debunked," *IEEE Power and Energy Magazine*, vol. 7, no. 6, pp. 89–99, 2009. 92

[119] A. Nasri, A. J. Conejo, S. J. Kazempour, and M. Ghandhari, "Minimzing wind power splillage using an OPF with FACTS devices," *IEEE Trans. Power Syst.*, vol. 29, no. 5, pp. 2150–2159, Sep. 2014. 92

[120] X. Fang, Q. Hu, F. Li, B. Wang, and Y. Li, "Coupon-based demand response considering wind power uncertainty: a strategic bidding model for load serving entities," *IEEE Transactions on Power Systems*, vol. 31, no. 2, pp. 1025–1037, Mar. 2016. 93

[121] X. Fang, Y. Wei, and F. Li, "Evaluation of lmp intervals considering wind uncertainty," *IEEE Transactions on Power Systems*, vol. 31, no. 3, pp. 2495–2496, May 2016. 93

[122] L. Yang, Y. Ma, J. Wang, J. Wang, X. Zhang, L. M. Tolbert, F. Wang, and K. Tomsovic, "Development of converter based reconfigurable power grid emulator," in *Energy Conversion Congress and Exposition (ECCE), 2014 IEEE*. Pittsburgh, PA, USA: IEEE, Sep. 14–18, 2014, pp. 3990–3997. 93

[123] L. Yang, X. Zhang, Y. Ma, J. Wang, L. Hang, K. Lin, L. M. Tolbert, F. Wang, and K. Tomsovic, "Stability analysis of inverter based generator emulator in test-bed for power systems," in *Energy Conversion Congress and Exposition (ECCE), 2013 IEEE*. Denver, CO, USA: IEEE, Sep. 15–19, 2013, pp. 5410–5417. 93

[124] L. Yang, J. Wang, Y. Ma, J. Wang, X. Zhang, L. M. Tolbert, F. F. Wang, and K. Tomsovic, "Three-phase power converter-based real-time synchronous generator emulation," *IEEE Transactions on Power Electronics*, vol. 32, no. 2, pp. 1651–1665, Feb. 2017. 93

[125] L. Yang, X. Zhang, Y. Ma, J. Wang, L. Hang, K. Lin, L. M. Tolbert, F. Wang, and K. Tomsovic, "Hardware implementation and control design of generator emulator in multi-converter system," in *Applied Power Electronics Conference*

and Exposition (APEC), 2013 Twenty-Eighth Annual IEEE. Long Beach, CA, USA: IEEE, Mar. 17–21, 2013, pp. 2316–2323. 93

[126] B. Liu, S. Zhang, S. Zheng, Y. Ma, F. Wang, and L. M. Tolbert, "Design consideration of converter based transmission line emulation," in *Applied Power Electronics Conference and Exposition (APEC), 2016 IEEE*. Long Beach, CA, USA: IEEE, Mar. 20–24, 2016, pp. 966–973. 93

[127] J. Wang, L. Yang, Y. Ma, X. Shi, X. Zhang, L. Hang, K. Lin, L. M. Tolbert, F. Wang, and K. Tomsovic, "Regenerative power converters representation of grid control and actuation emulator," in *Energy Conversion Congress and Exposition (ECCE), 2012 IEEE*. Raleigh, NC, USA: IEEE, Sep. 15–20, 2012, pp. 2460–2465. 93

[128] W. Cao, Y. Ma, J. Wang, L. Yang, J. Wang, F. Wang, and L. M. Tolbert, "Two-stage pv inverter system emulator in converter based power grid emulation system," in *Energy Conversion Congress and Exposition (ECCE), 2013 IEEE*. Denver, CO, USA: IEEE, Sep. 15–19, 2013, pp. 4518–4525. 93

[129] W. Cao, Y. Ma, J. Wang, and F. Wang, "Virtual series impedance emulation control for remote pv or wind farms," in *Applied Power Electronics Conference and Exposition (APEC), 2014 Twenty-Ninth Annual IEEE*. Fort Worth, TX, USA: IEEE, Mar. 16–20, 2014, pp. 411–418. 93

[130] Y. Ma, L. Yang, J. Wang, F. Wang, and L. M. Tolbert, "Emulating full-converter wind turbine by a single converter in a multiple converter based emulation system," in *Applied Power Electronics Conference and Exposition (APEC), 2014 Twenty-Ninth Annual IEEE*. Fort Worth, TX, USA: IEEE, Mar. 16–20, 2014, pp. 3042–3047. 93

Appendices

Appendix A

Modified Jacobian Matrix for the Power Balance Equations

The optimization variable $\boldsymbol{w}$ can be expressed as the following:

$$\boldsymbol{w} = [\boldsymbol{\theta}\ \boldsymbol{V}\ \boldsymbol{P_g}\ \boldsymbol{Q_g}\ \boldsymbol{x^V}\ \xi]^T \tag{A.1}$$

To compute the Jacobian matrix of the power balance equations, constraint (4.11) and (4.12) are first written as:

$$g_{Pi}(\boldsymbol{w}) = P_{gi} - \mu \cdot P_{di} - g_i V_i^2 - \sum_{j \in \mathcal{B}_i} P_{ij}, \quad i \in \mathcal{B} \tag{A.2}$$

$$g_{Qi}(\boldsymbol{w}) = Q_{gi} - \mu \cdot Q_{di} + b_i V_i^2 - \sum_{j \in \mathcal{B}_i} Q_{ij}, \quad i \in \mathcal{B} \tag{A.3}$$

The structure of the modified Jacobian matrix is expressed as

$$\boldsymbol{J} = \begin{bmatrix} \boldsymbol{J_A} & \boldsymbol{J_B} & \boldsymbol{J_C} \end{bmatrix} \tag{A.4}$$

where

$$\boldsymbol{J_A} = \begin{bmatrix} \frac{\partial \boldsymbol{g_P}}{\partial \boldsymbol{\theta}} & \frac{\partial \boldsymbol{g_P}}{\partial \boldsymbol{V}} & \frac{\partial \boldsymbol{g_P}}{\partial \boldsymbol{P_g}} & \frac{\partial \boldsymbol{g_P}}{\partial \boldsymbol{Q_g}} \\ \frac{\partial \boldsymbol{g_Q}}{\partial \boldsymbol{\theta}} & \frac{\partial \boldsymbol{g_Q}}{\partial \boldsymbol{V}} & \frac{\partial \boldsymbol{g_Q}}{\partial \boldsymbol{P_g}} & \frac{\partial \boldsymbol{g_Q}}{\partial \boldsymbol{Q_g}} \end{bmatrix} \tag{A.5}$$

$$\boldsymbol{J_B} = \begin{bmatrix} \frac{\partial \boldsymbol{g_P}}{\partial \boldsymbol{x^V}} \\ \frac{\partial \boldsymbol{g_Q}}{\partial \boldsymbol{x^V}} \end{bmatrix} \tag{A.6}$$

$$\boldsymbol{J_C} = \begin{bmatrix} \frac{\partial \boldsymbol{g_P}}{\partial \xi} \\ \frac{\partial \boldsymbol{g_Q}}{\partial \xi} \end{bmatrix} \tag{A.7}$$

$\boldsymbol{J_A}$ is the standard Jacobian matrix which is provided by MATPOWER [87]. The element of $\boldsymbol{J_B}$ is derived as

$$\begin{aligned} \frac{\partial g_{Pi}}{\partial x_{ij}^V} &= \frac{\partial g_{Pi}}{\partial P_{ij}} \frac{\partial P_{ij}}{g_{ij}} \frac{\partial g_{ij}}{\partial x_{ij}^V} + \frac{\partial g_{Pi}}{\partial P_{ij}} \frac{\partial P_{ij}}{b_{ij}} \frac{\partial b_{ij}}{\partial x_{ij}^V} \\ &= (V_i^2 - V_i V_j \cos(\theta_i - \theta_j)) \cdot \frac{2r_{ij}(x_{ij} + x_{ij}^V)}{(r_{ij}^2 + (x_{ij} + x_{ij}^V)^2)^2} \\ &\quad + (-V_i V_j \sin(\theta_i - \theta_j)) \cdot \frac{r_{ij}^2 - (x_{ij} + x_{ij}^V)^2}{(r_{ij}^2 + (x_{ij} + x_{ij}^V)^2)^2}, \\ &\qquad (i,\ j) \in \Omega_V,\ i \in \mathcal{B} \end{aligned} \tag{A.8}$$

$$\begin{aligned} \frac{\partial g_{Qi}}{\partial x_{ij}^V} &= \frac{\partial g_{Qi}}{\partial Q_{ij}} \frac{\partial Q_{ij}}{g_{ij}} \frac{\partial g_{ij}}{\partial x_{ij}^V} + \frac{\partial g_{Qi}}{\partial Q_{ij}} \frac{\partial Q_{ij}}{b_{ij}} \frac{\partial b_{ij}}{\partial x_{ij}^V} \\ &= V_i V_j \sin(\theta_i - \theta_j) \cdot \frac{2r_{ij}(x_{ij} + x_{ij}^V)}{(r_{ij}^2 + (x_{ij} + x_{ij}^V)^2)^2} \\ &\quad + (V_i V_j \cos(\theta_i - \theta_j) - V_i^2) \cdot \frac{r_{ij}^2 - (x_{ij} + x_{ij}^V)^2}{(r_{ij}^2 + (x_{ij} + x_{ij}^V)^2)^2}, \\ &\qquad (i,\ j) \in \Omega_V,\ i \in \mathcal{B} \end{aligned} \tag{A.9}$$

The element of $\boldsymbol{J_C}$ can be expressed as

$$\frac{\partial g_{Pi}}{\partial \mu} = -P_{di}, \quad i \in \mathcal{B} \tag{A.10}$$

$$\frac{\partial g_{Qi}}{\partial \mu} = -Q_{di}, \quad i \in \mathcal{B} \tag{A.11}$$

Vita

Xiaohu Zhang received the B.S. degree in electrical engineering from Huazhong University of Science and Technology, Wuhan, China, and the M.S. degree in electrical engineering from Royal Institute of Technology, Stockholm, Sweden, in 2009 and 2011 respectively. His research interests are power system operation, planning and stability analysis.